Supporting Information for:

Exploring the Stability of Inhibitor Binding to SIK2 Using Molecular Dynamics Simulation and Binding Free Energy Calculation

Mingsong Shi[1#], Min Zhao[1#], Lun Wang[1], Kongjun Liu[1], Penghui Li[2], Jiang Liu[1], Xiaoying Cai[1], Lijuan Chen[1]* and Dingguo Xu[2,3]*

1 *State Key Laboratory of Biotherapy/Collaborative Innovation Center of Biotherapy and Cancer Center, West China Hospital of Sichuan University, Chengdu, Sichuan 610041, China*

2 *College of Chemistry, MOE Key Laboratory of Green Chemistry and Technology, Sichuan University, Chengdu, Sichuan 610064, China*

3 *Research Center for Material Genome Engineering, Sichuan University, Chengdu, Sichuan 610065, China*

* To whom correspondence should be addressed: dgxu@scu.edu.cn (D. X); chenlijuan125@163.com (L. C).

Contents

Method for Binding Free Energy Estimation

In this work, the molecular mechanics generalized Born surface area (MM/GBSA) approach[1, 2] were employed to calculate the binding free energies of those four inhibitors to SIK2 protein kinase. It is an efficient method to improve the ability evaluation of ligand and enzyme systems[3-5]. The MM/GBSA framework has been discussed extensively[6-8]. Only a short description is summarized here. The total binding free energy for the binding of inhibitor of SIK2, namely $\Delta G_{binding}$ was provide in the following:

$$\Delta G_{binding} = \Delta G_{complex} - \Delta G_{protein} - \Delta G_{ligand} \quad (1)$$

$$G = E_{gas} + G_{sol} - TS \quad (2)$$

$$E_{gas} = E_{int} + E_{vdW} + E_{ele} \quad (3)$$

$$G_{sol} = G_{el} + G_{nonel} \quad (4)$$

$\Delta G_{complex}$, $\Delta G_{protein}$ and ΔG_{ligand} are denoted as free energies of the inhibitor/SIK2, SIK2 and inhibitor, respectively. The $\Delta G_{binding}$ can be decomposed into the enthalpy part ($\Delta H = E_{gas} + G_{sol}$) and the entropy part ($T\Delta S$). The molecular mechanical energies (E_{gas}) consist of the intramolecular energy (E_{int}), van der Waals forces (E_{vdW}) and electrostatic forces (E_{ele}) which get these values via a statistical average way based on the AMBER force field. The solvation free energy (G_{sol}) can be principally divided into both electrostatic (G_{el}) and non-electrostatic (G_{nonel}) terms. The G_{nonel} comes from the combined effect of unfavorable cost of surface formation and the favorable van der Waals interactions between the solute and solvent, which can be evaluated by the equation of $\gamma \cdot SA + b$, where γ =0.0072 kcal/Å^2 and b=0.0 kcal/mol. The solvent accessible surface area (SA) which was estimated using the LCPO method[9]. The G_{el} is calculated by the Generalized Born (GB) equation[10, 11]. The solute dielectric constant was set to 1, and the exterior dielectric constant was set to 80. We used MM/GBSA method to get these former terms via a statistical average way from the last 200 ns MD trajectory. Meanwhile, entropy contributions to the binding free energy may be added to improve the accuracy. The entropy can be estimated using the normal model analysis with quasi harmonic model based on the conformational snapshots from the same MD trajectory[12]. For each complex system, binding energies were averaged over 1000 frames and the $-TS$ was averaged with interval 2 ns. Those energy was calculated with the MMPBA.py program[13].

Reference

1. Srinivasan, J.; Cheatham, T. E.; Cieplak, P.; Kollman, P. A.; Case, D. A., Continuum solvent studies of the stability of DNA, RNA, and phosphoramidate - DNA helices. *J. Am. Chem. Soc.* **1998,** *120* (37), 9401-9409.

2. Lee, M. S.; Salsbury, F. R.; Olson, M. A., An efficient hybrid explicit/implicit solvent method for biomolecular simulations. *J. Comput. Chem.* **2004,** *25* (16), 1967-1978.

3. Shi, M.; Xu, D., Molecular dynamics investigations suggest a non-specific recognition strategy of 14-3-3σ protein by tweezer: Implication for the inhibition mechanism. *Front. Chem.* **2019,** *7* (237).

4. Wang, J. Y.; Chen, Q.; Wang, M.; Zhong, C., The opening/closure of the P-loop and hinge of BCR-ABL1 decodes the low/high bioactivities of dasatinib and axitinib. *Phys. Chem. Chem. Phys.* **2017,** *19* (33), 22444-22453.

5. Tse, A.; Verkhivker, G. M., Molecular Dynamics Simulations and Structural Network Analysis of c-Abl and c-Src Kinase Core Proteins: Capturing Allosteric Mechanisms and Communication Pathways from Residue Centrality. *J. Chem. Inf. Model.* **2015,** *55* (8), 1645-1662.

6. Honig, B.; Nicholls, A., Classical electrostatics in biology and chemistry. *Science* **1995,** *268* (5214), 1144-1149.

7. Genheden, S.; Ryde, U., The MM/PBSA and MM/GBSA methods to estimate ligand-binding affinities. *Expert. Opin. Drug Discov.* **2015,** *10* (5), 449-461.

8. Onufriev, A. V.; Case, D. A., Generalized Born Implicit Solvent Models for Biomolecules. In *Annual Review of Biophysics, Vol 48*, Dill, K. A., Ed. Annual Reviews: Palo Alto, 2019; Vol. 48, pp 275-296.

9. Weiser, J.; Shenkin, P. S.; Still, W. C., Approximate atomic surfaces from linear combinations of pairwise overlaps (LCPO). *J. Comput. Chem.* **1999,** *20* (2), 217-230.

10. Still, W. C.; Tempczyk, A.; Hawley, R. C.; Hendrickson, T., Semianalytical treatment of solvation for molecular mechanics and dynamics. *J. Am. Chem. Soc.* **1990,** *112* (16), 6127-6129.

11. Srinivasan, J.; Trevathan, M. W.; Beroza, P.; Case, D. A., Application of a pairwise generalized Born model to proteins and nucleic acids: inclusion of salt effects. *Theor. Chem. Acc.* **1999,** *101* (6), 426-434.

12. Gao, P. C.; Li, Z. L., Computation of the Boltzmann entropy of a landscape: a review and a generalization. *Landsc. Ecol.* **2019,** *34* (9), 2183-2196.

13. Miller, B. R.; McGee, T. D.; Swails, J. M.; Homeyer, N.; Gohlke, H.; Roitberg, A. E., MMPBSA.py: An Efficient Program for End-State Free Energy Calculations. *Journal of Chemical Theory and Computation* **2012,** *8* (9), 3314-3321.

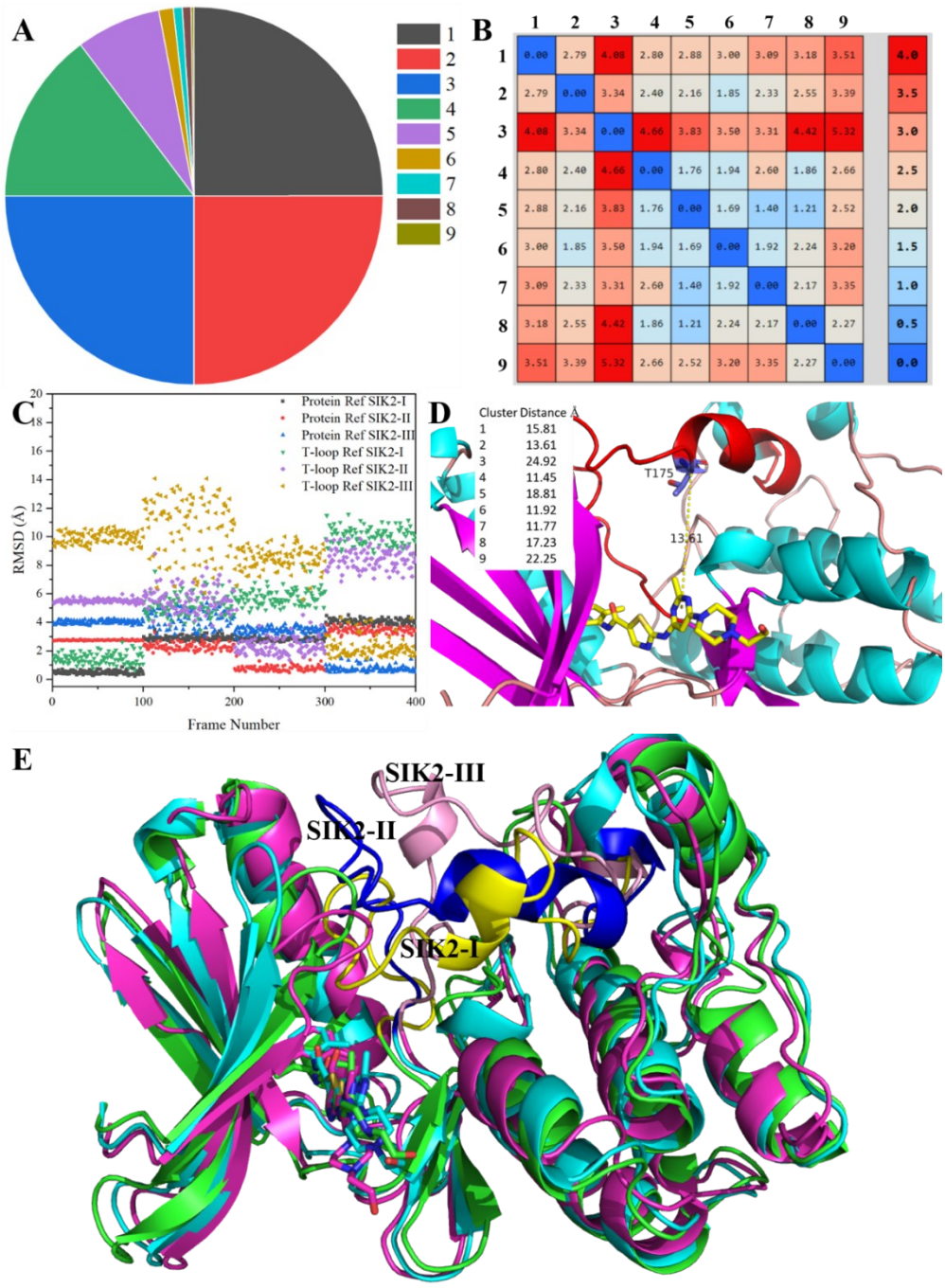

Figure S1. The cluster analysis results for the SAMD simulations.

(A) Cluster analysis of the 400 conformations from the SAMD simulation; (B) RMSD values of representative frames for the nine clusters; (C) RMSD values for the backbone atoms of protein and T-loop with SIK2-I, SIK2-II and SIK2-III as the reference states; (D) distances between the Cα atom of T175 and the center of mass of the pyrimidine ring of dasatinib for the representative structure of the nine clusters; (E) the selected conformations of SIK2-I, SIK2-II and SIK2-III when dasatinib bind into the ATP-binding site.

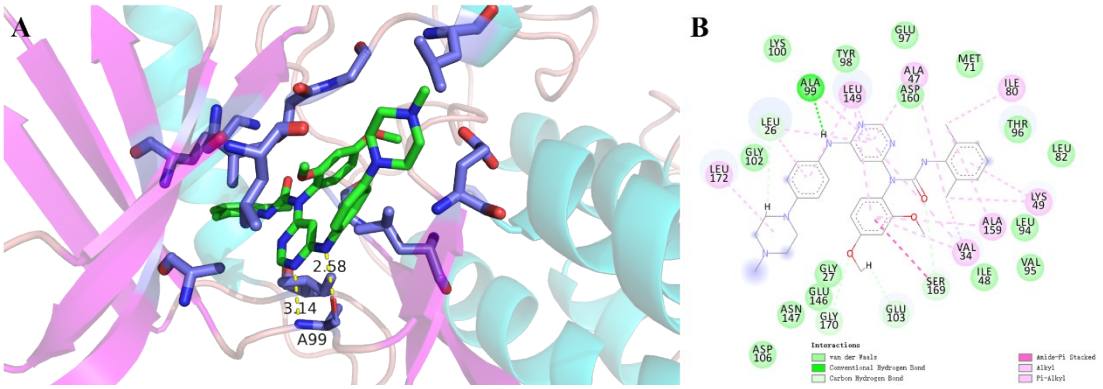

Figure S2. The putative binding mode of inhibitor HG-9-91-01 in the kinase domain of SIK2-I.

(A) for 3D, (B) for 2D.

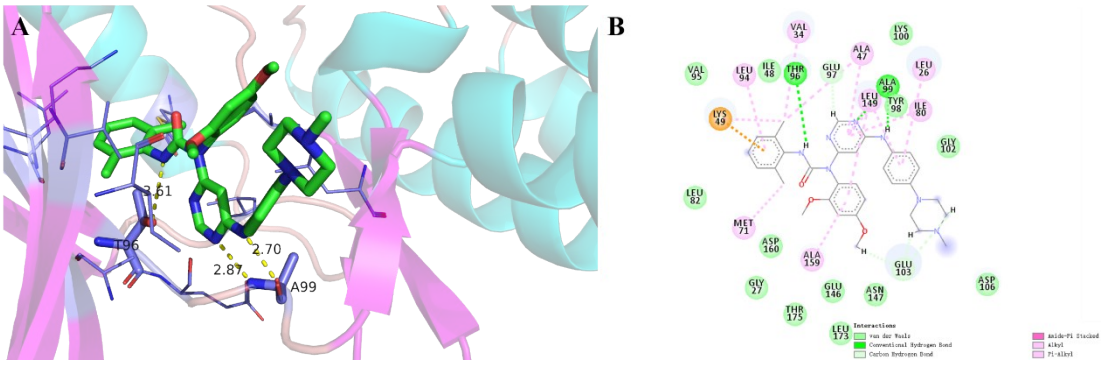

Figure S3. The putative binding mode of inhibitor HG-9-91-01 in the kinase domain of SIK2-II.

(A) for 3D, (B) for 2D.

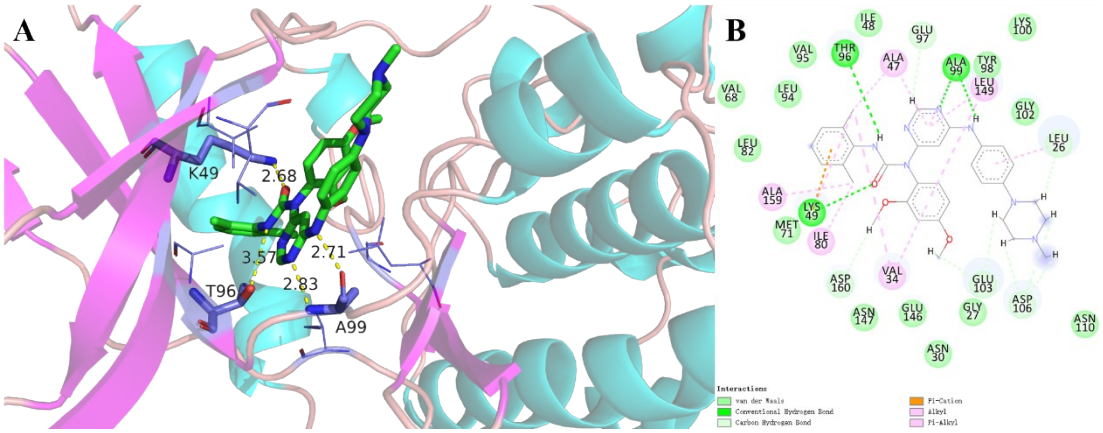

Figure S4. The putative binding mode of inhibitor HG-9-91-01 in the kinase domain of SIK2-III.

(A) for 3D, (B) for 2D.

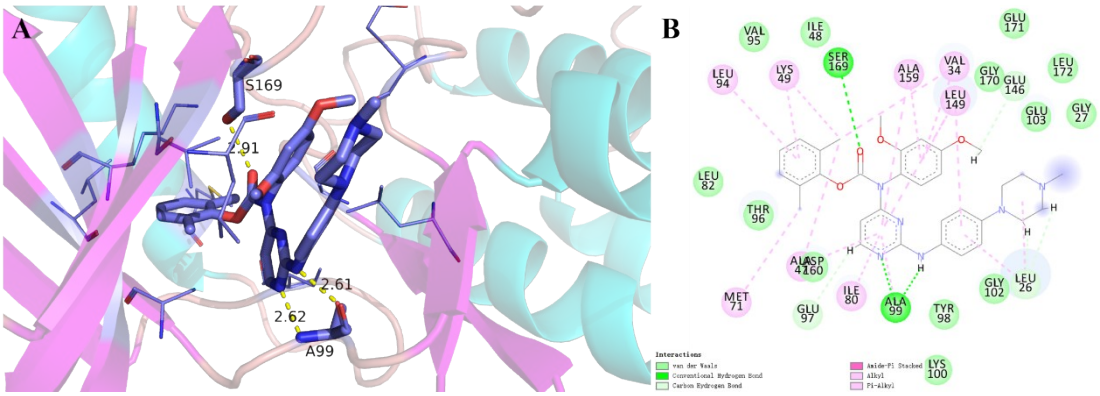

Figure S5. The putative binding mode of inhibitor KIN112 in the kinase domain of SIK2-I.

(A) for 3D, (B) for 2D.

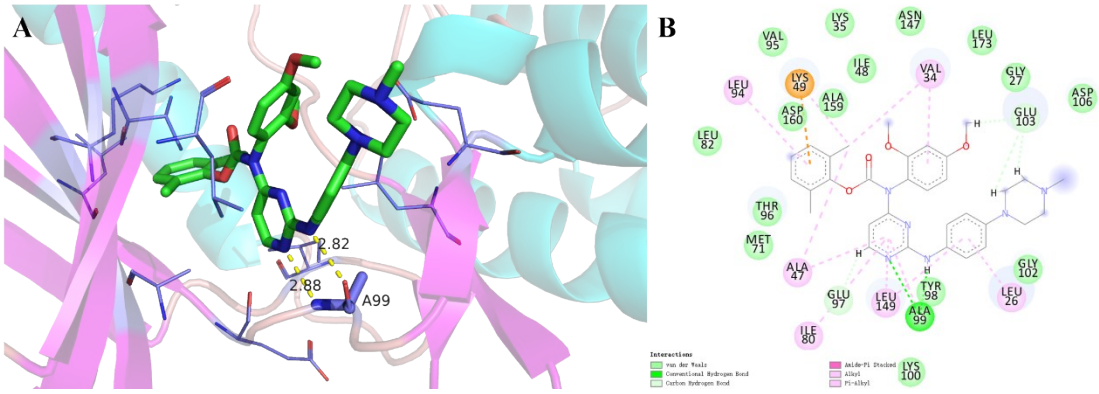

Figure S6. The putative binding mode of inhibitor KIN112 in the kinase domain of SIK2-II.

(A) for 3D, (B) for 2D.

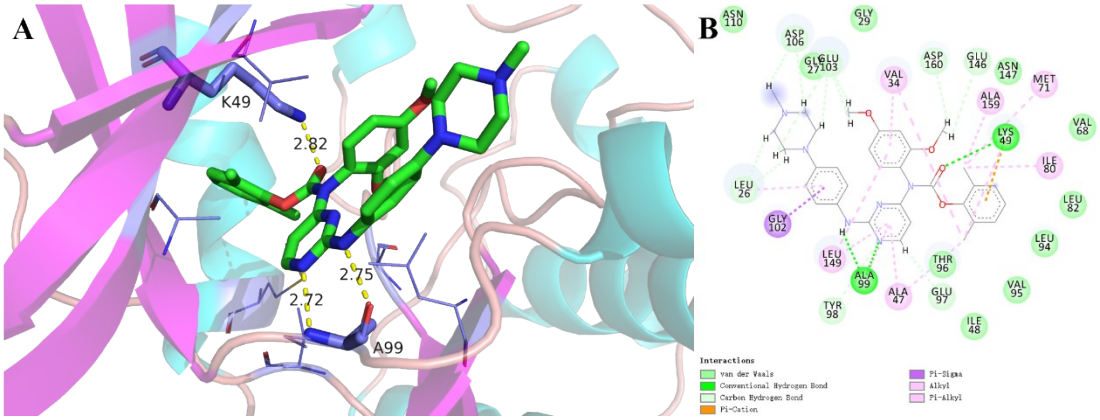

Figure S7. The putative binding mode of inhibitor KIN112 in the kinase domain of SIK2-III.

(A) for 3D, (B) for 2D.

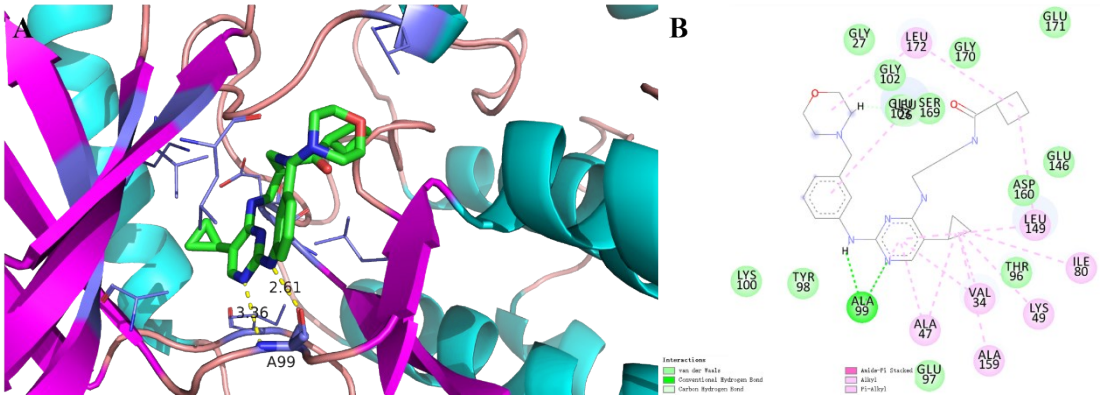

Figure S8. The putative binding mode of inhibitor MRT67307 in the kinase domain of SIK2-I.

(A) for 3D, (B) for 2D.

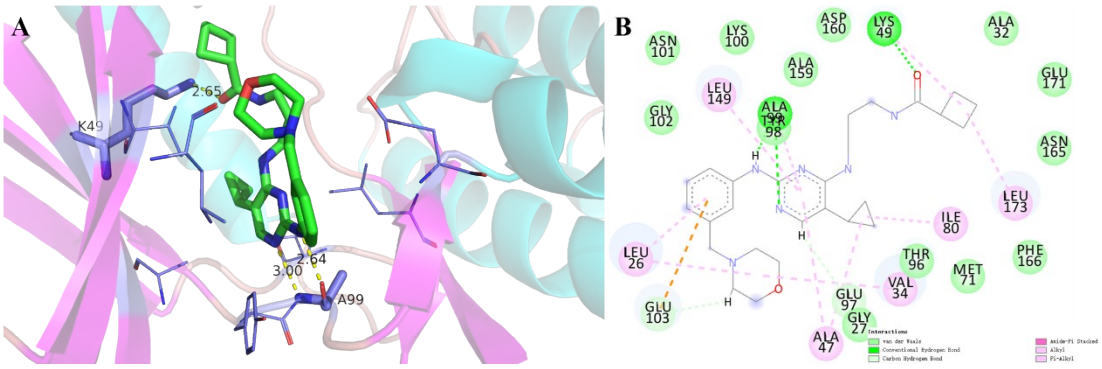

Figure S9. The putative binding mode of inhibitor MRT67307 in the kinase domain of SIK2-II.

(A) for 3D, (B) for 2D.

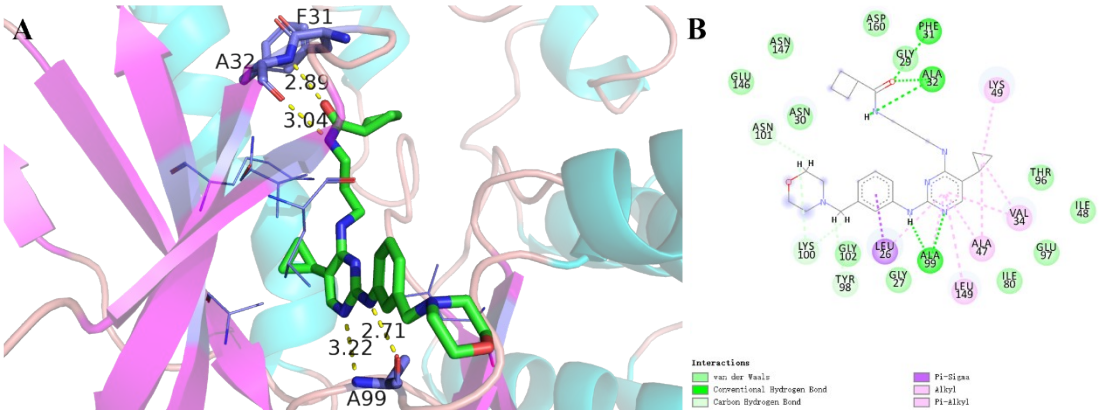

Figure S10. The putative binding mode of inhibitor MRT67307 in the kinase domain of SIK2-III.

(A) for 3D, (B) for 2D.

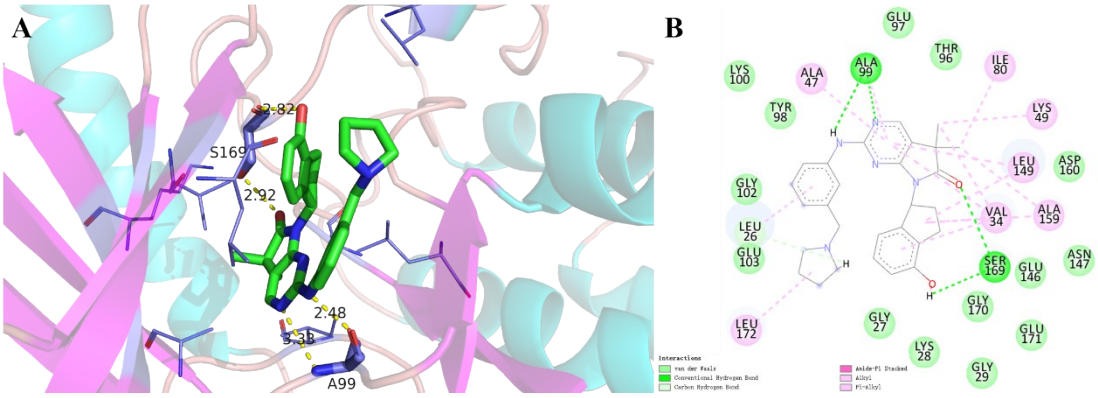

Figure S11. The putative binding mode of inhibitor MRT199665 in the kinase domain of SIK2-I.

(A) for 3D, (B) for 2D.

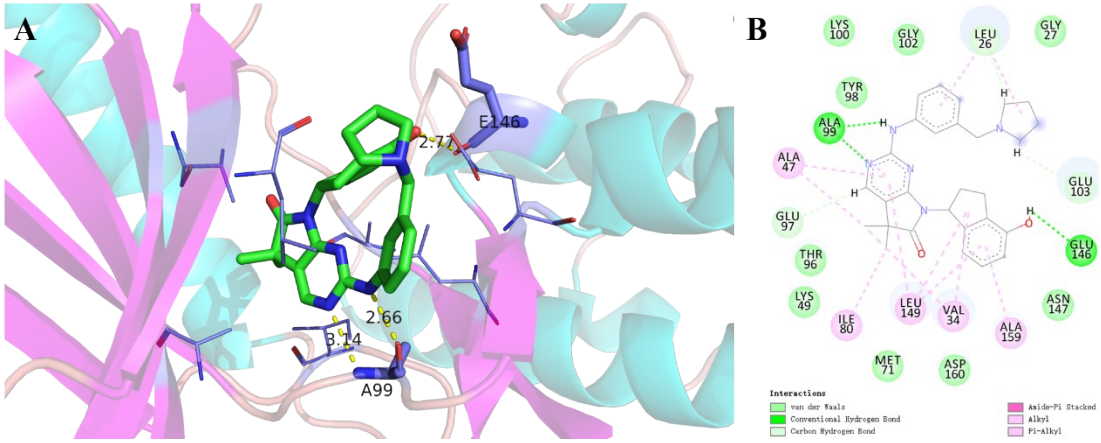

Figure S12. The putative binding mode of inhibitor MRT199665 in the kinase domain of SIK2-II.

(A) for 3D, (B) for 2D.

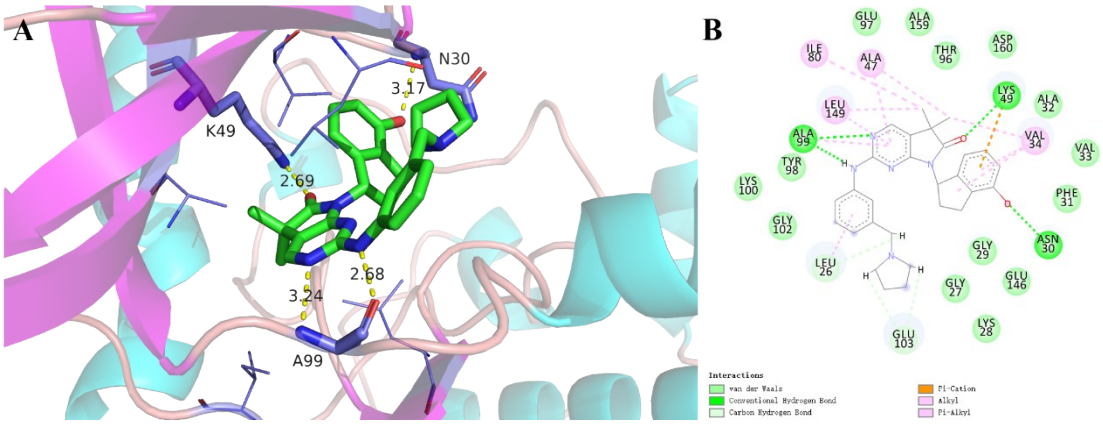

Figure S13. The putative binding mode of inhibitor MRT199665 in the kinase domain of SIK2-III.

(A) for 3D, (B) for 2D.

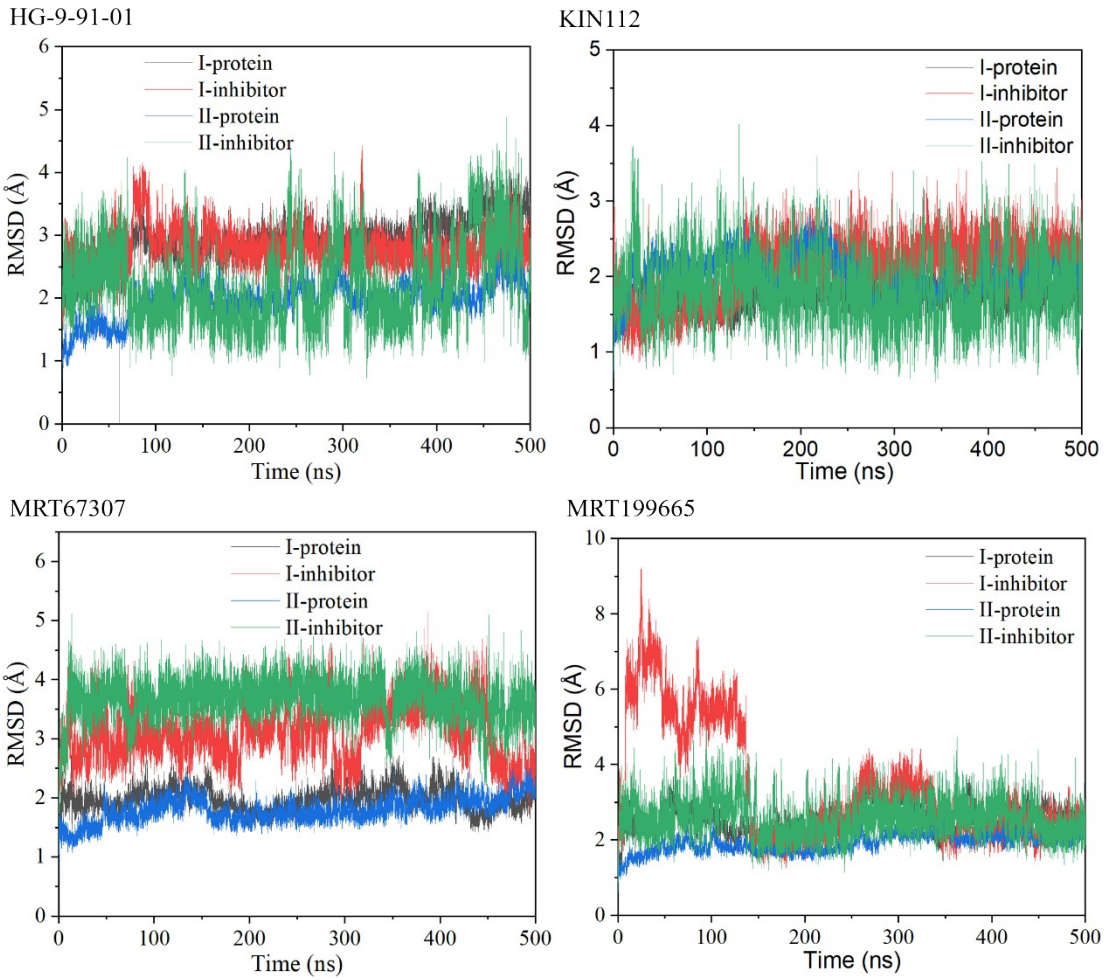

Figure S14. The root mean square deviation (RMSD) value of heavy atoms of backbone for protein and heavy atoms of inhibitor along 500 ns MD simulation for SIK2-I and SIK2-II systems.

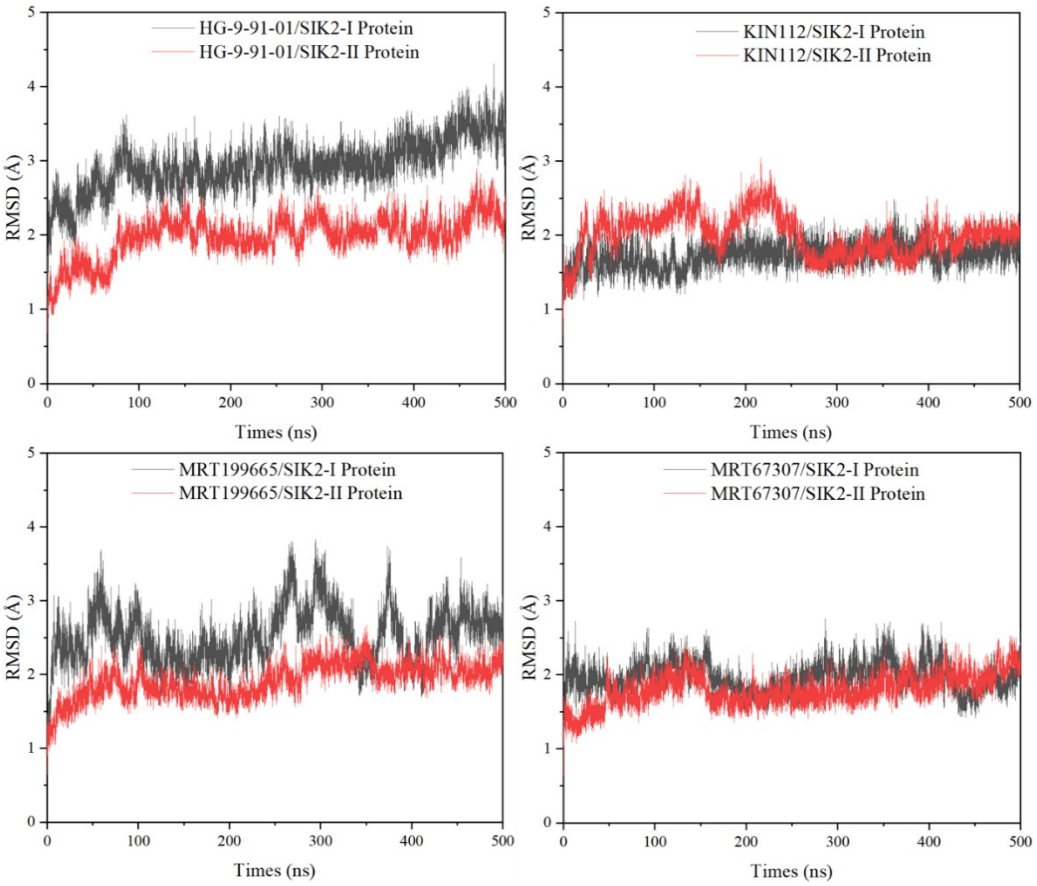

Figure S15. The root mean square deviation (RMSD) value of heavy atoms of protein along 500 ns MD simulation for SIK2-I and SIK2-II systems.

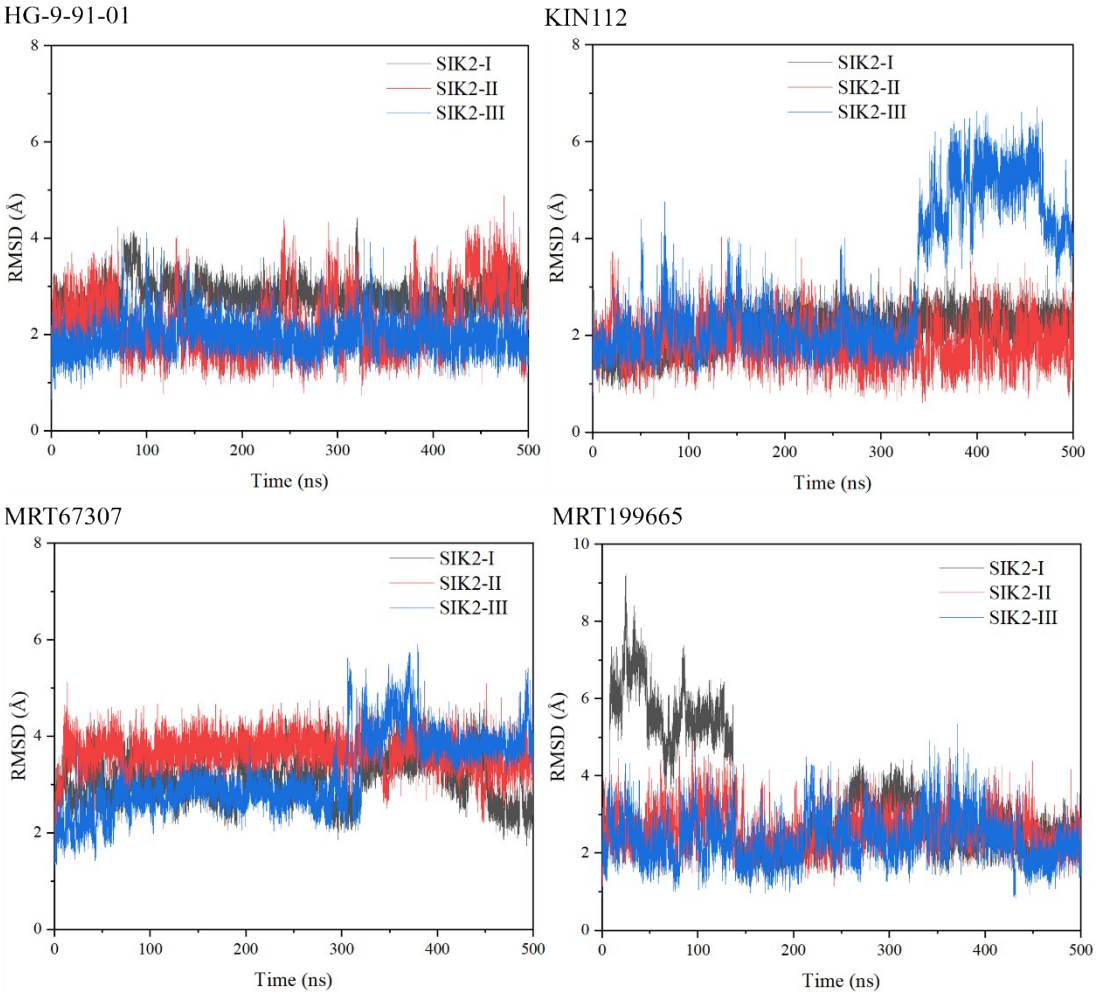

Figure S16. The root mean square deviation (RMSD) value of heavy atoms of backbone for protein along 500 ns MD simulation for SIK2-I, SIK2-II, and SIK2-III systems.

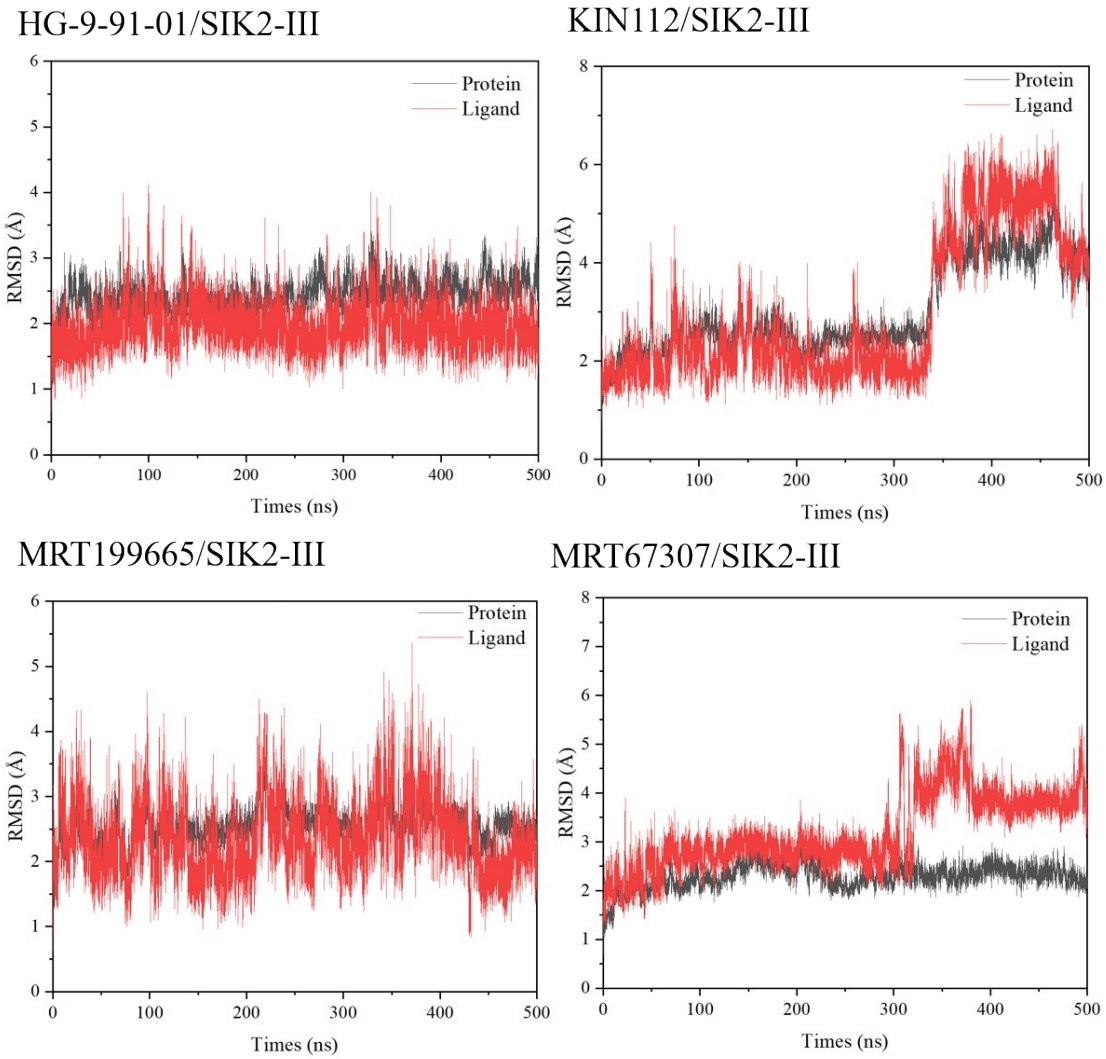

Figure S17. The root mean square deviation (RMSD) value of heavy atoms of backbone of protein and the heavy atoms of inhibitor along 500 ns MD simulation for SIK2-III systems.

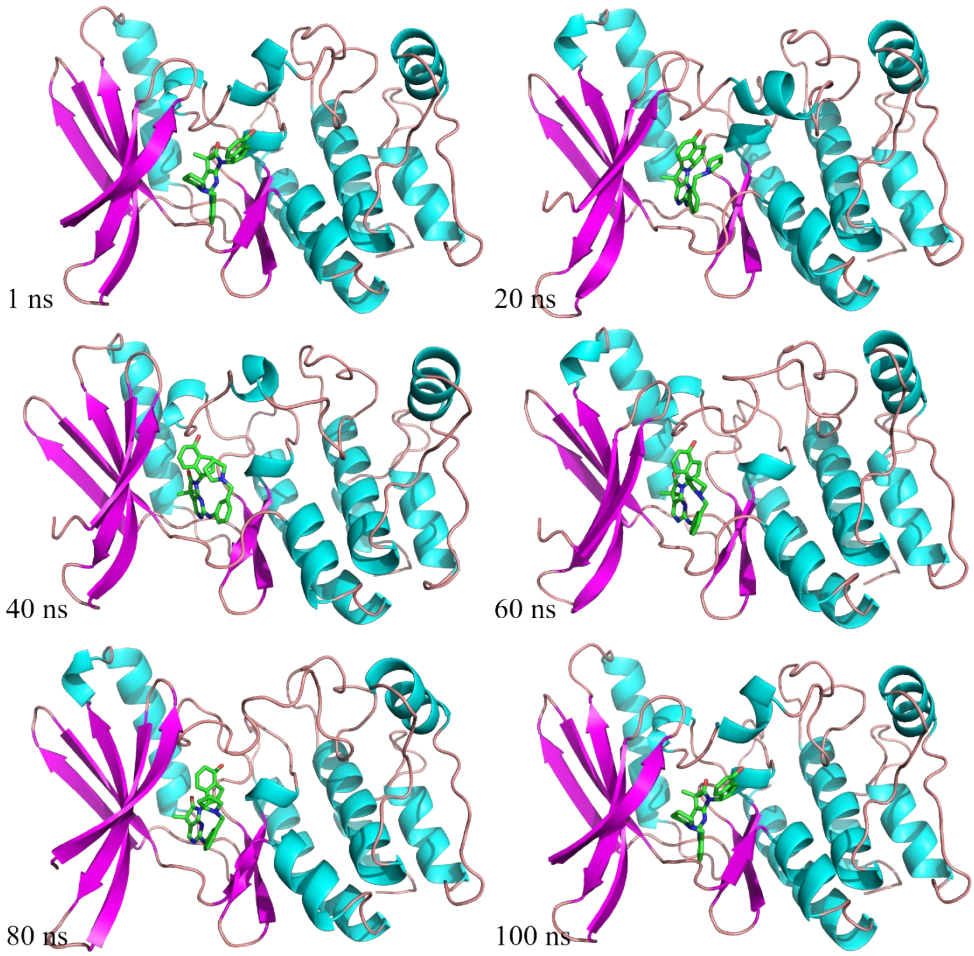

Figure S18. Snapshots of the MRT199665/SIK2-I along the dynamic simulation time for 1, 20, 40, 60, and 80 ns.

For clarity, the water molecules have been removed. The MRT199665 is plotted using stick style, while cartoon style for SIK2.

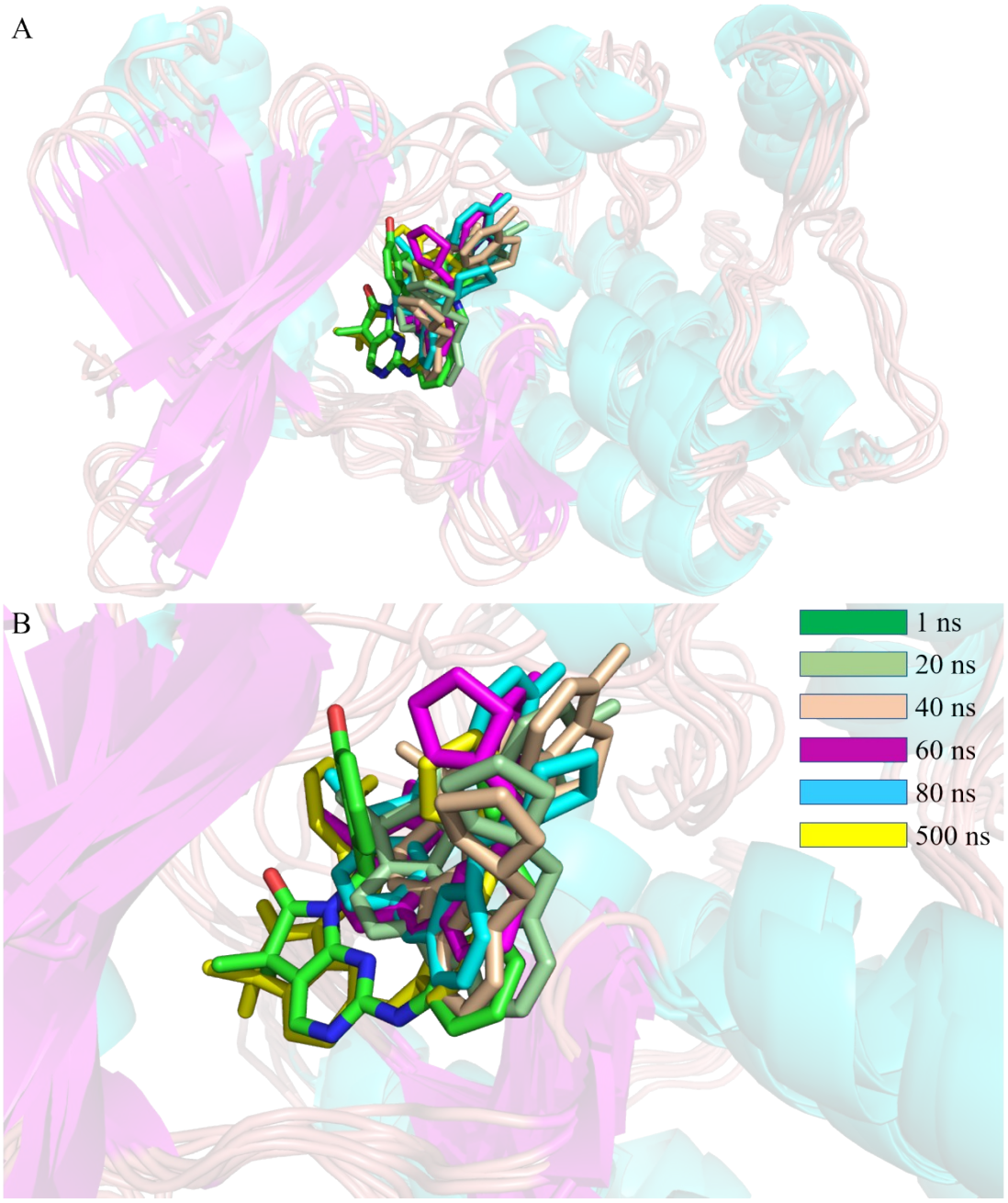

Figure S19. Aligned snapshots of the MRT199665/SIK2-I along the dynamic simulation time for 1, 20, 40, 60, 80, and 500 ns.

For clarity, the water molecules have been removed. The MRT199665 is plotted using stick style, while cartoon style for SIK2. (A) for overall structures and (B) for the active site.

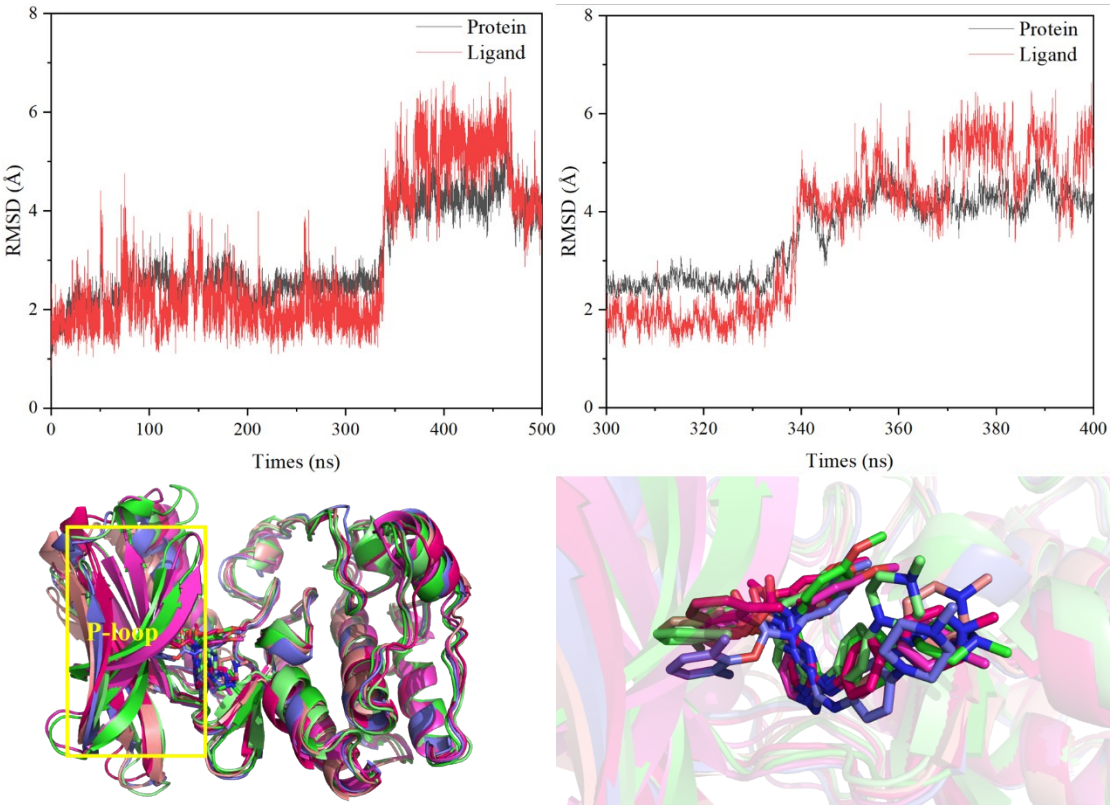

Figure S20. The change between 300 ns to 400 ns for KIN112/SIK2-III complex system.

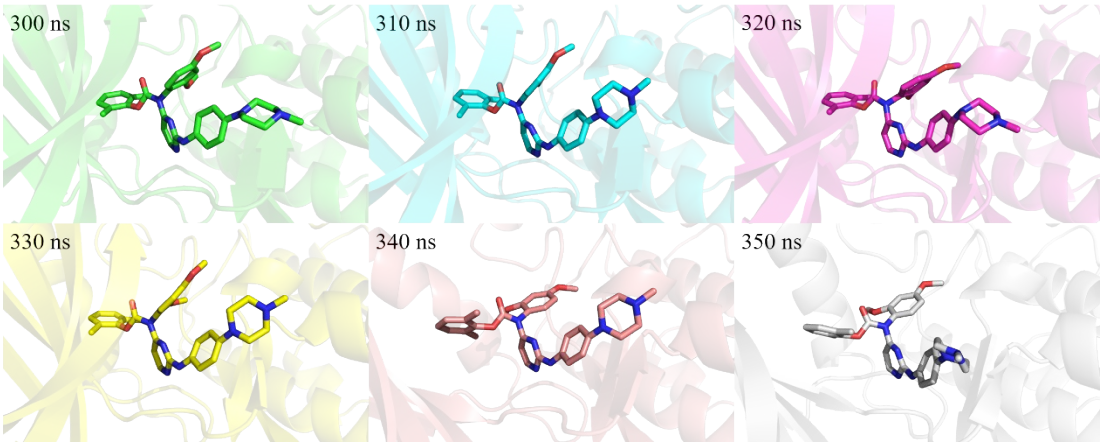

Figure S21. Snapshots of the KIN112/SIK2-III along the dynamic simulation time for 300, 310, 320, 330, 340, and 350 ns.

For clarity, the water molecules have been removed. The KIN112 is plotted using stick style, while cartoon style for SIK2.

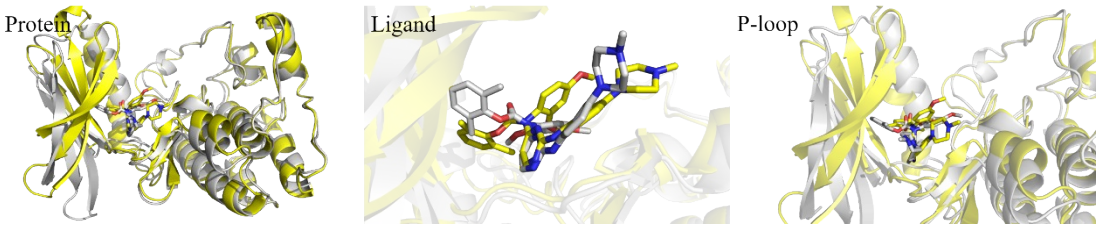

Figure S22. Snapshots of the KIN112/SIK2-III for the dynamic simulation time for 330 ns (yellow) and 350 ns (gray).

For clarity, the water molecules have been removed. The KIN112 is plotted using stick style, while cartoon style for SIK2.

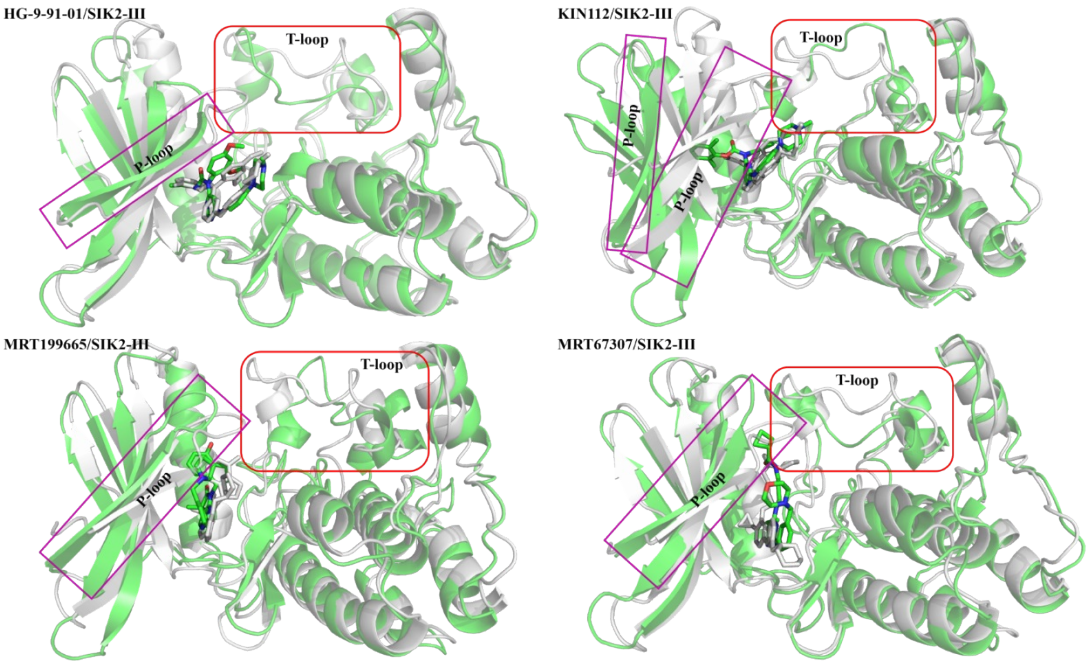

Figure S23. The frames of inhibitor/SIK2-III complex systems for initial and 500th ns.

Green indicates the initial frame and grey indicates the frame from 500th ns MD simulation.

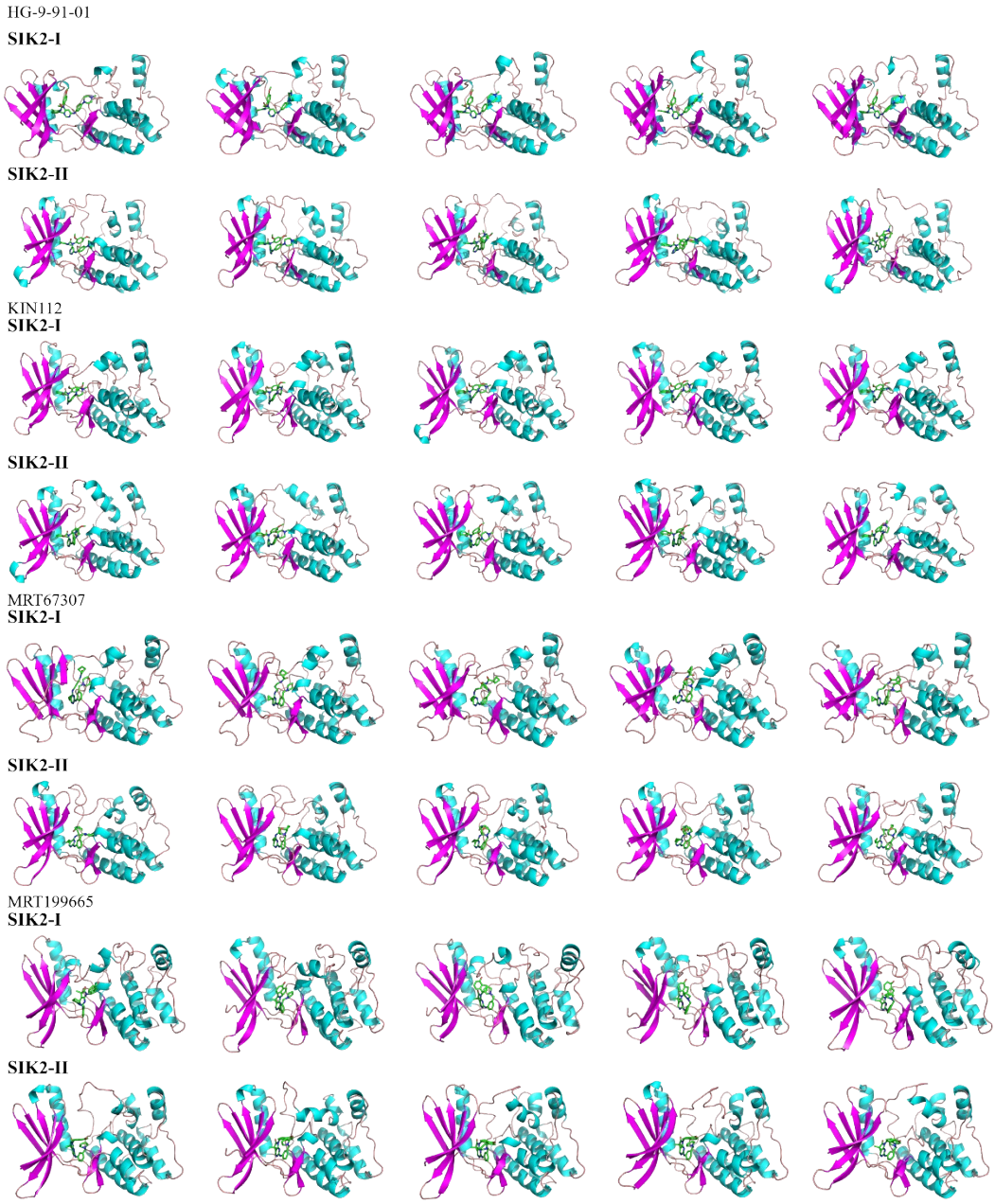

Figure S24. Snapshots of the inhibitor/SIK2 along the dynamic simulation time for 100, 200, 300, 400, and 500 ns.

For clarity, the water molecules have been removed. The inhibitor is plotted using stick style, while cartoon style for SIK2.

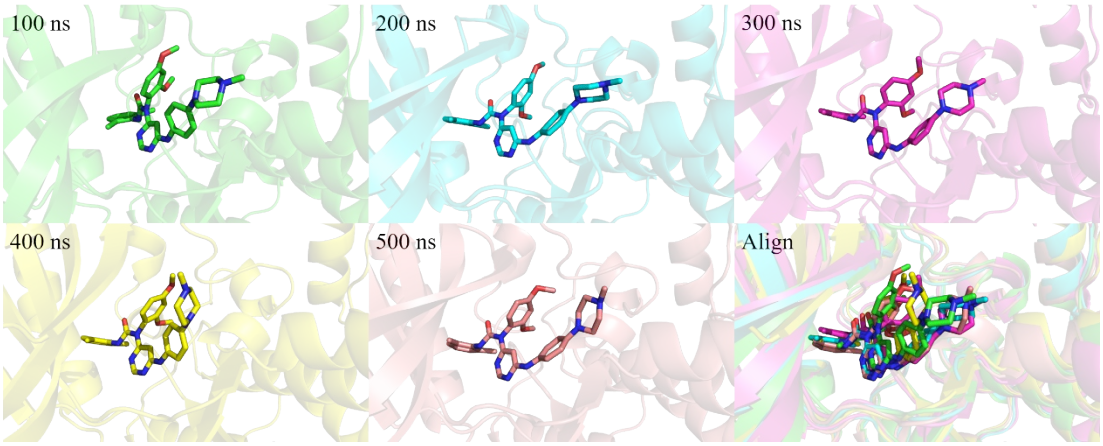

Figure S25. Snapshots of the HG-9-91-01/SIK2-III along the dynamic simulation time for 100, 200, 300, 400, and 500 ns.

For clarity, the water molecules have been removed. The inhibitor is plotted using stick style, while cartoon style for SIK2.

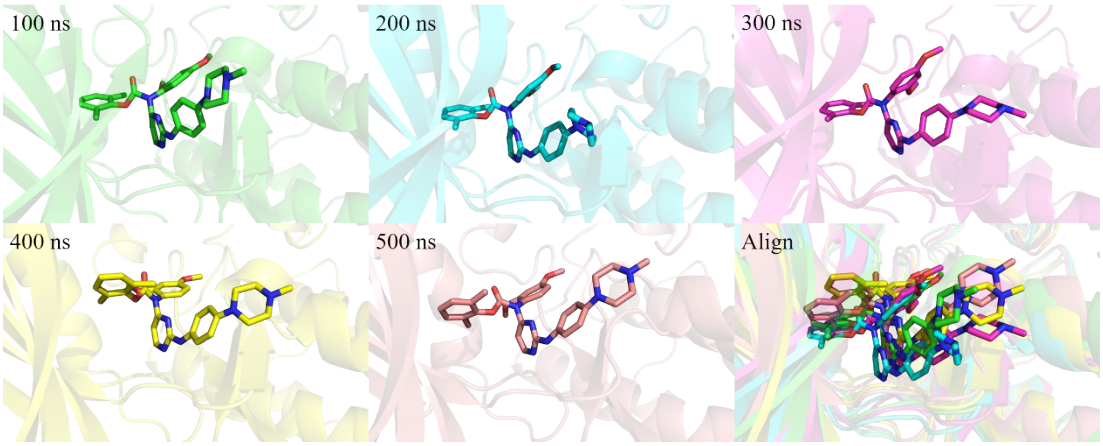

Figure S26. Snapshots of the KIN112/SIK2-III along the dynamic simulation time for 100, 200, 300, 400, and 500 ns.

For clarity, the water molecules have been removed. The inhibitor is plotted using stick style, while cartoon style for SIK2.

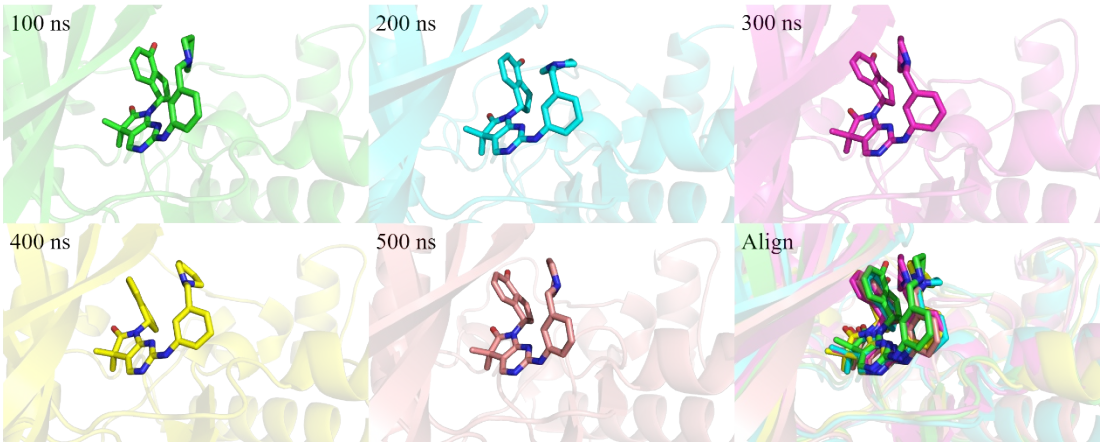

Figure S27. Snapshots of the MRT199665/SIK2-III along the dynamic simulation time for 100, 200, 300, 400, and 500 ns.

For clarity, the water molecules have been removed. The inhibitor is plotted using stick style, while cartoon style for SIK2.

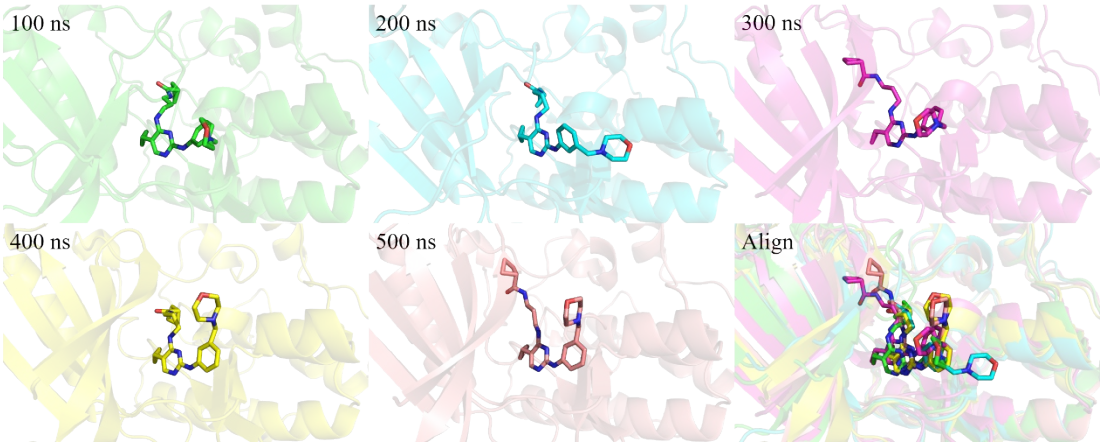

Figure S28. Snapshots of the MRT67307/SIK2-III along the dynamic simulation time for 100, 200, 300, 400, and 500 ns.

For clarity, the water molecules have been removed. The inhibitor is plotted using stick style, while cartoon style for SIK2.

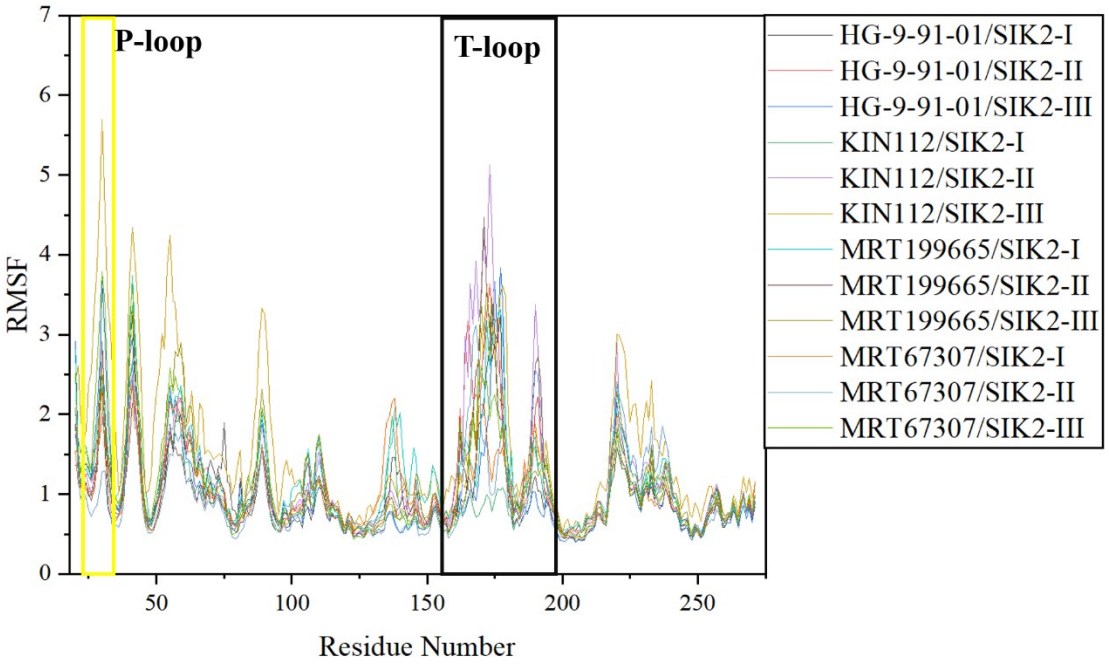

Figure S29. RMSF of the Cα atoms from simulation trajectory of inhibitor/SIK2 systems at 300K with 500 ns MD.

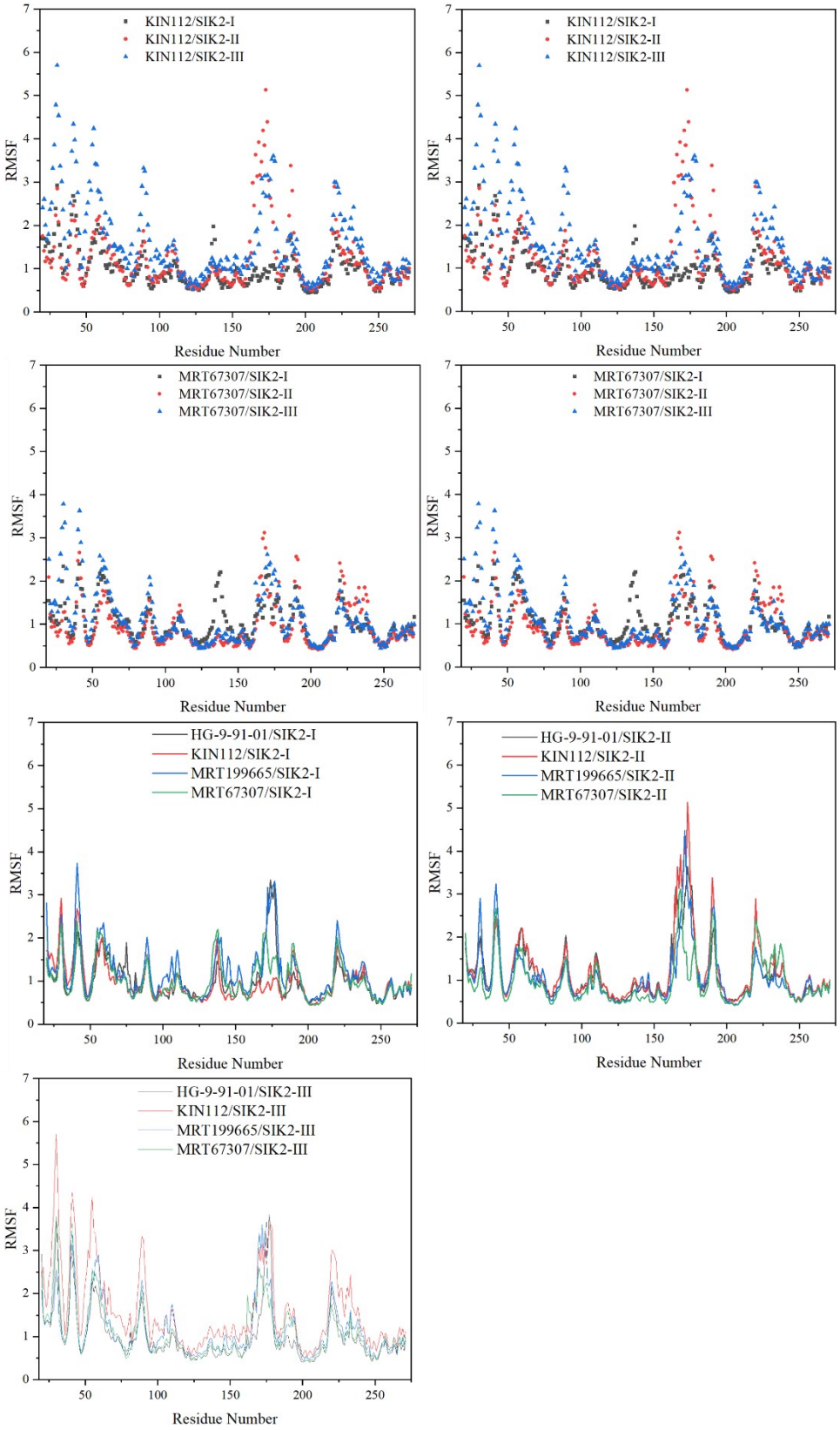

Figure S30. Compare analysis RMSF of the Cα atoms from simulation trajectory of inhibitor/SIK2 systems at 300K with 500 ns MD.

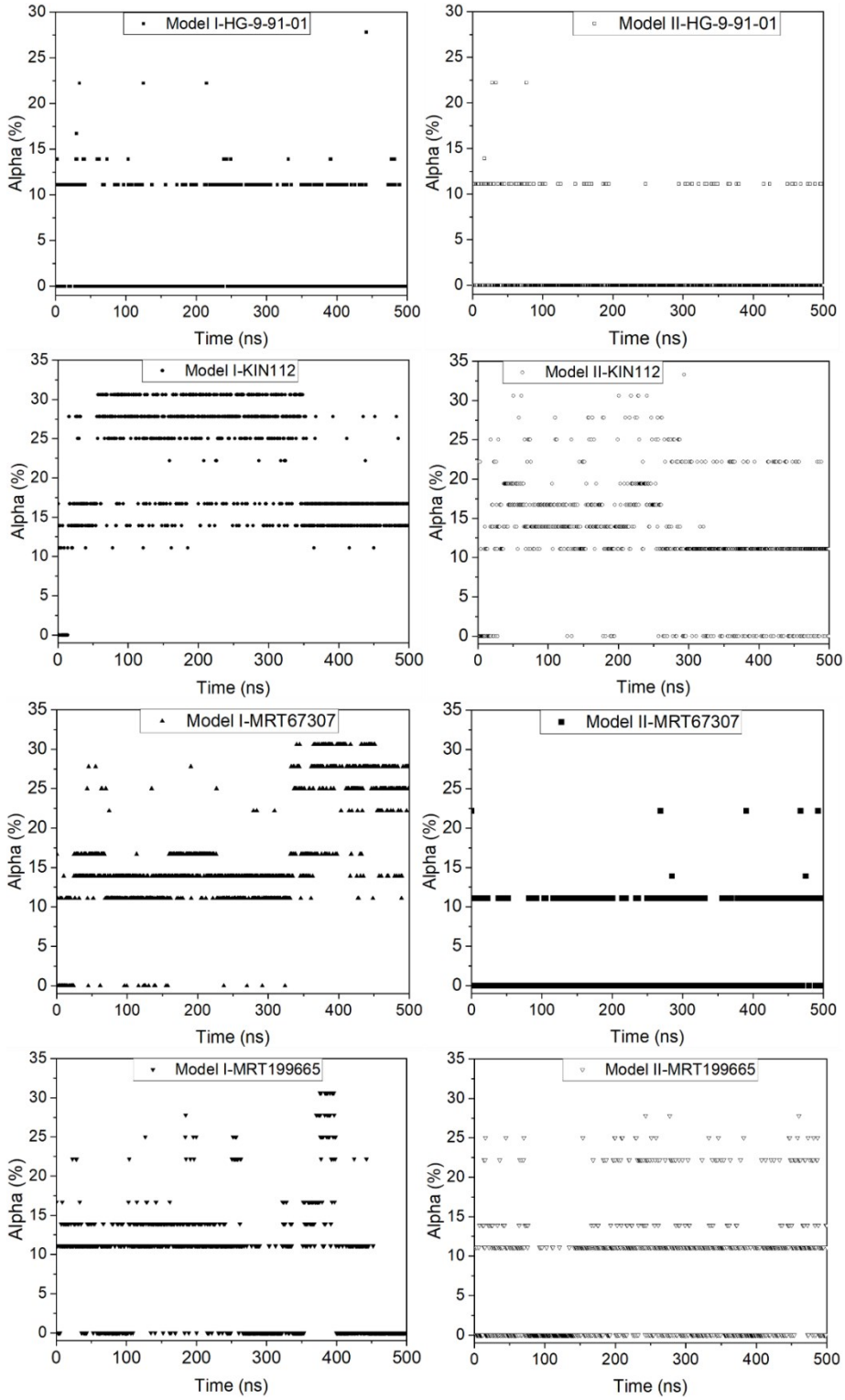

Figure S31. Secondary structure analyzed in the simulation of inhibitor/SIK2-I and inhibitor/SIK2-II complex systems.

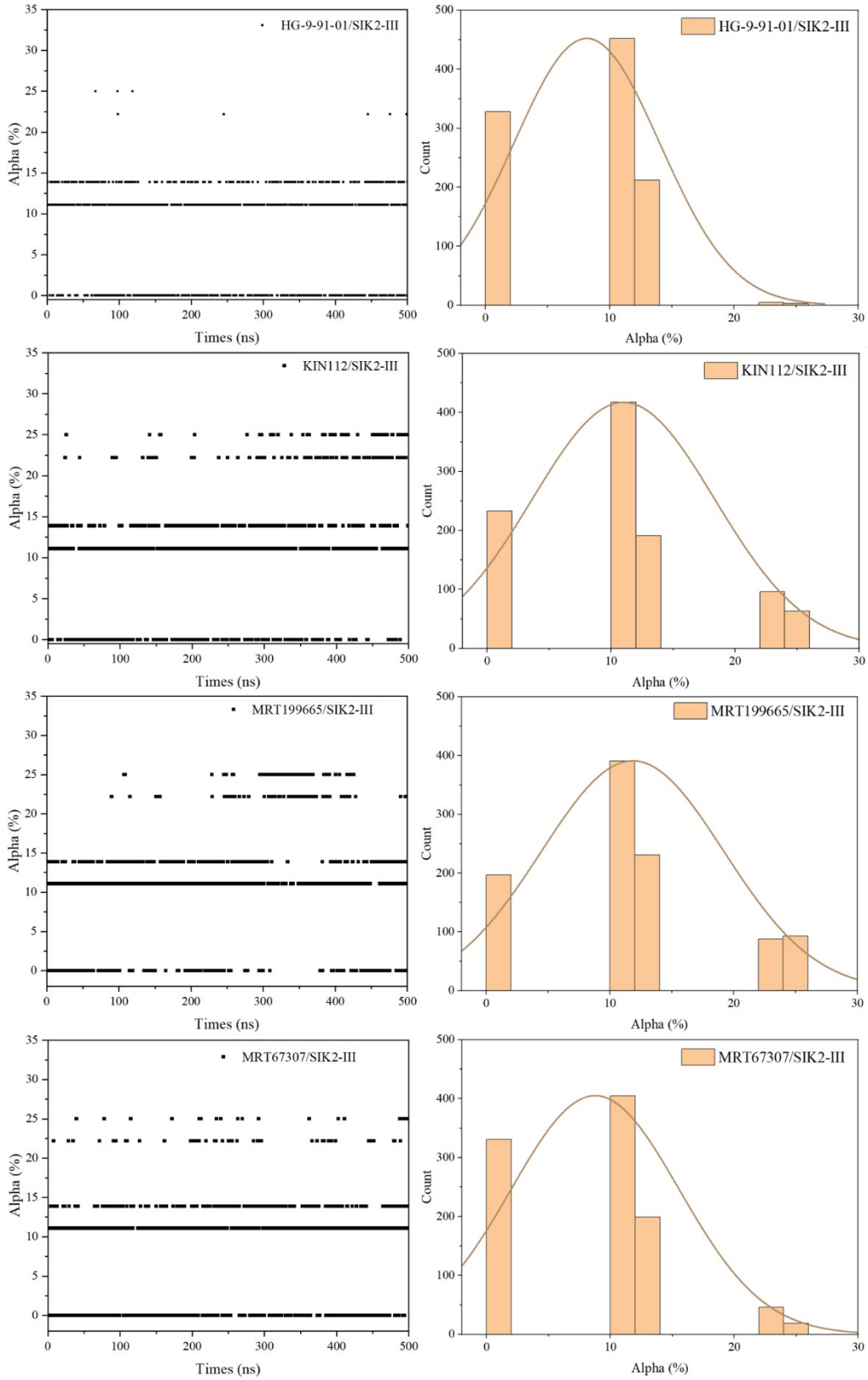

Figure S32. Secondary structure analyzed in the simulation of inhibitor/SIK2-III complex systems.

Total 1000 frames were extracted from the 500 ns MD simulations.

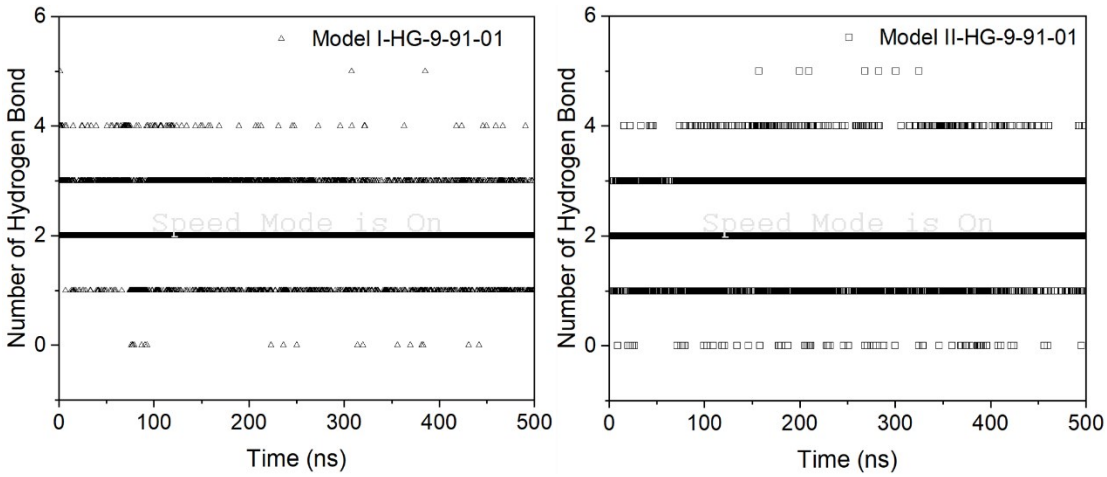

Figure S33. Statistical hydrogen bond number profile along the 500-ns MD simulation for HG-9-91-01/SIK2.

Hydrogen bond is defined as the distance between the acceptor and donor atoms < 3.5 Å, with an internal angle between the H-acceptor and H-donor > 120º.

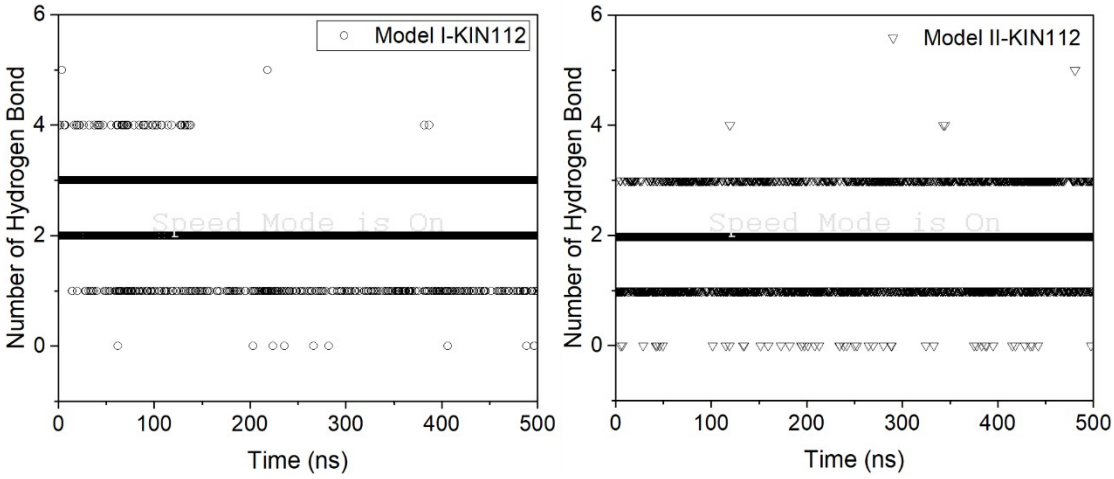

Figure S34. Statistical hydrogen bond number profile along the 500-ns MD simulation for KIN112/SIK2.

Hydrogen bond is defined as the distance between the acceptor and donor atoms < 3.5 Å, with an internal angle between the H-acceptor and H-donor > 120º.

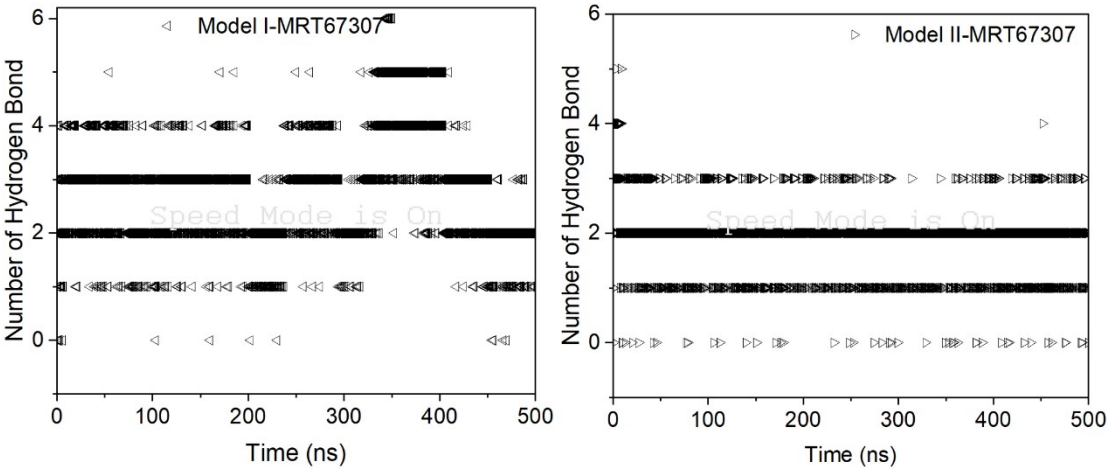

Figure S35. Statistical hydrogen bond number profile along the 500-ns MD simulation for MRT67307/SIK2.

Hydrogen bond is defined as the distance between the acceptor and donor atoms < 3.5 Å, with an internal angle between the H-acceptor and H-donor > 120º.

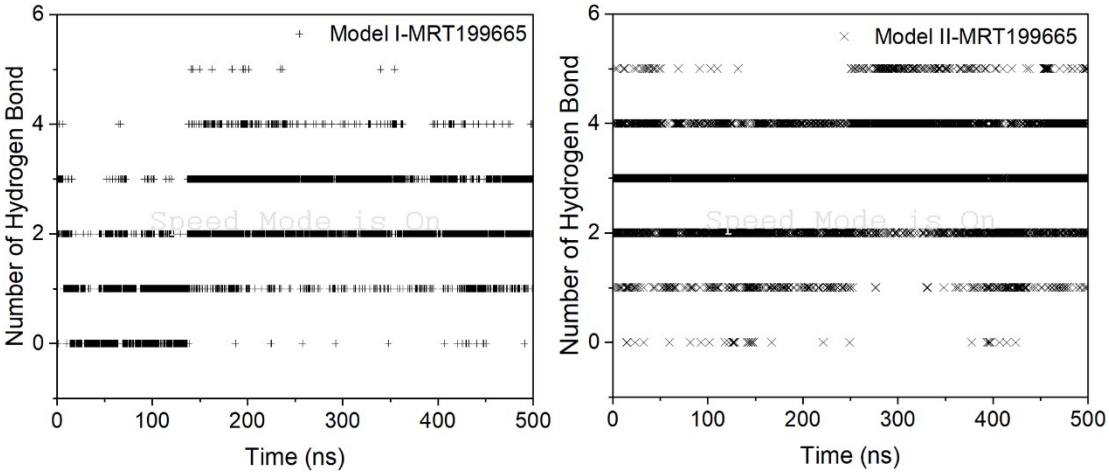

Figure S36. Statistical hydrogen bond number profile along the 500-ns MD simulation for MRT199665/SIK2.

Hydrogen bond is defined as the distance between the acceptor and donor atoms < 3.5 Å, with an internal angle between the H-acceptor and H-donor > 120º.

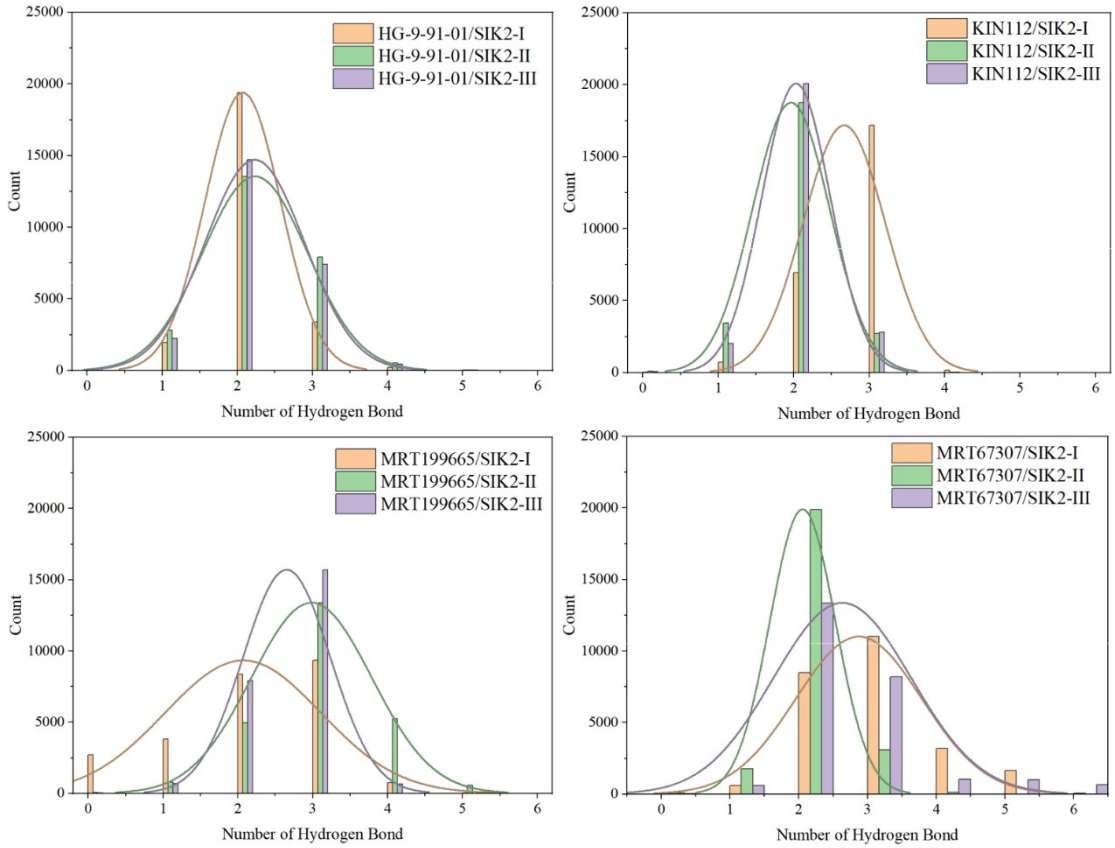

Figure S37. Distribution of number of hydrogen bond for the HG-9-91-01, KIN112, MRT199665 and MRT67307 with SIK2-I and SIK2-II.

Hydrogen bond is defined as the distance between the acceptor and donor atoms < 3.5 Å, with an internal angle between the H-acceptor and H-donor > 120º.

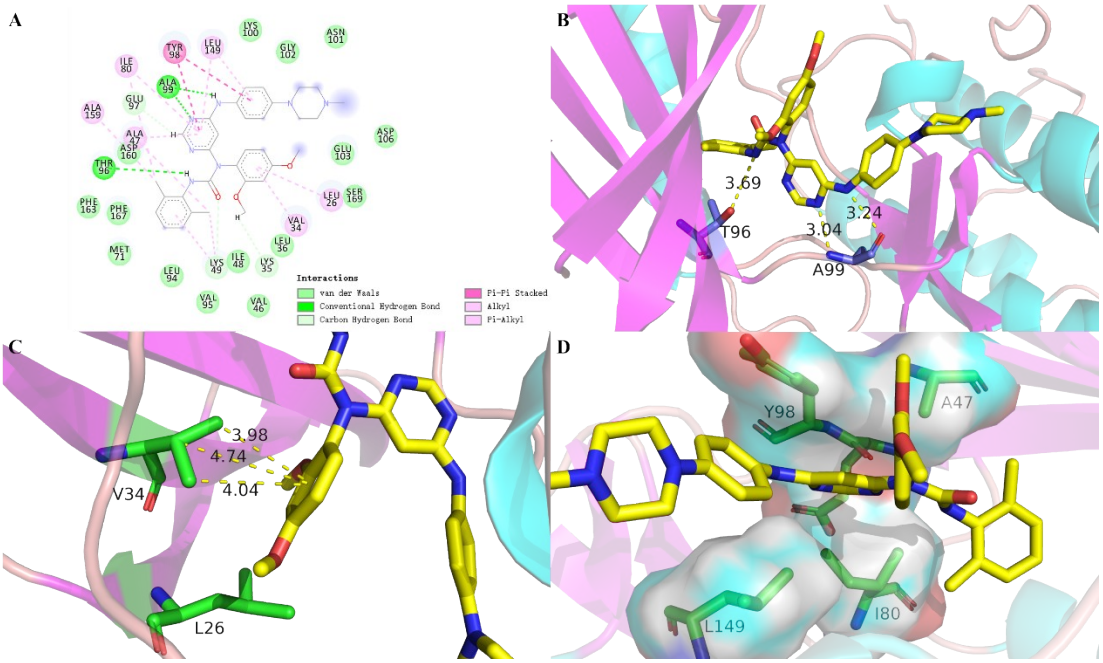

Figure S38. Interaction between HG-9-91-01 and SIK2-I complex system for the representative conformation of the largest cluster from the cluster analysis.

(A) 2D interaction, (B) hydrogen bond for hinge loop, (C) hydrophobic interaction and (D) interaction for pyrimidine-amino.

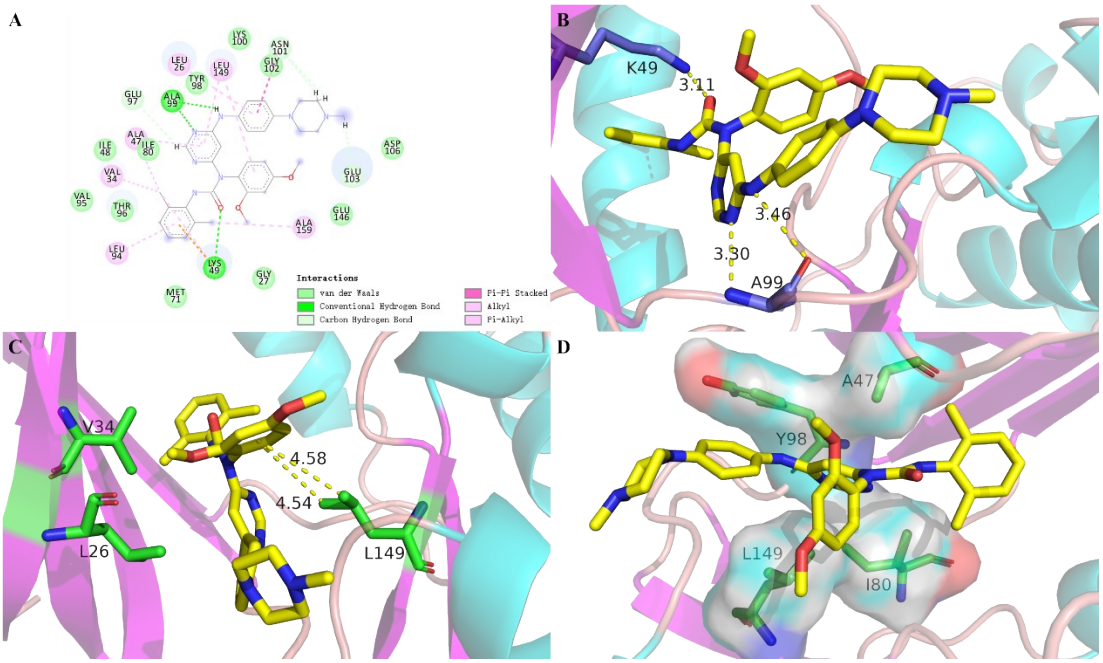

Figure S39. Interaction between HG-9-91-01 and SIK2-II complex system for the representative conformation of the largest cluster from the cluster analysis.

(A) 2D interaction, (B) hydrogen bond for hinge loop, (C) hydrophobic interaction and (D) interaction for pyrimidine-amino.

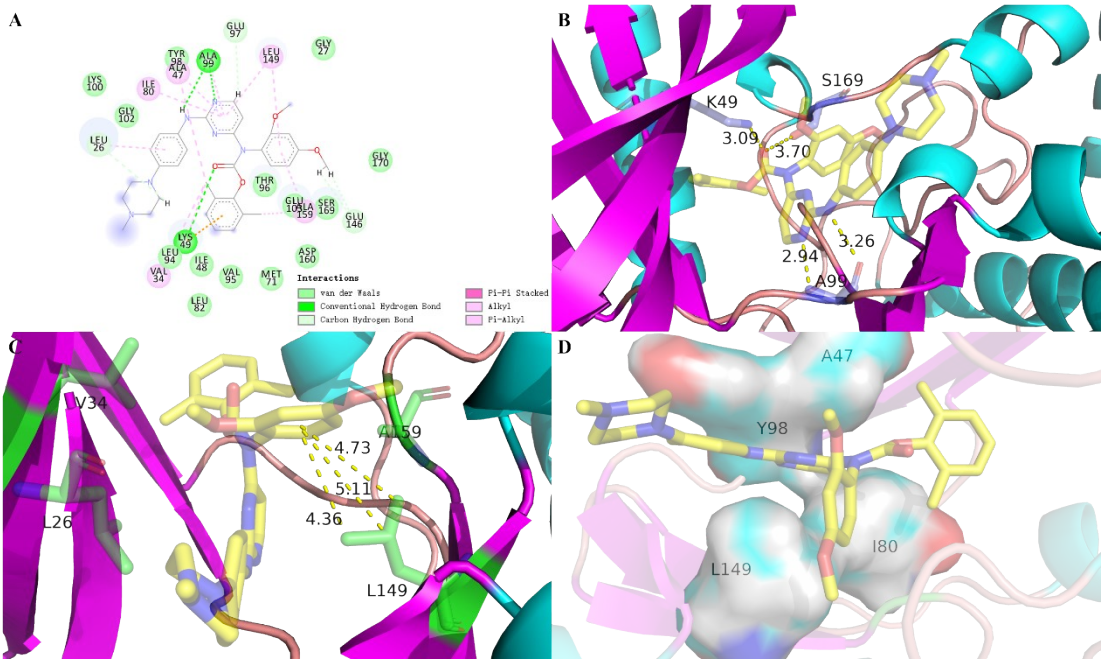

Figure S40. Interaction between KIN112 and SIK2-I complex system for the representative conformation of the largest cluster from the cluster analysis.

(A) 2D interaction, (B) hydrogen bond for hinge loop, (C) hydrophobic interaction and (D) interaction for pyrimidine-amino.

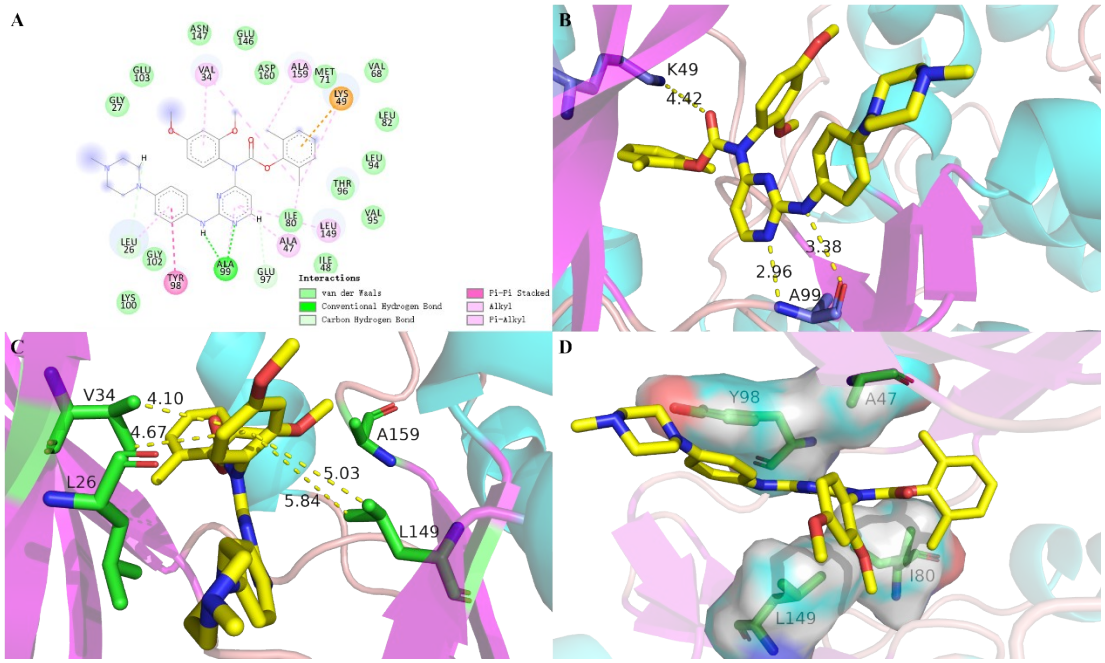

Figure S41. Interaction between KIN112 and SIK2-II complex system for the representative conformation of the largest cluster from the cluster analysis.

(A) 2D interaction, (B) hydrogen bond for hinge loop, (C) hydrophobic interaction and (D) interaction for pyrimidine-amino.

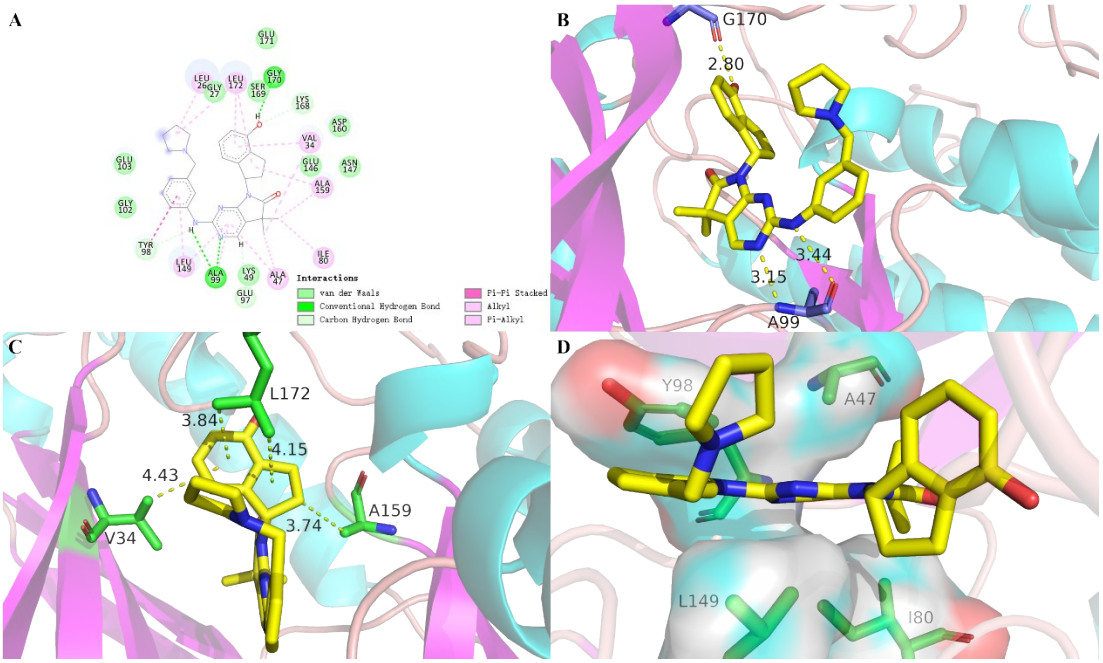

Figure S42. Interaction between MRT199665 and SIK2-I complex system for the representative conformation of the largest cluster from the cluster analysis.

(A) 2D interaction, (B) hydrogen bond for hinge loop, (C) hydrophobic interaction and (D) interaction for pyrimidine-amino.

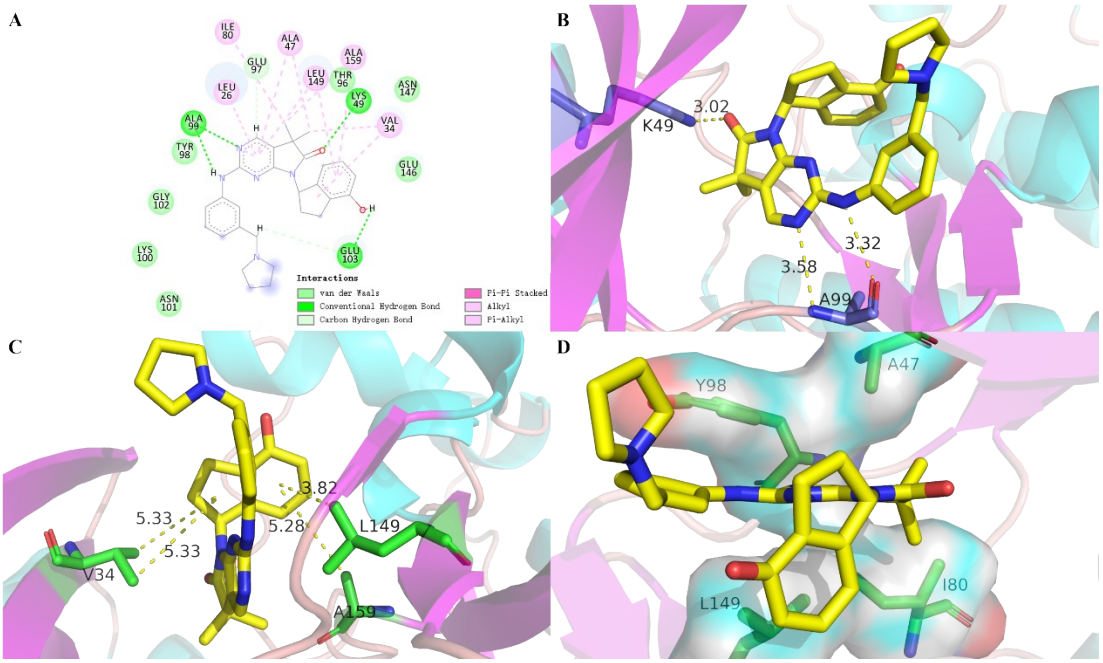

Figure S43. Interaction between MRT199665 and SIK2-II complex system for the representative conformation of the largest cluster from the cluster analysis.

(A) 2D interaction, (B) hydrogen bond for hinge loop, (C) hydrophobic interaction and (D) interaction for pyrimidine-amino.

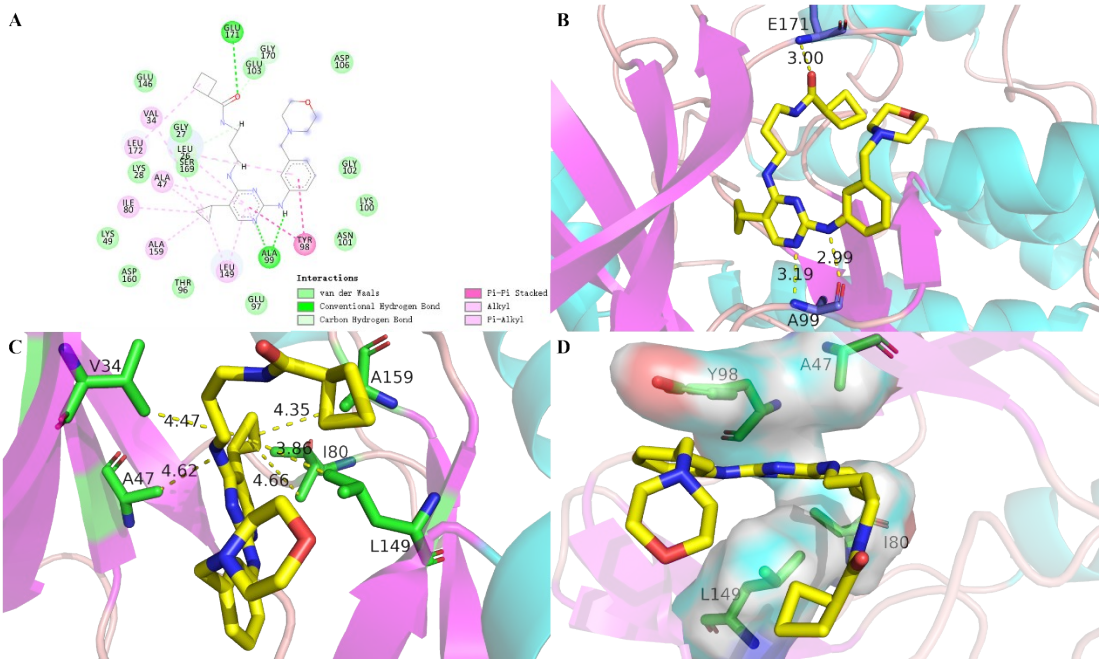

Figure S44. Interaction between MRT67307 and SIK2-I complex system for the representative conformation of the largest cluster from the cluster analysis.

(A) 2D interaction, (B) hydrogen bond for hinge loop, (C) hydrophobic interaction and (D) interaction for pyrimidine-amino.

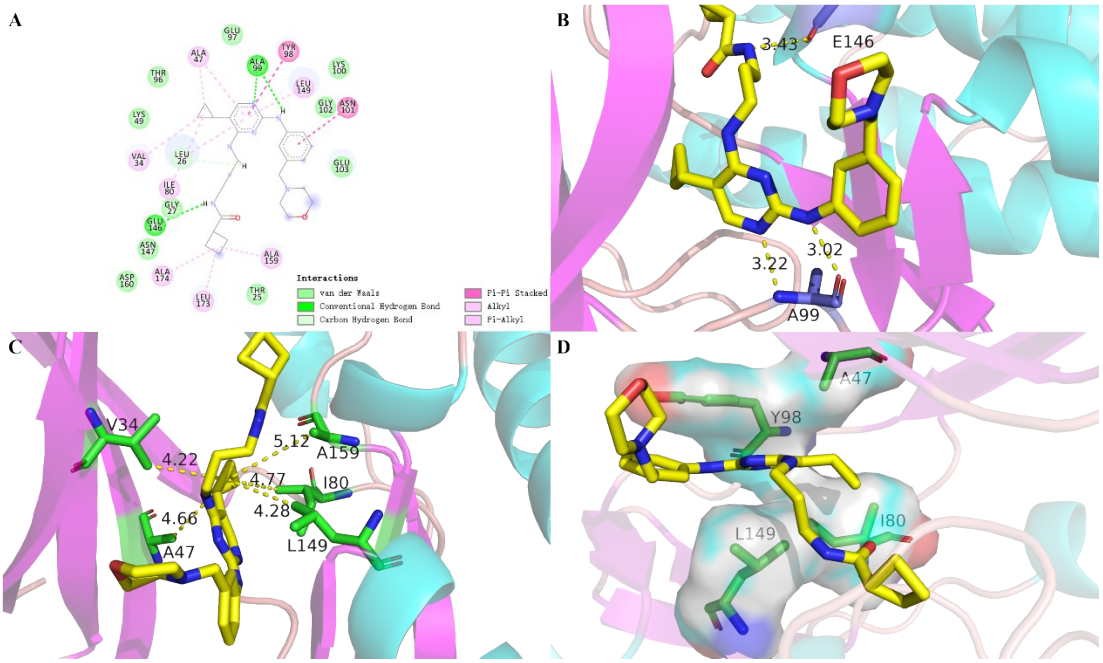

Figure S45. Interaction between MRT67307 and SIK2-I complex system for the representative conformation of the largest cluster from the cluster analysis.

(A) 2D interaction, (B) hydrogen bond for hinge loop, (C) hydrophobic interaction and (D) interaction for pyrimidine-amino.

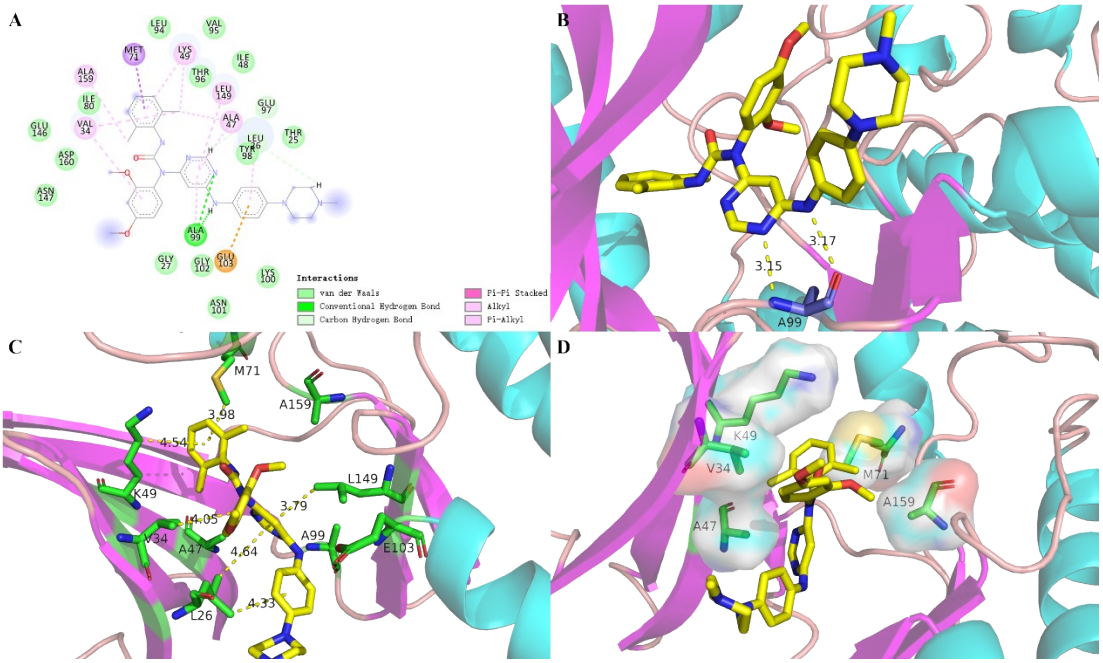

Figure S46. Interaction between HG-9-91-01 and SIK2-III complex system for the representative conformation of the largest cluster from the cluster analysis.

(A) 2D interaction, (B) hydrogen bond for hinge loop, (C) hydrophobic interaction and (D) interaction for pyrimidine-amino.

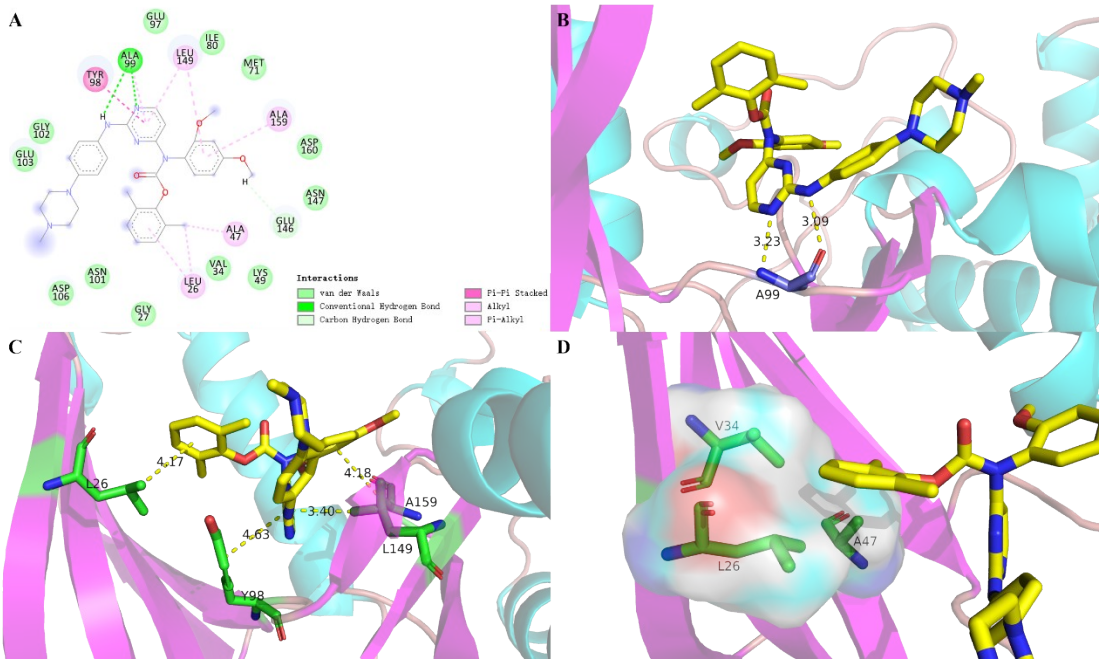

Figure S47. Interaction between KIN112 and SIK2-III complex system for the representative conformation of the largest cluster from the cluster analysis.

(A) 2D interaction, (B) hydrogen bond for hinge loop, (C) hydrophobic interaction and (D) interaction for pyrimidine-amino.

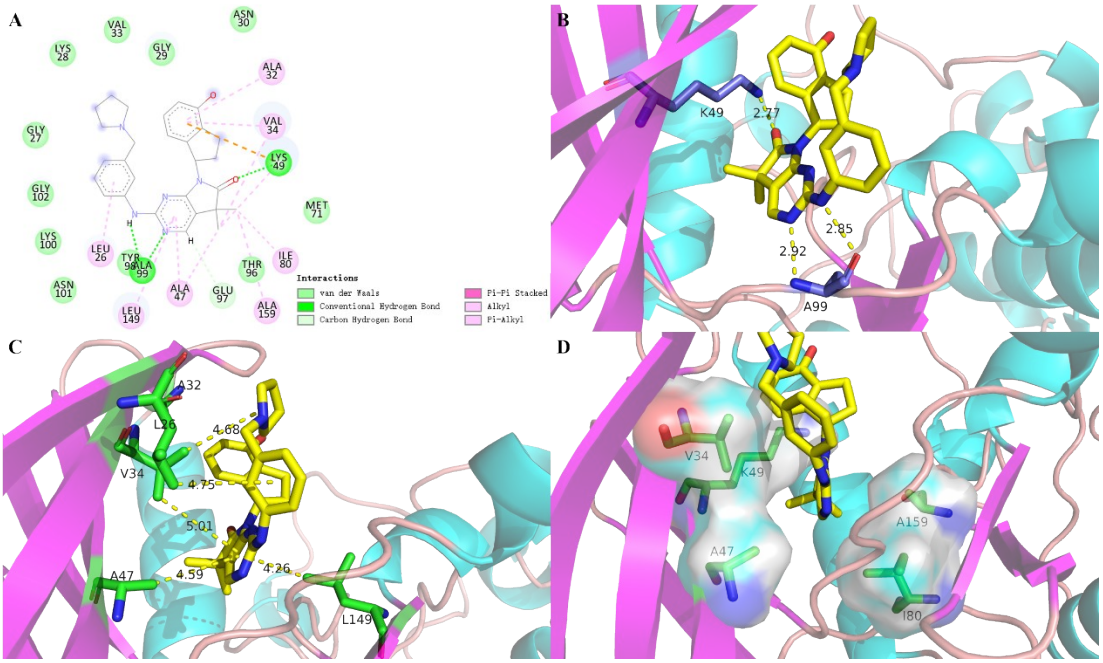

Figure S48. Interaction between MRT199665 and SIK2-III complex system for the representative conformation of the largest cluster from the cluster analysis.

(A) 2D interaction, (B) hydrogen bond for hinge loop, (C) hydrophobic interaction and (D) interaction for pyrimidine-amino.

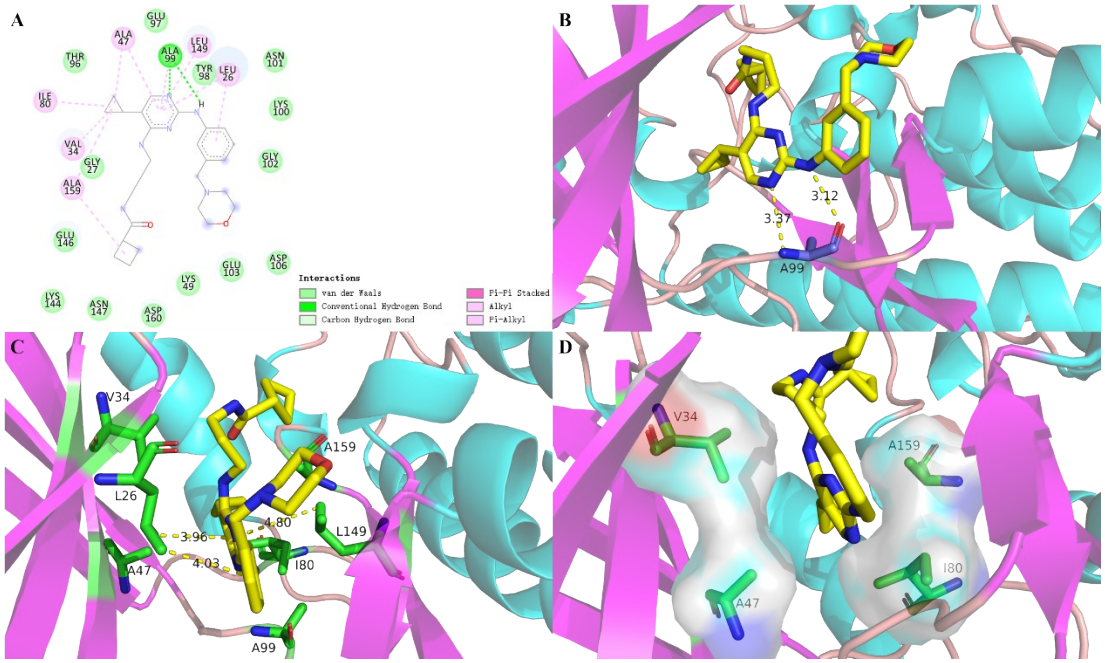

Figure S49. Interaction between MRT67307 and SIK2-III complex system for the representative conformation of the largest cluster from the cluster analysis.

(A) 2D interaction, (B) hydrogen bond for hinge loop, (C) hydrophobic interaction and (D) interaction for pyrimidine-amino.

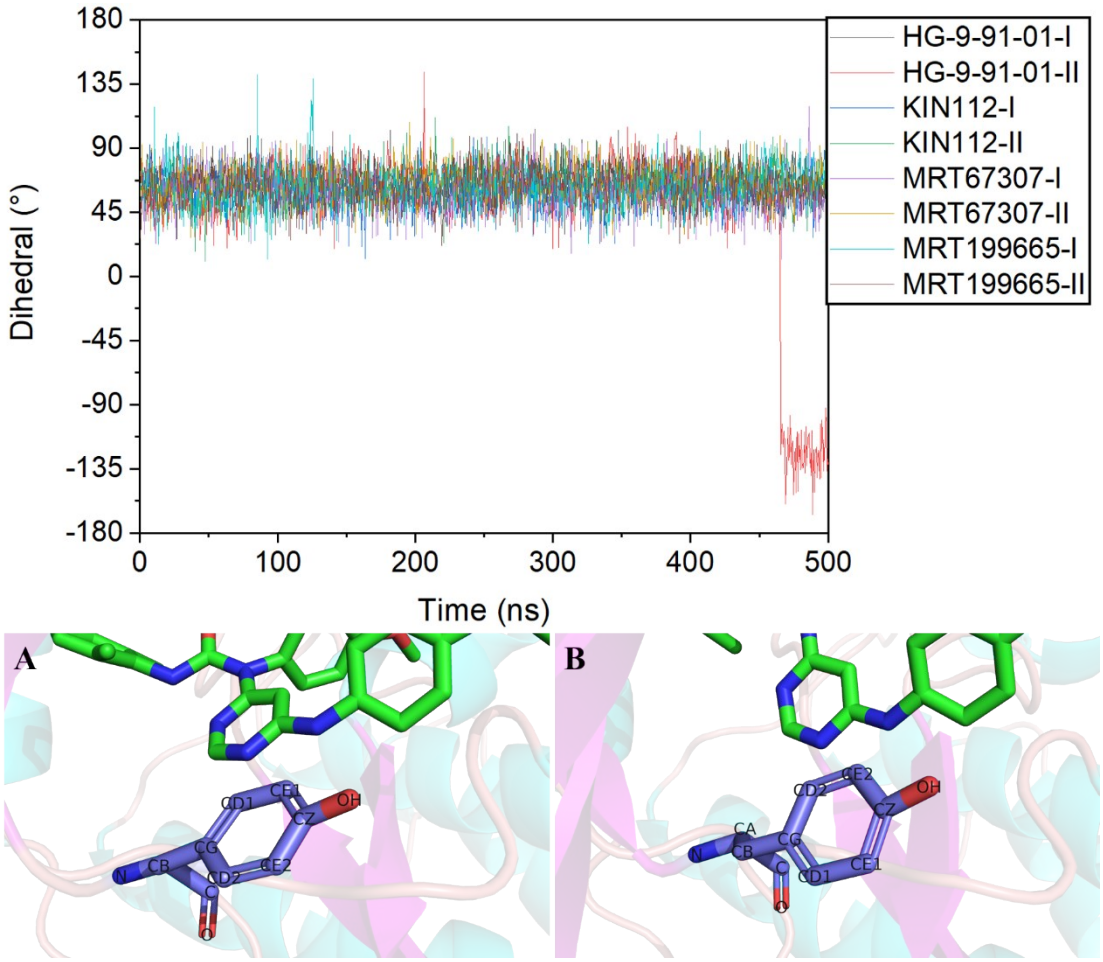

Figure S50. The dihedral angle of CD1, CG, CB and CA atom of the Y98.

The upper for dihedral with the MD time, (A) for the main orientation and (B) for the other orientation of Y98.

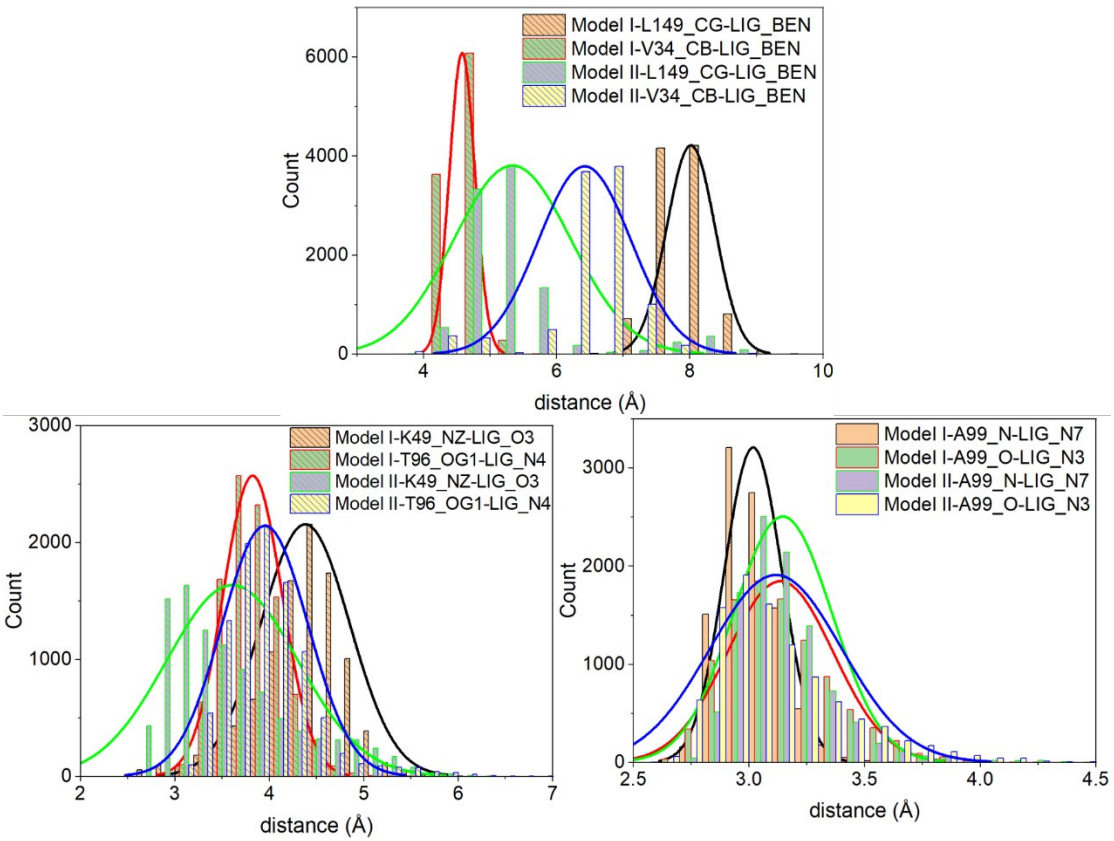

Figure S51. The distance between HG-9-91-01 and residues of SIK2 although the 500 ns MD simulation.

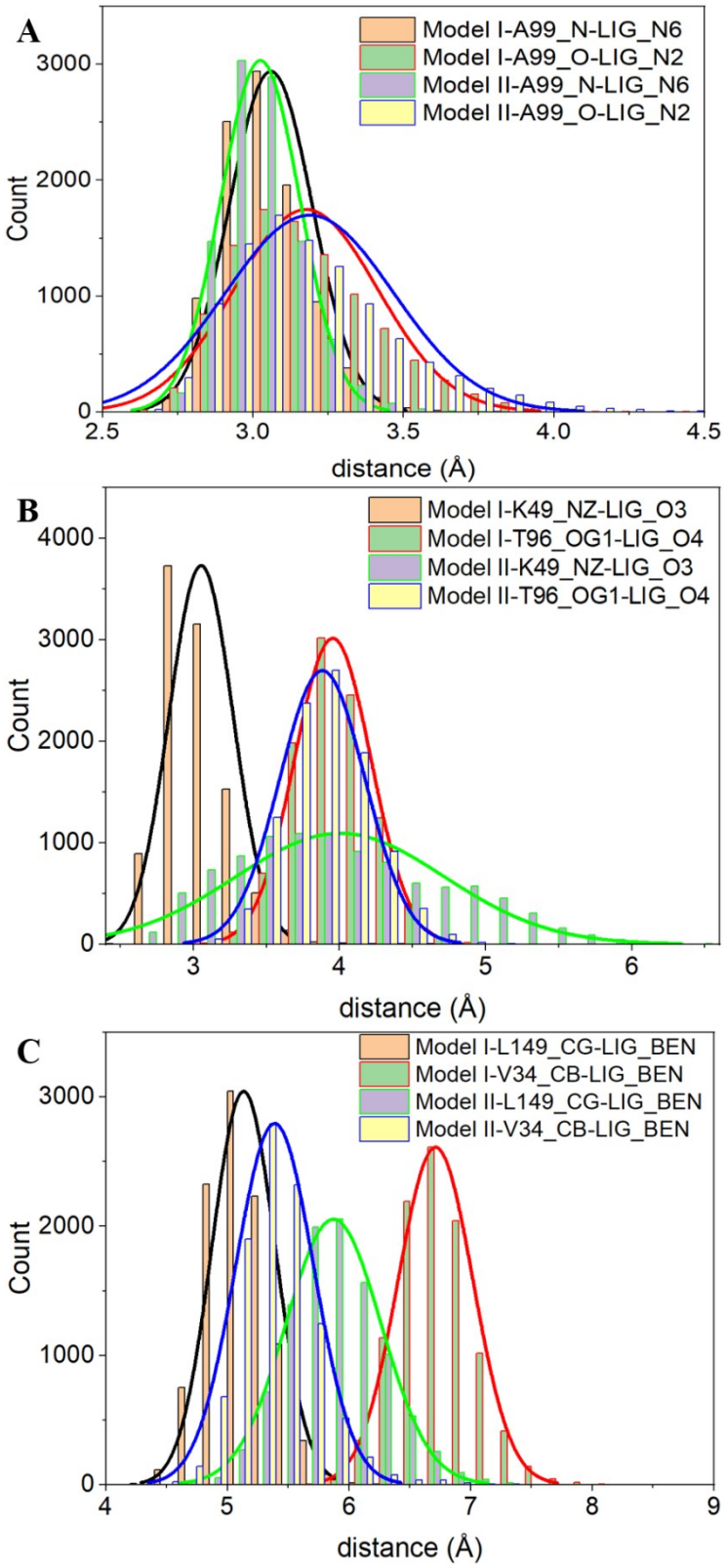

Figure S52. The distance between KIN112 and residues of SIK2 although the 500 ns MD simulation.

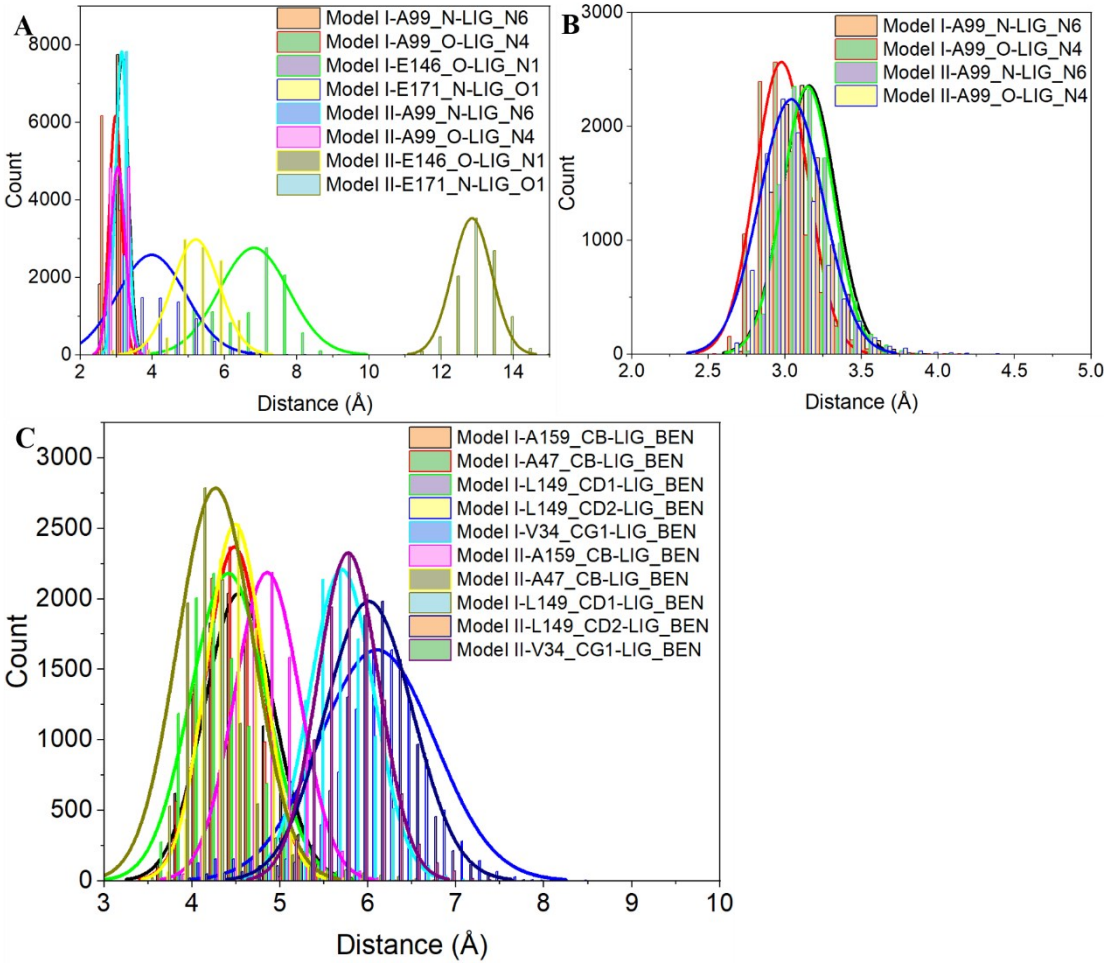

Figure S53. The distance between MRT67307 and residues of SIK2 although the 500 ns MD simulation.

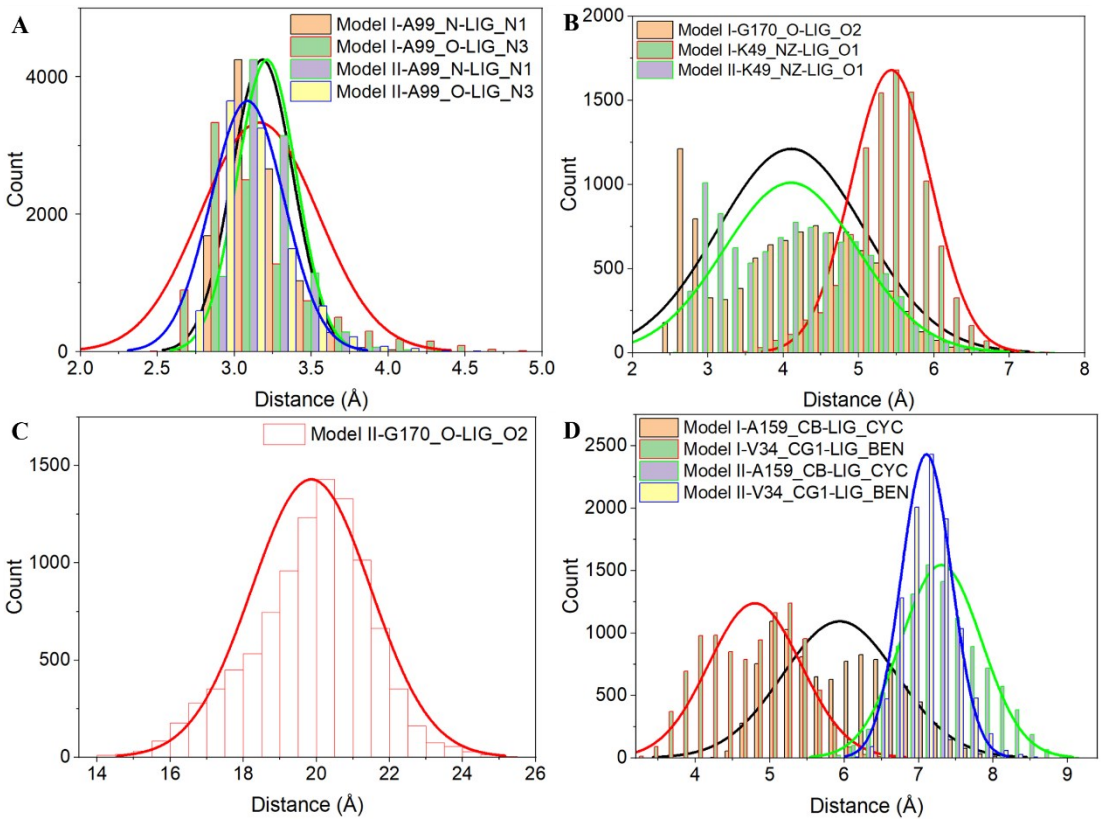

Figure S54. The distance between MRT199665 and residues of SIK2 although the 500 ns MD simulation.

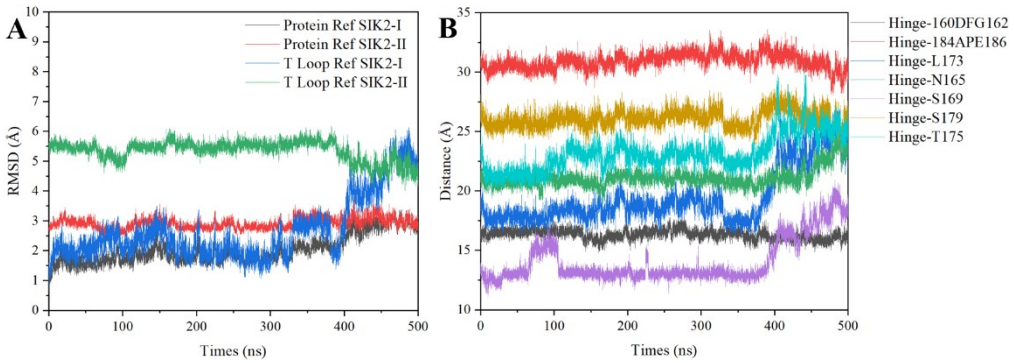

Figure S55. Transition of T-loop for dasatinib/SIK2-I.

(A) for the RMSD and (B) for the distance.

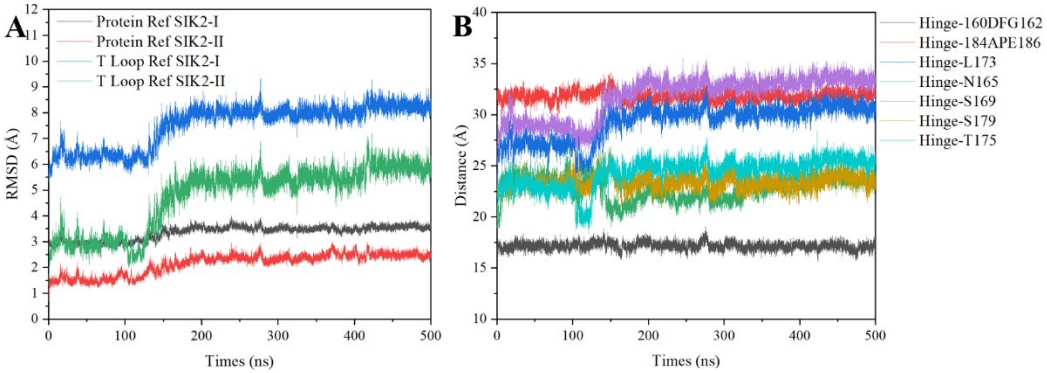

Figure S56. Transition of T-loop for dasatinib/SIK2-II.

(A) for the RMSD and (B) for the distance.

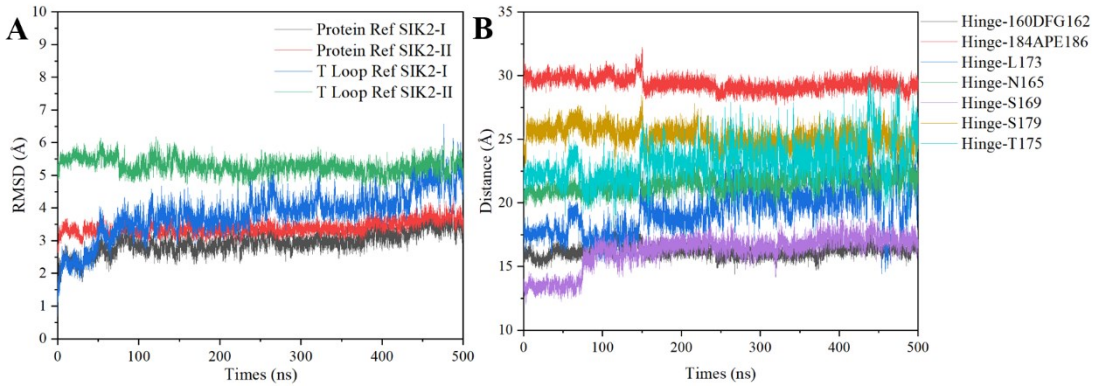

Figure S57. Transition of T-loop for HG-9-91-01/SIK2-I.

(A) for the RMSD and (B) for the distance.

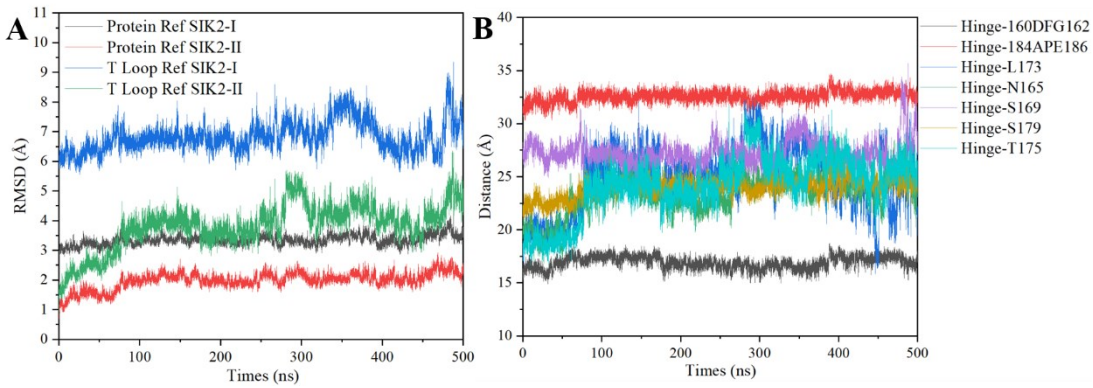

Figure S58. Transition of T-loop for HG-9-91-01/SIK2-II.

(A) for the RMSD and (B) for the distance.

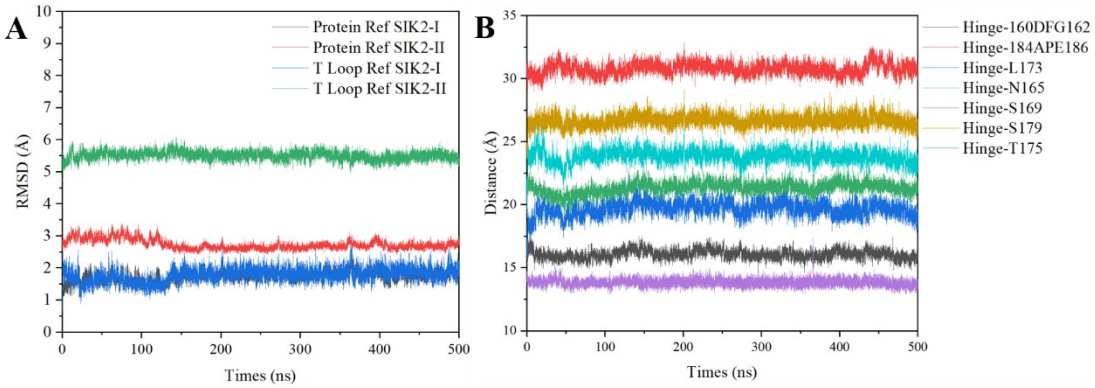

Figure S59. Transition of T-loop for KIN112/SIK2-I.

(A) for the RMSD and (B) for the distance.

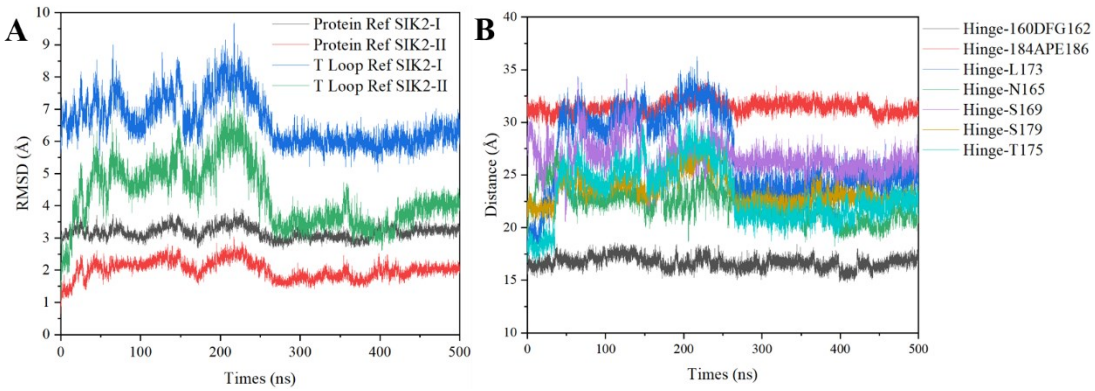

Figure S60. Transition of T-loop for KIN112/SIK2-II.

(A) for the RMSD and (B) for the distance.

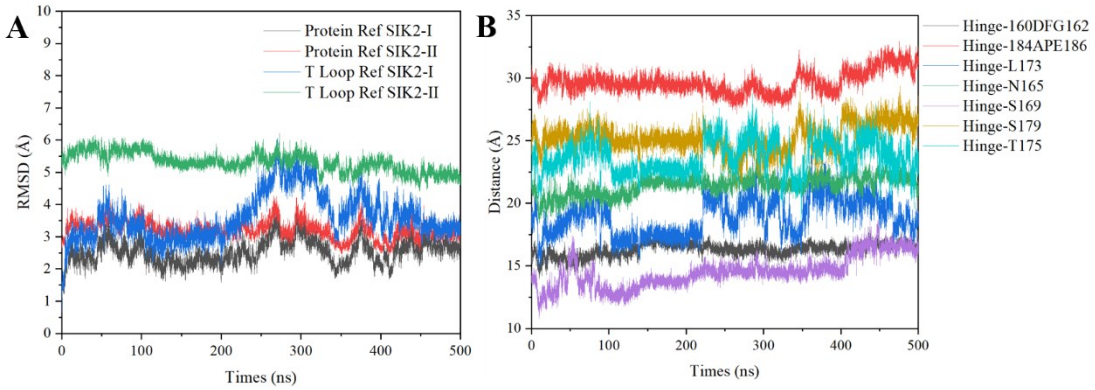

Figure S61. Transition of T-loop for MRT199665/SIK2-I.

(A) for the RMSD and (B) for the distance.

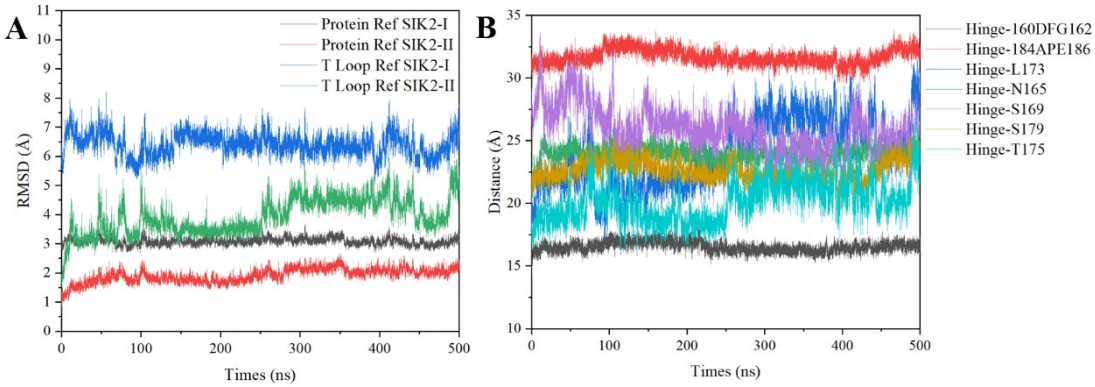

Figure S62. Transition of T-loop for MRT199665/SIK2-II.

(A) for the RMSD and (B) for the distance.

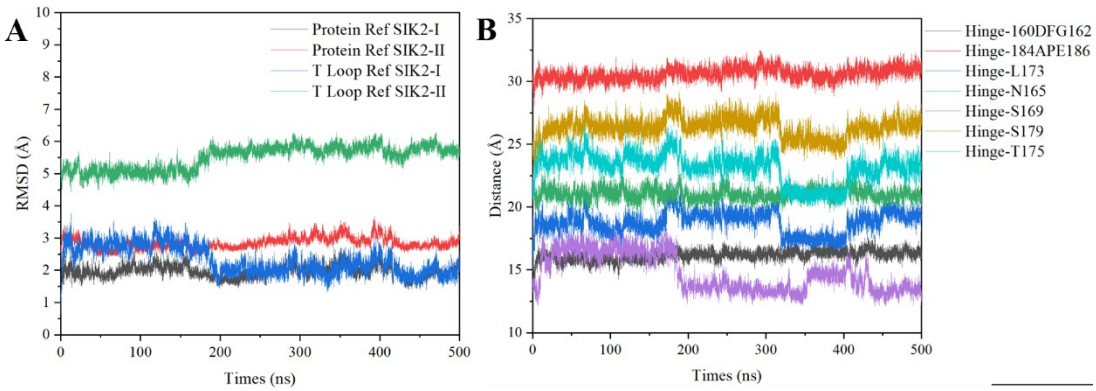

Figure S63. Transition of T-loop for MRT67307/SIK2-I.

(A) for the RMSD and (B) for the distance.

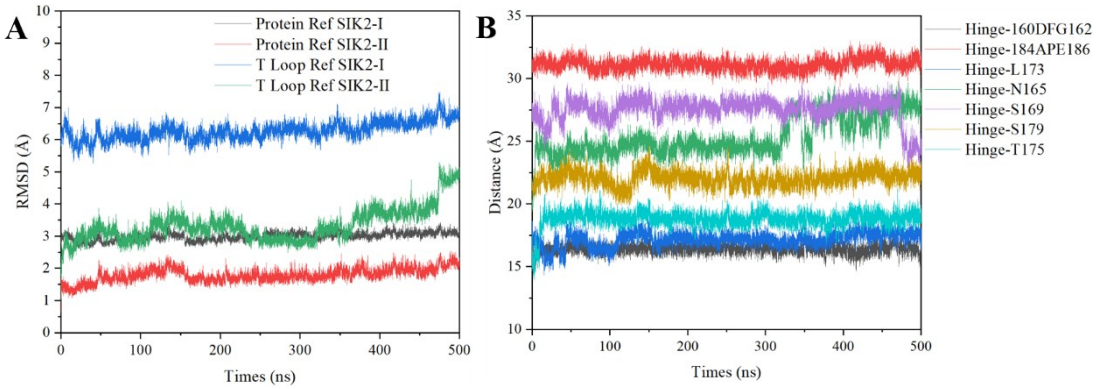

Figure S64. Transition of T-loop for MRT67307/SIK2-II.

(A) for the RMSD and (B) for the distance.

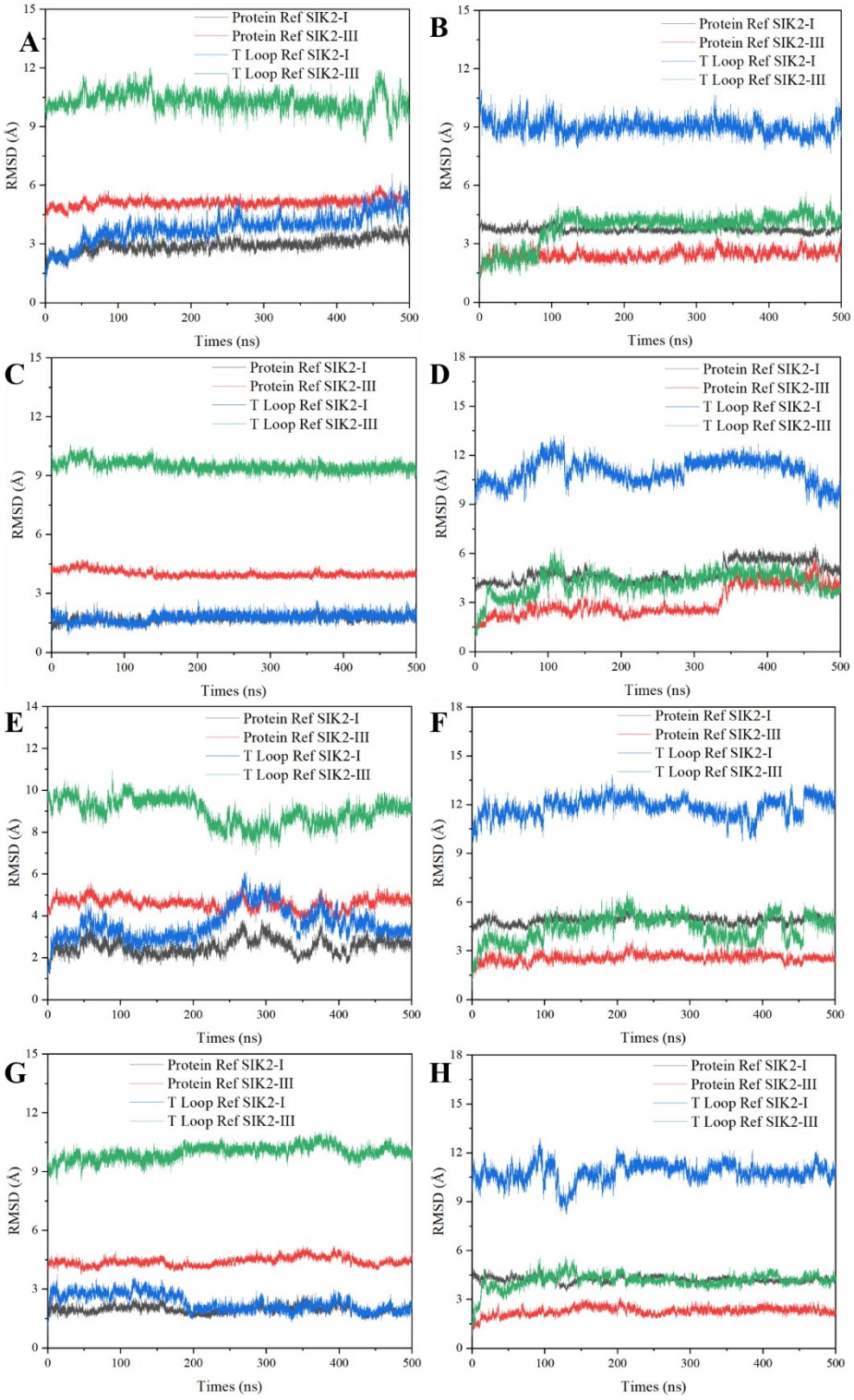

Figure S65. The RMSD vs Times among the MD simulation for SIK2-I and SIK2-III bound with HG-9-91-01, KIN112, MRT199665, and MRT67307.

SIK2-I (left) and SIK2-III (right) bound with HG-9-91-01 (A and B), KIN112 (C and D), MRT199665 (E and F), and MRT67307 (G and H).

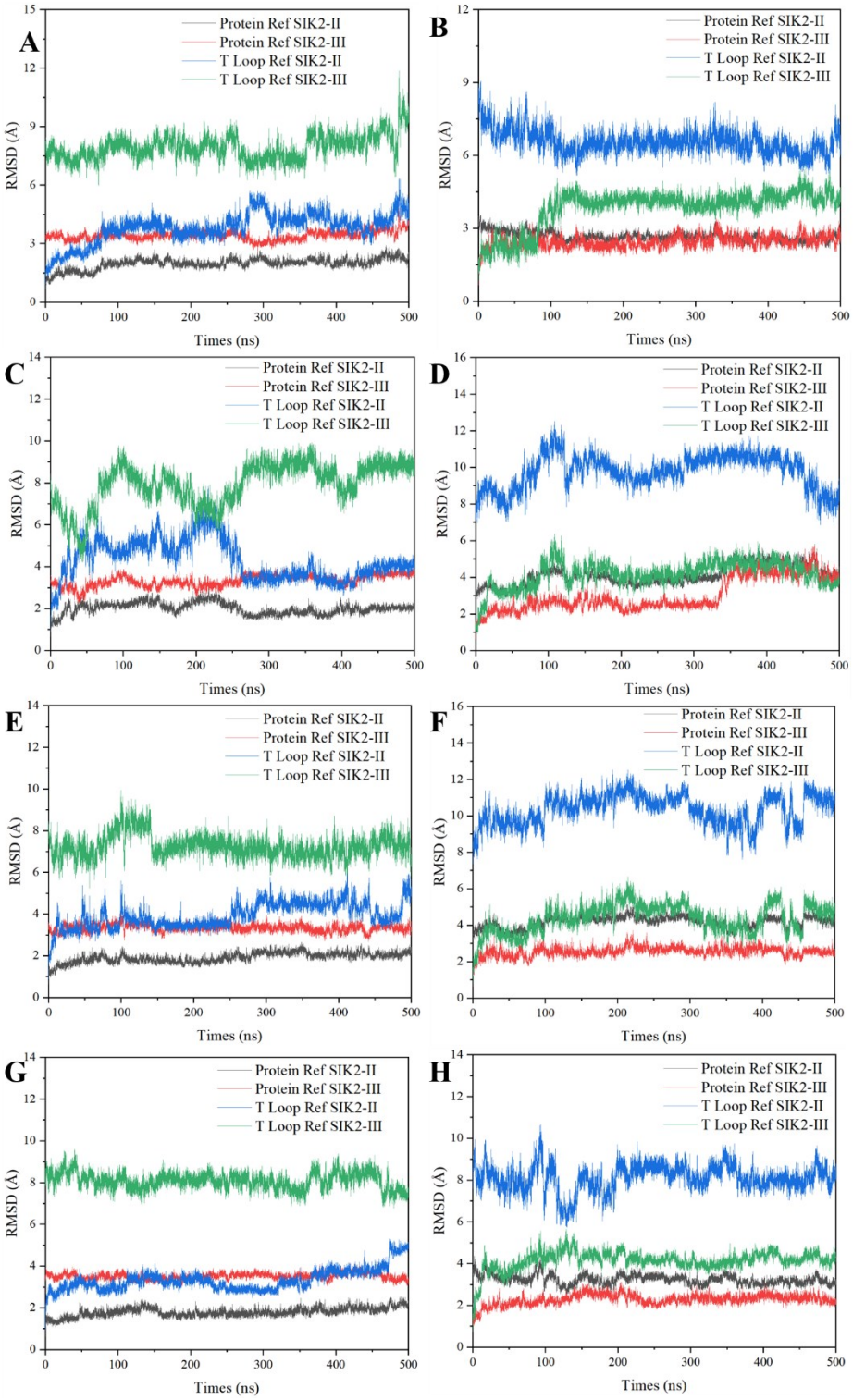

Figure S66. The RMSD vs Times among the MD simulation for SIK2-II and SIK2-III bound with HG-9-91-01, KIN112, MRT199665, and MRT67307.

SIK2-II (left) and SIK2-III (right) bound with HG-9-91-01 (A and B), KIN112 (C and D), MRT199665 (E and F), and MRT67307 (G and H).

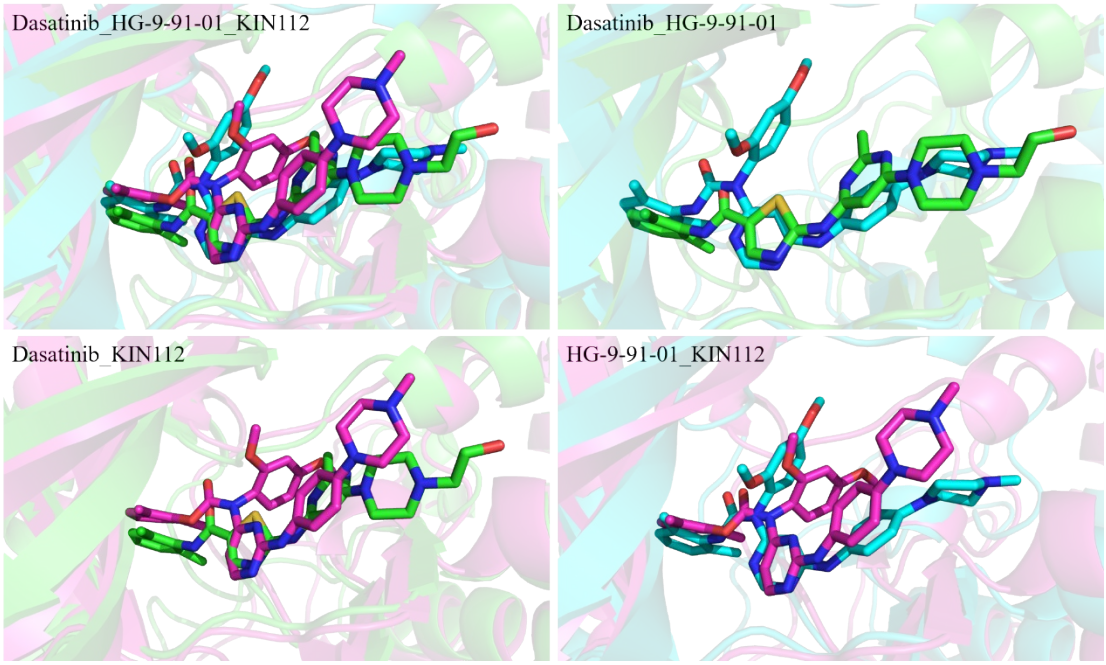

Figure S67. The align conformation of dasatinib/SIK2-I, HG-9-91-01/SIK2-I, and KIN112/SIK2-I.

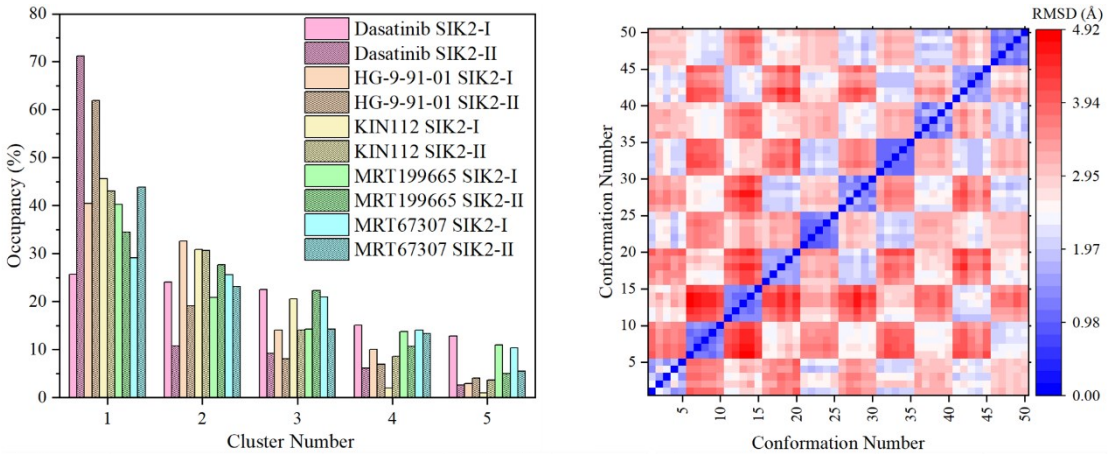

Conformation Number	Label	Conformation Number	Label	Conformation Number	Label	Conformation Number	Label	Conformation Number	Label
1	Dasatinib-I-1	11	HG-9-91-01-I-1	21	KIN112-I-1	31	MRT67307-I-1	41	MRT199665-I-1
2	Dasatinib-I-2	12	HG-9-91-01-I-2	22	KIN112-I-2	32	MRT67307-I-2	42	MRT199665-I-2
3	Dasatinib-I-3	13	HG-9-91-01-I-3	23	KIN112-I-3	33	MRT67307-I-3	43	MRT199665-I-3
4	Dasatinib-I-4	14	HG-9-91-01-I-4	24	KIN112-I-4	34	MRT67307-I-4	44	MRT199665-I-4
5	Dasatinib-I-5	15	HG-9-91-01-I-5	25	KIN112-I-5	35	MRT67307-I-5	45	MRT199665-I-5
6	Dasatinib-II-1	16	HG-9-91-01-II-1	26	KIN112-II-1	36	MRT67307-II-1	46	MRT199665-II-1
7	Dasatinib-II-2	17	HG-9-91-01-II-2	27	KIN112-II-2	37	MRT67307-II-2	47	MRT199665-II-2
8	Dasatinib-II-3	18	HG-9-91-01-II-3	28	KIN112-II-3	38	MRT67307-II-3	48	MRT199665-II-3
9	Dasatinib-II-4	19	HG-9-91-01-II-4	29	KIN112-II-4	39	MRT67307-II-4	49	MRT199665-II-4
10	Dasatinib-II-5	20	HG-9-91-01-II-5	30	KIN112-II-5	40	MRT67307-II-5	50	MRT199665-II-5

Figure S68. The cluster analysis results.

The cluster analysis was classed as five cluster for the 1000 frames for every complex system from the last 200 ns MD simulation.

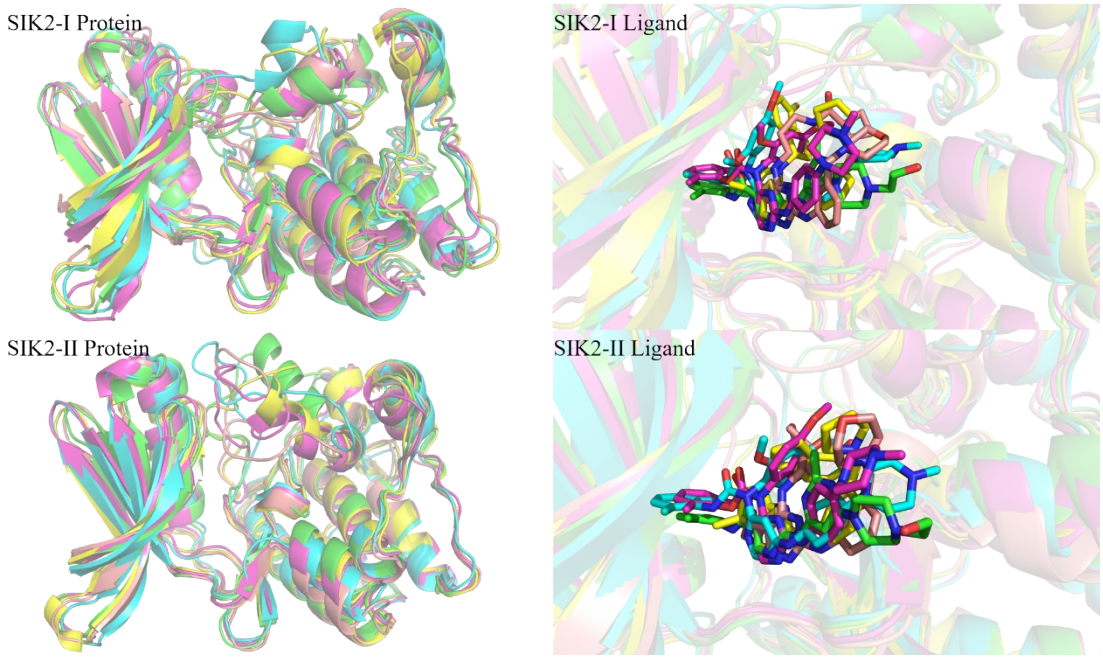

Figure S69. The representative conformations for ensemble docking.

The Dasatinib-I-1, HG-9-91-01-I-1, KIN112-I-1, MRT199665-I-1, MRT67307-I-1 from SIK2-I and Dasatinib-II-1, HG-9-91-01-II-1, KIN112-II-1, MRT199665-II-1, MRT67307-II-1 from SIK2-II were selected as the protein conformations for ensemble docking.

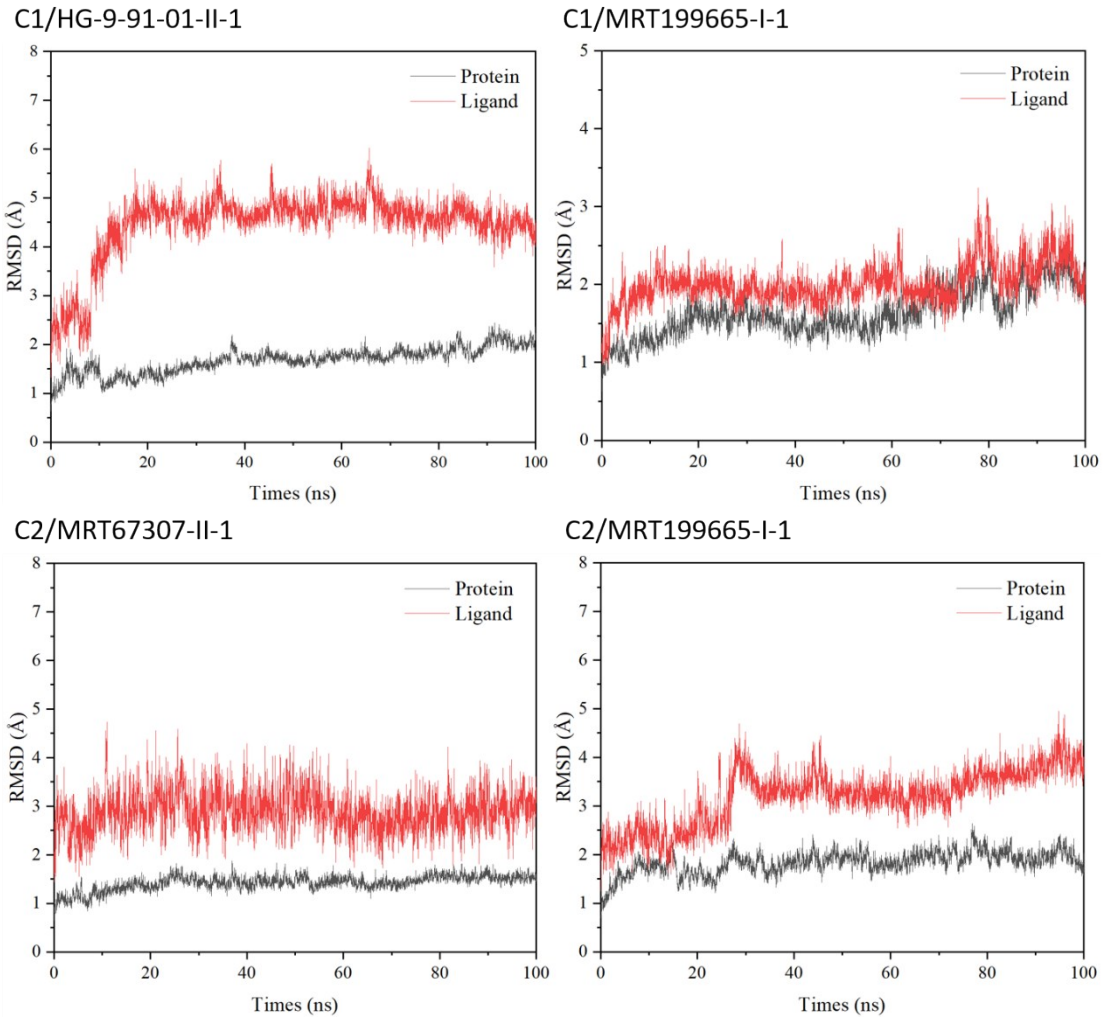

Figure S70. The root mean square deviation (RMSD) value of heavy atoms of protein along 100 ns MD simulations.

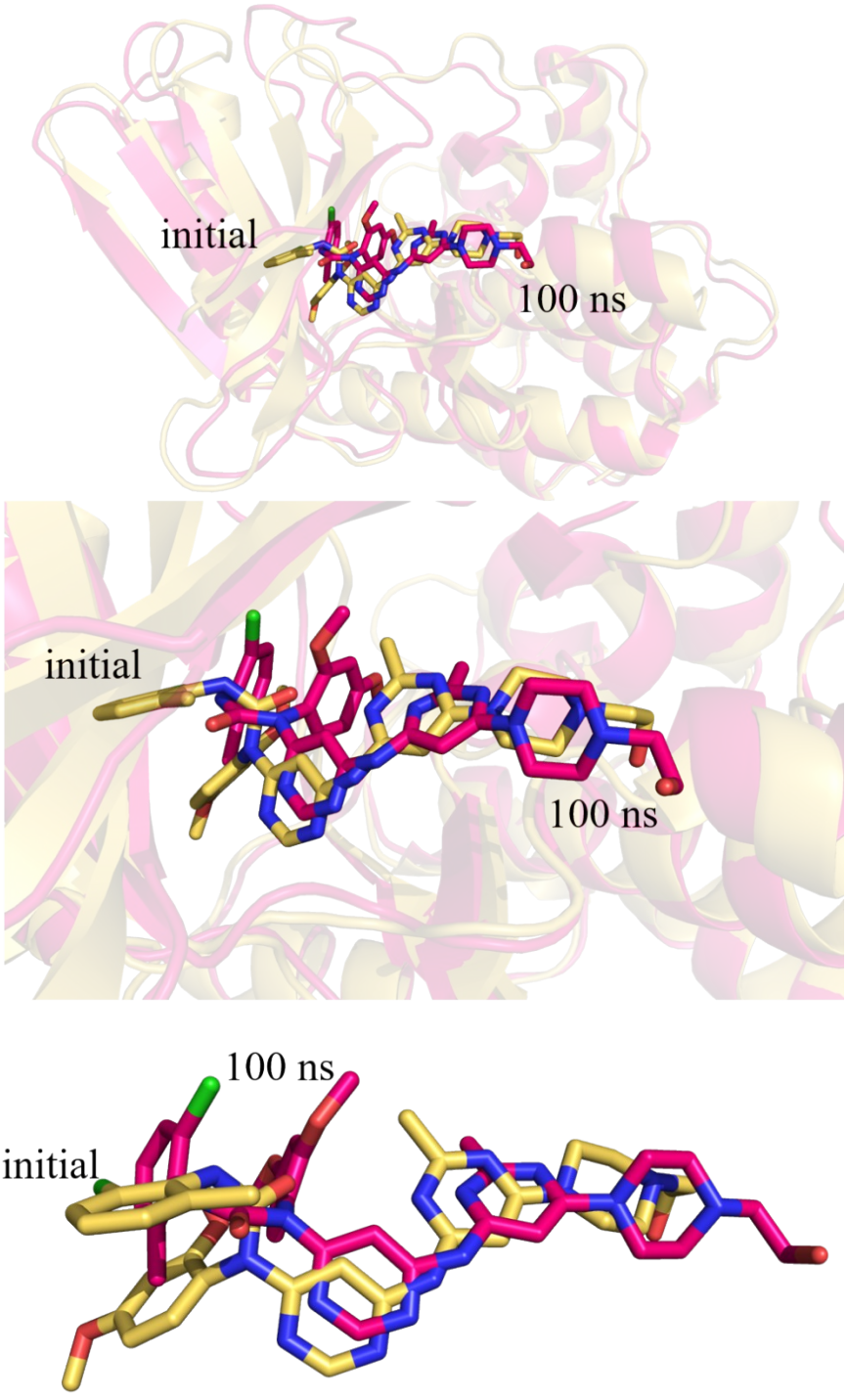

Figure S71. Structures of the C1/HG-9-91-01-II-1 for initial and 100 ns.

For clarity, the water molecules have been removed. The inhibitor is plotted using stick style, while cartoon style for SIK2.

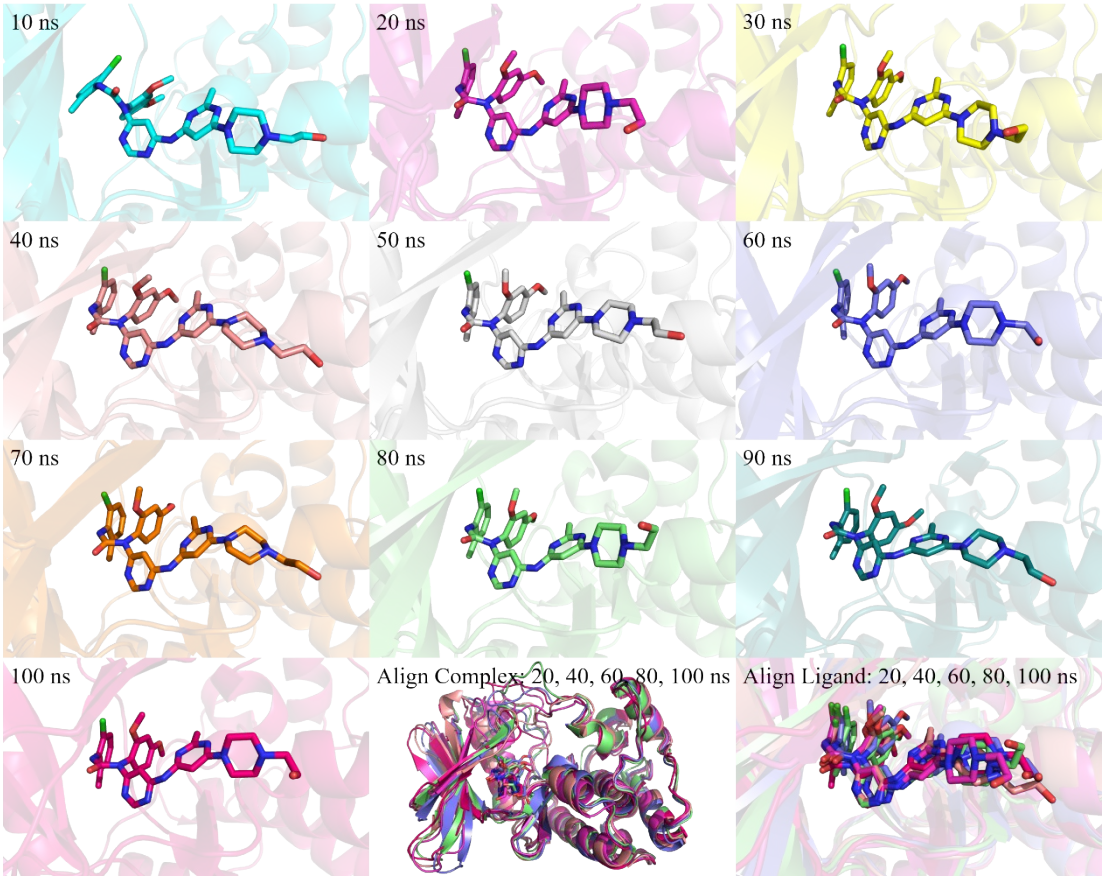

Figure S72. Snapshots of the C1/HG-9-91-01-II-1 along the dynamic simulation time for 10, 20, 30, 40, 50, 60, 70, 80, 90, and 100 ns.

For clarity, the water molecules have been removed. The inhibitor is plotted using stick style, while cartoon style for SIK2.

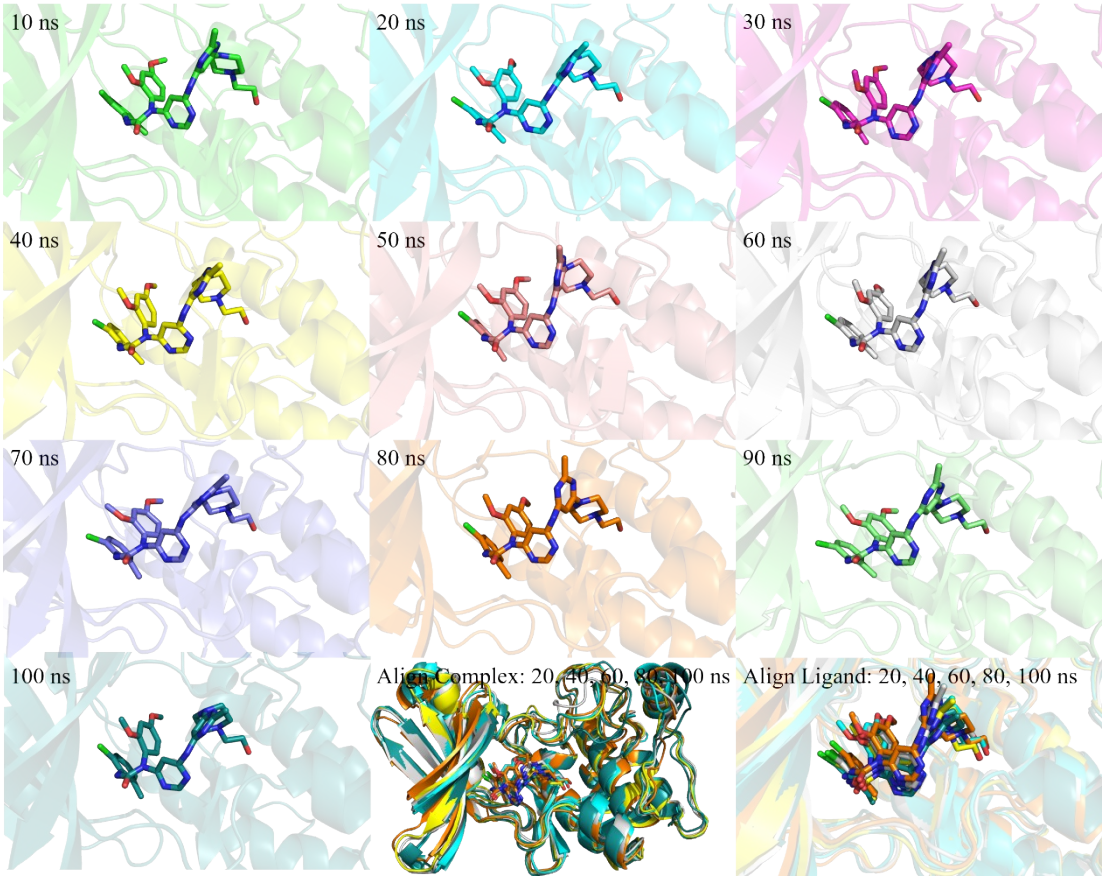

Figure S73. Snapshots of the C1/MRT199665-I-1 along the dynamic simulation time for 10, 20, 30, 40, 50, 60, 70, 80, 90, and 100 ns.

For clarity, the water molecules have been removed. The inhibitor is plotted using stick style, while cartoon style for SIK2.

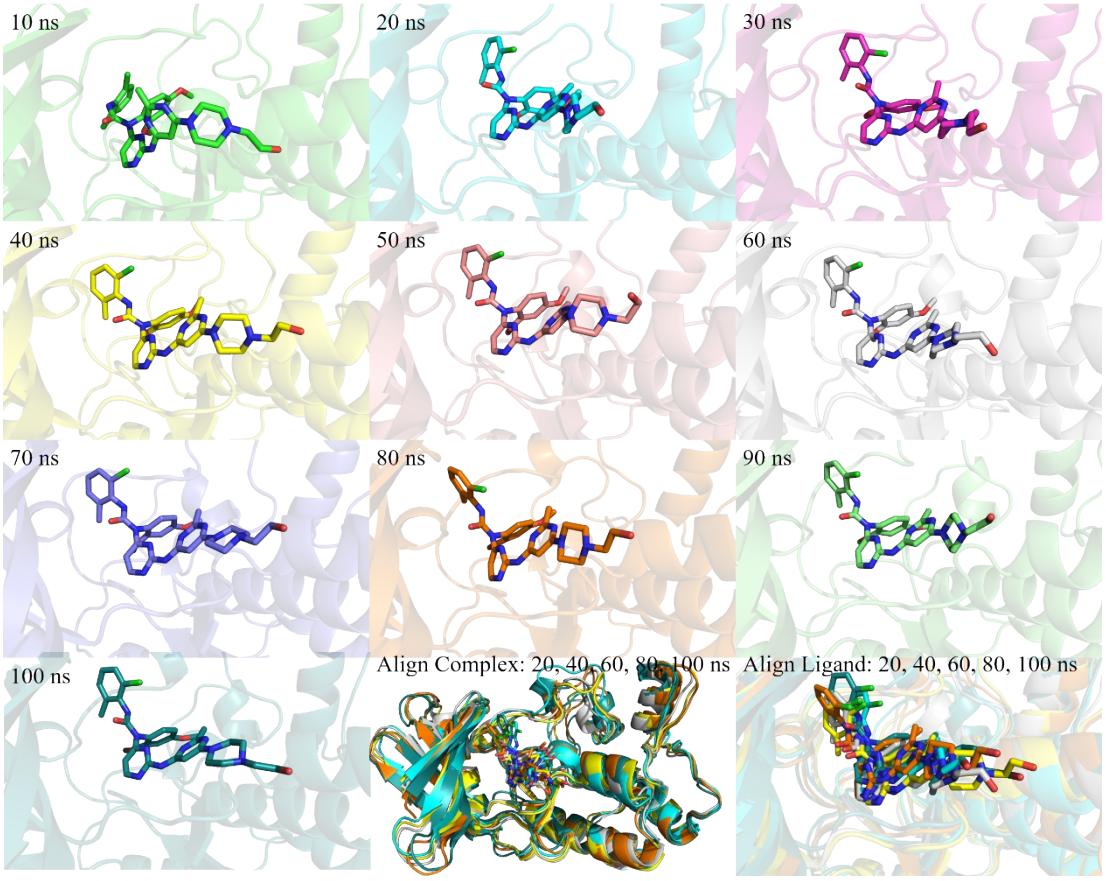

Figure S74. Snapshots of the C2/MRT199665-I-1 along the dynamic simulation time for 10, 20, 30, 40, 50, 60, 70, 80, 90, and 100 ns.

For clarity, the water molecules have been removed. The inhibitor is plotted using stick style, while cartoon style for SIK2.

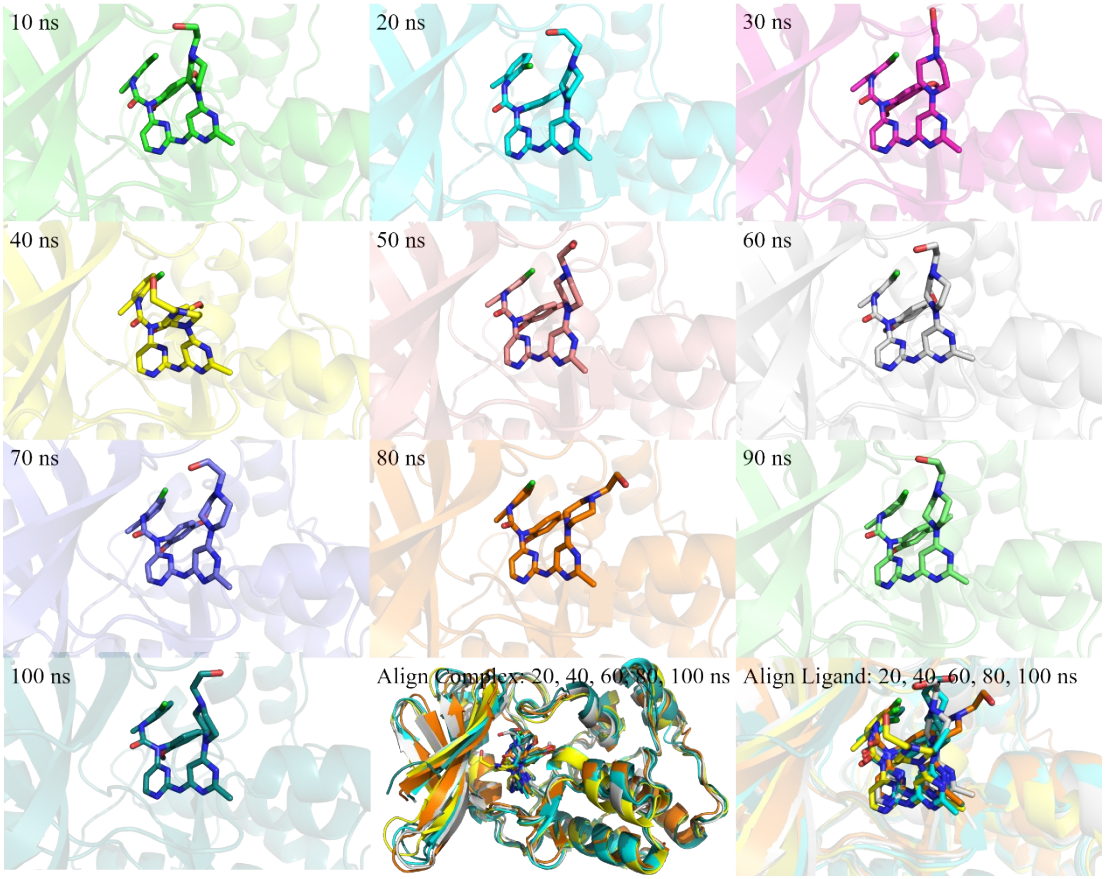

Figure S75. Snapshots of the C2/MRT67307-II-1 along the dynamic simulation time for 10, 20, 30, 40, 50, 60, 70, 80, 90, and 100 ns.

For clarity, the water molecules have been removed. The inhibitor is plotted using stick style, while cartoon style for SIK2.

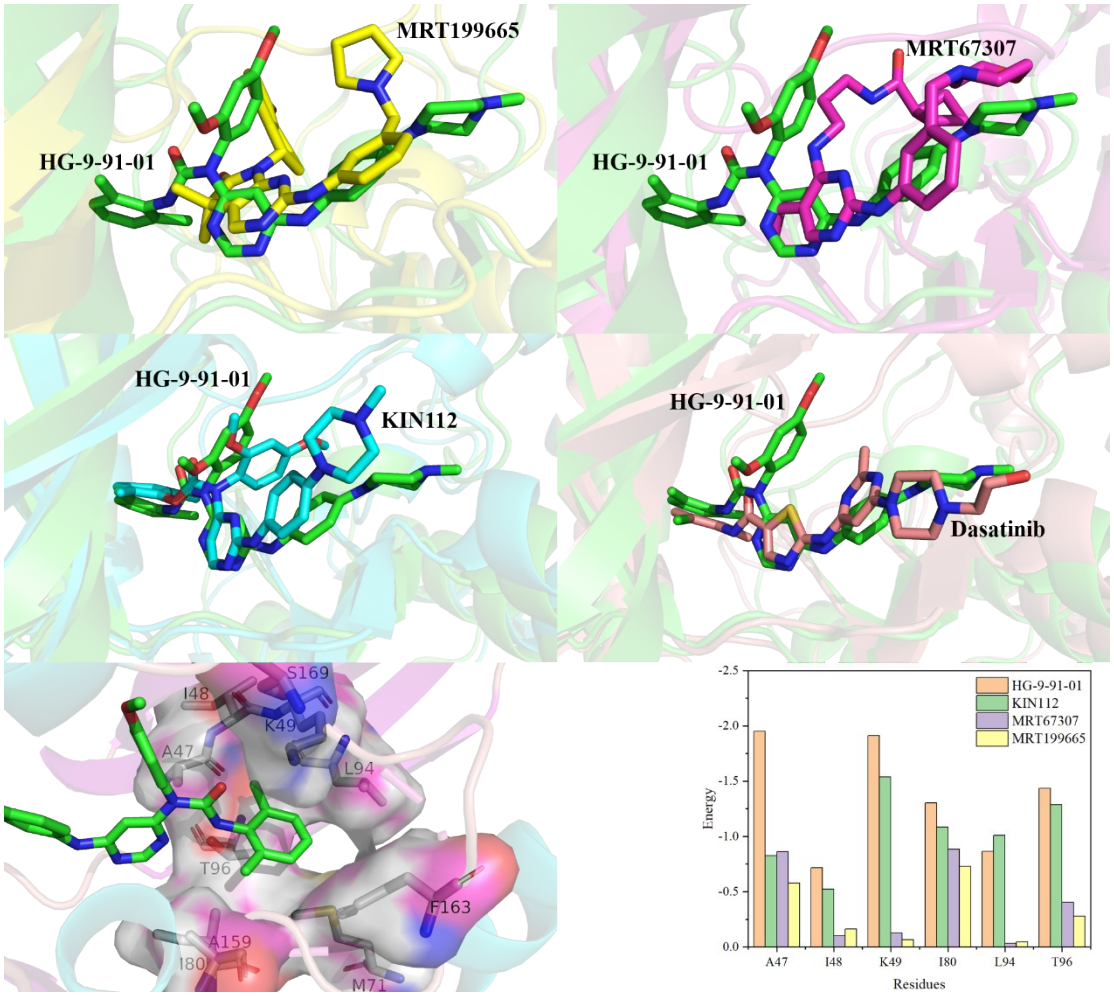

Figure S76. The structures and contribution energy of some residues for the hydrophobic cavity.

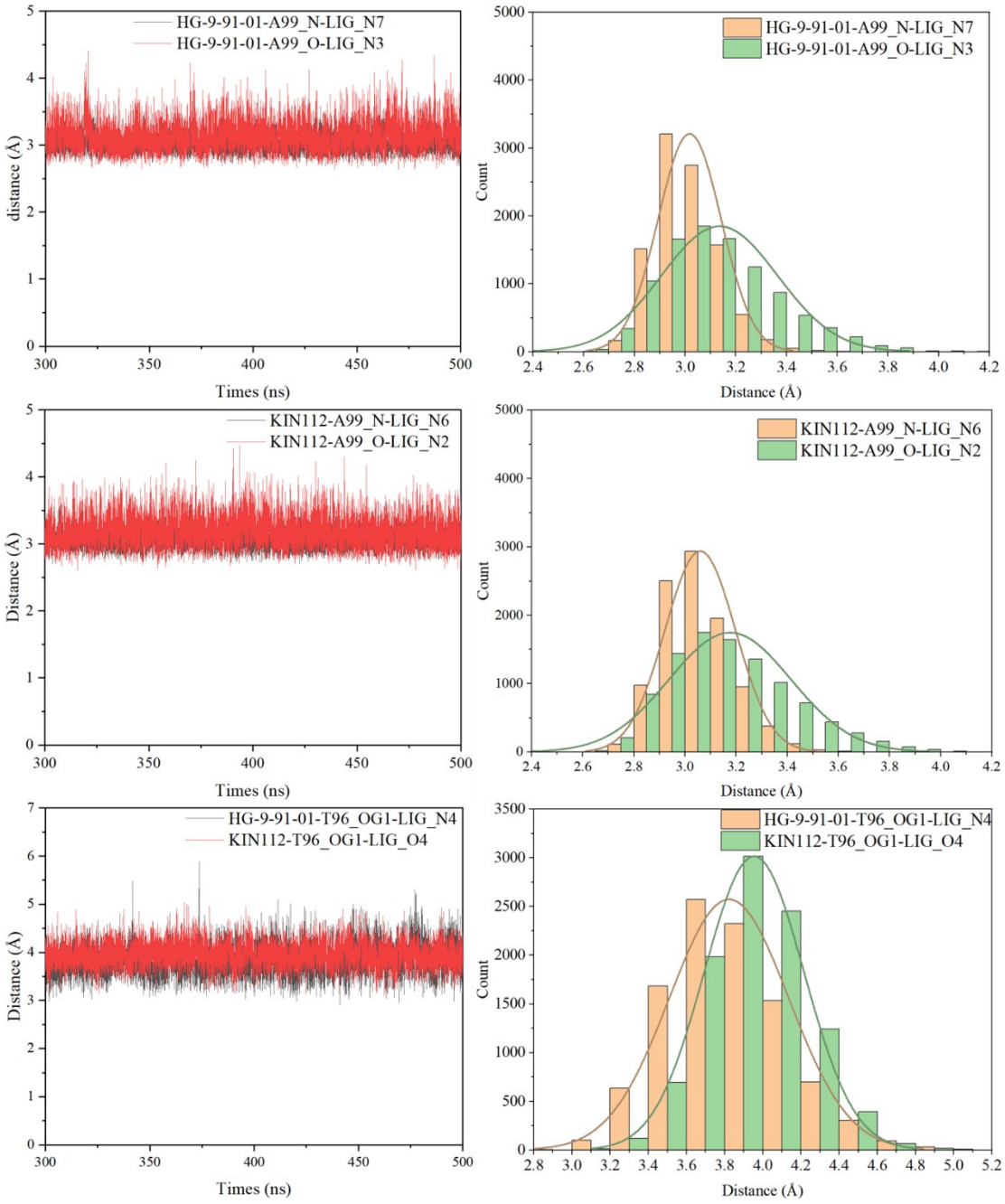

Figure S77. Distance along the last 200 ns MD simulation and distribution of the distance between inhibitors and SIK2.

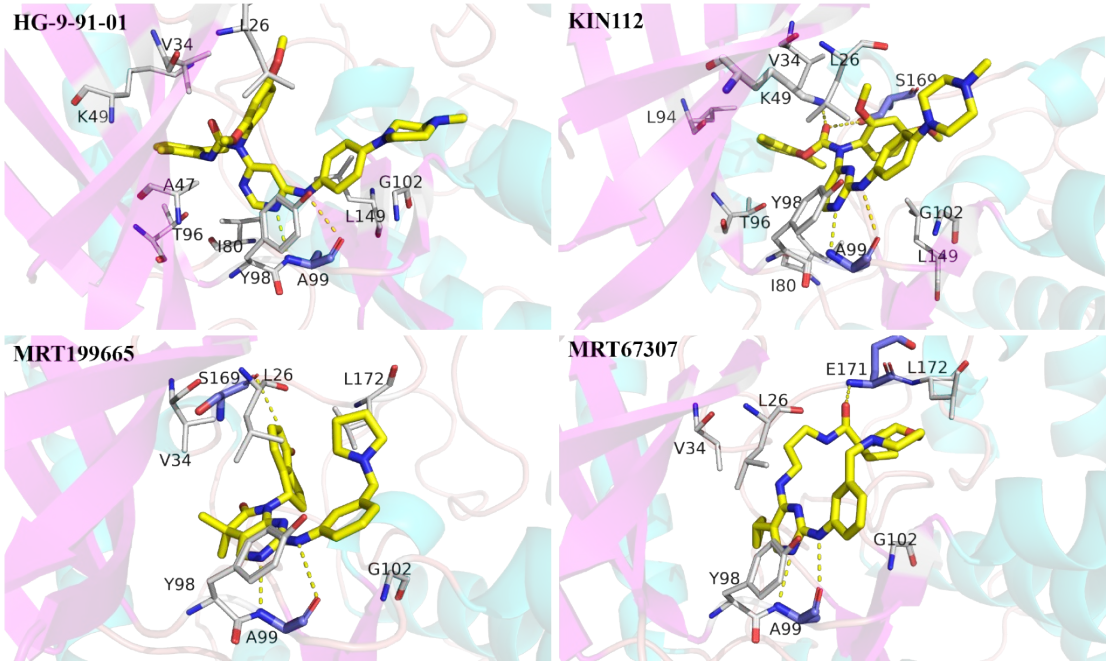

Figure S78. Interaction between the HG-9-91-01, KIN112, MRT199665, MRT67307 and SIK2.

Yellow for ligands, blue for residues of hydrogen bonds and gray for hydrophobic interactions. Sticks for ligand and key residues, cartoon for proteins.

Table S1. Distance for the two hydrogen bonds between A99 of SIK2 and the inhibitors from docking results.

Distance (Å)	**SIK2-I**	**SIK2-II**	**SIK2-III**
HG-9-91-01	2.58/3.14	2.7/2.87	2.71/2.83
KIN112	2.61/2.62	2.82/2.88	2.72/2.75
MRT67307	2.61/3.36	2.64/3.00	2.71/3.22
MRT199665	2.48/3.38	2.66/3.14	2.68/3.24

Table S2. Hydrogen bond network analysis for interactions between inhibitors and SIK2-III.

Residues	Occupancy (%)			
	HG-9-91-1	KIN112	MRT67307	MRT199665
K49@NZ	30.02	12.65		23.59
A99@N	91.85	98.91	97.13	93.36
A99@O	91.74	90.51	97.43	97.06
E103@N				10.45

Hydrogen bond is defined as the distance between the acceptor and donor atoms < 3.5 Å, with an internal angle between the H-acceptor and H-donor > 120º.

Table S3. Distance for the two hydrogen bonds between A99 of SIK2 and the inhibitors from the representative conformation from cluster analysis.

Distance (Å)	**SIK2-I**	**SIK2-II**	**SIK2-III**
HG-9-91-01	2.58/3.14	2.7/2.87	2.71/2.83
KIN112	2.61/2.62	2.82/2.88	2.72/2.75
MRT67307	2.61/3.36	2.64/3.00	2.71/3.22
MRT199665	2.48/3.38	2.66/3.14	2.68/3.24

Table S4. Binding free energy (ΔG_{bind}^{cal}) for dasatinib/SIK2-I complexes and decomposition to electrostatic interaction (E_{ele}), van der Walls interaction (E_{vdW}), solvation free energies (E_{GB}), and entropy (TS_{total}).

	Complex		Receptor		Ligand		Delta	
	Average	Std. Dev.	Average	Std. Dev.	Average	Std. Dev.	Average	Std. Dev.
E_{vdW}	-2065.25	26.01	-2003.79	25.15	-4.24	1.43	-57.23	3.46
E_{ele}	-17844.82	170.65	-17960.05	169.08	141.15	4.08	-25.92	6.45
E_{GB}	-3030.06	145.82	-3043.19	145.11	-25.34	0.87	38.47	5.08
E_{surf}	96.93	3.14	98.89	2.96	4.35	0.04	-6.32	0.35
G_{gas}	-3086.18	164.58	-2743.72	161.61	-259.31	5.41	-83.15	7.67
G_{solv}	-2933.13	143.67	-2944.30	143.16	-20.98	0.86	32.15	4.99
$E_{gas} + G_{sol}$	-6019.31	49.59	-5688.02	48.54	-280.29	5.30	-51.00	4.76
TS_{total}	2920.78	8.12	2881.43	8.16	65.53	1.08	-26.18	4.93
ΔG_{bind}^{cal}							-24.82	6.85

Energies are in kcal/mol.

Table S5. Binding free energy (ΔG_{bind}^{cal}) for dasatinib/SIK2-II complexes and decomposition to electrostatic interaction (E_{ele}), van der Walls interaction (E_{vdW}), solvation free energies (E_{GB}), and entropy (TS_{total}).

	Complex		Receptor		Ligand		Delta	
	Average	Std. Dev.	Average	Std. Dev.	Average	Std. Dev.	Average	Std. Dev.
E_{vdW}	-2115.03	20.43	-2055.13	20.10	-4.31	1.41	-55.59	3.43
E_{ele}	-18051.43	112.60	-18167.43	112.22	140.51	4.14	-24.51	6.24
E_{GB}	-2865.63	94.62	-2877.59	94.19	-25.27	0.85	37.23	5.71
E_{surf}	91.53	1.92	93.38	1.87	4.34	0.04	-6.19	0.30
G_{gas}	-3328.08	112.31	-2989.04	110.80	-258.94	5.59	-80.10	7.12
G_{solv}	-2774.11	93.58	-2784.21	93.26	-20.93	0.84	31.03	5.64
$E_{gas} + G_{sol}$	-6102.19	48.35	-5773.26	47.57	-279.87	5.50	-49.07	3.52
TS_{total}	2893.93	9.98	2855.25	9.61	65.20	1.16	-26.52	5.97
ΔG_{bind}^{cal}							-22.54	6.93

Energies are in kcal/mol.

Table S6. Free energy decomposition for the HG-9-91-01/SIK2-I complex at the level of individual residues basis into contributions from van der Waals energy (ΔE_{vdW}), electrostatic interaction energy (ΔE_{ele}), nonpolar solvation free energy ($\Delta G_{sol,np}$), polar solvation free energy ($\Delta G_{sol,GB}$), or from backbone energy ($B\Delta G_{subtotal}$) and side chain energy ($S\Delta G_{subtotal}$).

Residues	ΔE_{vdW}	ΔE_{ele}	$\Delta G_{sol,GB}$	$\Delta G_{sol,np}$	$S\Delta G_{subtotal}$	$B\Delta G_{subtotal}$	$\Delta G_{subtotal}$
L26	-1.37	-0.44	0.89	-0.22	-1.11	-0.03	-1.14
G27	-0.31	0.29	-0.13	-0.02	-0.10	-0.07	-0.17
V34	-2.15	-0.48	0.34	-0.26	-2.23	-0.33	-2.56
L36	-0.84	0.10	-0.18	-0.01	-0.61	-0.33	-0.93
V46	-0.22	-0.25	-0.03	0.00	-0.11	-0.40	-0.51
A47	-1.85	-0.24	0.31	-0.16	-1.44	-0.51	-1.95
I48	-0.91	0.31	-0.12	0.00	-0.28	-0.44	-0.72
K49	-1.82	-7.41	7.49	-0.18	-1.64	-0.27	-1.91
M52	-0.60	-0.14	0.22	-0.06	-0.54	-0.03	-0.58
I80	-1.22	0.11	-0.10	-0.10	-1.19	-0.11	-1.30
L94	-0.86	0.02	0.01	-0.03	-0.56	-0.30	-0.86
V95	-0.38	-0.02	-0.26	0.00	-0.15	-0.51	-0.66
T96	-1.91	0.33	0.29	-0.14	-1.03	-0.41	-1.44
Y98	-3.15	-1.00	1.82	-0.30	-2.05	-0.58	-2.63
A99	-0.85	-2.77	2.12	-0.05	-0.59	-0.97	-1.56
N101	-0.49	-0.24	0.24	-0.03	-0.07	-0.45	-0.52
G102	-1.23	-0.53	0.15	-0.15	-0.41	-1.36	-1.77
E103	-2.05	-1.64	3.88	-0.24	-0.09	0.03	-0.06
L149	-1.72	-0.12	0.10	-0.23	-1.78	-0.19	-1.96
A159	-0.62	-0.02	0.20	-0.05	-0.44	-0.05	-0.49
D160	-1.00	2.26	0.43	-0.18	1.36	0.15	1.51
F167	-0.65	0.40	-0.31	-0.06	-0.55	-0.08	-0.62
S169	-0.35	-0.02	0.39	-0.04	-0.09	0.07	-0.03
G170	-0.16	0.06	0.06	-0.04	-0.05	-0.02	-0.07
E171	-0.11	-0.36	0.47	-0.01	0.02	-0.03	-0.01
L172	-0.46	0.09	-0.01	-0.15	-0.51	-0.03	-0.54

Energies are in kcal/mol.

Table S7. Free energy decomposition for the KIN112/SIK2-I complex at the level of individual residues basis into contributions from van der Waals energy ($^{\Delta E_{vdW}}$), electrostatic interaction energy ($^{\Delta E_{ele}}$), nonpolar solvation free energy ($^{\Delta G_{sol,np}}$), polar solvation free energy ($^{\Delta G_{sol,GB}}$), or from backbone energy ($^{B\Delta G_{subtotal}}$) and side chain energy ($^{S\Delta G_{subtotal}}$).

Residues	ΔE_{vdW}	ΔE_{ele}	$\Delta G_{sol,GB}$	$\Delta G_{sol,np}$	$S\Delta G_{subtotal}$	$B\Delta G_{subtotal}$	$\Delta G_{subtotal}$
L26	-3.15	-0.70	1.96	-0.49	-2.60	0.23	-2.38
G27	-0.47	0.12	0.09	-0.06	-0.16	-0.16	-0.32
V34	-1.71	-0.31	0.27	-0.19	-1.72	-0.22	-1.94
L36	-0.20	-0.02	0.05	0.00	-0.14	-0.03	-0.17
V46	-0.11	0.06	-0.23	0.00	-0.07	-0.21	-0.28
A47	-1.02	-0.24	0.52	-0.09	-0.74	-0.08	-0.83
I48	-0.74	0.25	-0.03	0.00	-0.30	-0.22	-0.52
K49	-2.28	-9.77	10.73	-0.22	-1.46	-0.08	-1.54
M52	-0.35	-0.03	0.11	-0.08	-0.34	0.00	-0.34
I80	-1.03	0.10	-0.08	-0.08	-1.01	-0.07	-1.08
L94	-0.92	-0.12	0.09	-0.06	-0.60	-0.41	-1.01
V95	-0.42	-0.04	-0.17	0.00	-0.17	-0.47	-0.64
T96	-1.74	0.30	0.34	-0.19	-0.90	-0.39	-1.29
Y98	-1.92	-1.43	1.30	-0.08	-1.22	-0.92	-2.13
A99	-0.80	-2.74	1.68	-0.06	-0.60	-1.32	-1.92
N101	-0.49	-0.17	0.19	-0.03	-0.09	-0.41	-0.50
G102	-1.15	-0.59	0.45	-0.17	-0.37	-1.08	-1.46
E103	-1.30	-0.16	1.98	-0.24	0.25	0.03	0.28
L149	-2.24	-0.23	0.23	-0.28	-2.32	-0.20	-2.52
A159	-0.81	0.22	-0.07	-0.09	-0.69	-0.06	-0.75
D160	-0.96	-0.13	2.53	-0.08	1.46	-0.10	1.36
F167	-0.07	0.27	-0.22	0.00	-0.03	0.01	-0.03
S169	-2.19	1.63	-0.58	-0.28	-1.27	-0.14	-1.42
G170	-0.49	0.28	-0.03	-0.06	-0.18	-0.12	-0.30
E171	-0.07	0.04	0.01	0.00	0.05	-0.07	-0.02
L172	-0.06	0.04	0.01	0.00	-0.05	0.02	-0.02

Energies are in kcal/mol.

Table S8. Free energy decomposition for the MRT67307/SIK2-I complex at the level of individual residues basis into contributions from van der Waals energy (ΔE_{vdW}), electrostatic interaction energy (ΔE_{ele}), nonpolar solvation free energy ($\Delta G_{sol,np}$), polar solvation free energy ($\Delta G_{sol,GB}$), or from backbone energy ($B\Delta G_{subtotal}$) and side chain energy ($S\Delta G_{subtotal}$).

Residues	ΔE_{vdW}	ΔE_{ele}	$\Delta G_{sol,GB}$	$\Delta G_{sol,np}$	$S\Delta G_{subtotal}$	$B\Delta G_{subtotal}$	$\Delta G_{subtotal}$
L26	-3.73	-2.24	3.06	-0.53	-3.00	-0.45	-3.44
G27	-1.01	-0.27	0.81	-0.09	-0.41	-0.14	-0.55
V34	-1.26	0.13	-0.21	-0.12	-1.15	-0.31	-1.46
L36	-0.21	-0.10	0.12	0.00	-0.13	-0.06	-0.19
V46	-0.07	0.07	-0.29	0.00	-0.05	-0.25	-0.30
A47	-0.77	0.01	-0.04	-0.05	-0.70	-0.16	-0.86
I48	-0.11	-0.03	0.04	0.00	-0.02	-0.08	-0.10
K49	-0.31	2.50	-2.27	-0.04	-0.08	-0.04	-0.12
M52	-0.03	0.01	0.01	0.00	-0.01	0.00	-0.01
I80	-0.70	0.03	-0.14	-0.06	-0.71	-0.17	-0.88
L94	-0.03	-0.06	0.06	0.00	-0.02	-0.01	-0.03
V95	-0.03	0.01	-0.17	0.00	-0.02	-0.17	-0.18
T96	-0.44	-0.10	0.18	-0.05	-0.18	-0.22	-0.40
Y98	-1.89	-1.37	1.22	-0.10	-1.04	-1.10	-2.14
A99	-0.81	-3.10	1.76	-0.05	-0.62	-1.58	-2.20
N101	-0.61	-0.14	-0.02	-0.03	-0.14	-0.65	-0.79
G102	-1.20	-0.56	0.42	-0.15	-0.37	-1.13	-1.50
E103	-1.18	0.58	0.38	-0.19	-0.27	-0.13	-0.41
L149	-2.32	-0.13	0.13	-0.34	-2.41	-0.25	-2.65
A159	-0.47	0.11	-0.18	-0.06	-0.44	-0.15	-0.60
D160	-0.30	-2.32	3.06	-0.02	0.36	0.06	0.42
F167	-0.04	-0.18	0.19	0.00	-0.02	-0.02	-0.04
S169	-1.31	-0.12	1.06	-0.14	-0.53	0.01	-0.52
G170	-0.93	-1.40	1.43	-0.12	-0.33	-0.70	-1.02
E171	-0.88	-0.27	0.47	-0.09	-0.21	-0.56	-0.76
L172	-1.40	-0.50	0.56	-0.32	-1.36	-0.29	-1.65

Energies are in kcal/mol.

Table S9. Free energy decomposition for the MRT199665/SIK2-I complex at the level of individual residues basis into contributions from van der Waals energy (ΔE_{vdW}), electrostatic interaction energy (ΔE_{ele}), nonpolar solvation free energy ($\Delta G_{sol,np}$), polar solvation free energy ($\Delta G_{sol,GB}$), or from backbone energy ($B\Delta G_{subtotal}$) and side chain energy ($S\Delta G_{subtotal}$).

Residues	ΔE_{vdW}	ΔE_{ele}	$\Delta G_{sol,GB}$	$\Delta G_{sol,np}$	$S\Delta G_{subtotal}$	$B\Delta G_{subtotal}$	$\Delta G_{subtotal}$
L26	-2.98	0.00	1.10	-0.44	-2.47	0.15	-2.32
G27	-0.66	0.12	0.26	-0.06	-0.20	-0.14	-0.35
V34	-1.57	-0.17	0.20	-0.19	-1.54	-0.20	-1.73
L36	-0.21	0.00	-0.01	0.00	-0.15	-0.07	-0.22
V46	-0.08	0.09	-0.11	0.00	-0.03	-0.07	-0.10
A47	-0.61	0.06	0.04	-0.06	-0.49	-0.08	-0.58
I48	-0.18	-0.02	0.04	0.00	-0.06	-0.10	-0.16
K49	-0.43	-3.19	3.60	-0.05	-0.11	0.04	-0.07
M52	-0.04	0.00	0.02	0.00	-0.03	0.01	-0.02
I80	-0.73	0.16	-0.09	-0.06	-0.73	0.00	-0.73
L94	-0.05	-0.02	0.02	0.00	-0.03	-0.02	-0.04
V95	-0.04	0.06	-0.11	0.00	-0.02	-0.07	-0.09
T96	-0.59	0.13	0.27	-0.08	-0.22	-0.06	-0.28
Y98	-1.99	-1.20	1.19	-0.15	-1.28	-0.87	-2.15
A99	-0.96	-3.16	2.04	-0.06	-0.65	-1.50	-2.15
N101	-0.42	-0.10	0.04	-0.01	-0.08	-0.41	-0.49
G102	-1.03	-0.42	0.21	-0.15	-0.33	-1.05	-1.38
E103	-1.19	-0.69	2.40	-0.20	0.38	-0.07	0.32
L149	-2.61	-0.03	0.09	-0.31	-2.69	-0.17	-2.86
A159	-0.69	-0.09	0.20	-0.12	-0.55	-0.15	-0.70
D160	-0.64	4.30	-3.31	-0.08	0.35	-0.09	0.27
F167	-0.06	0.22	-0.28	0.00	-0.10	-0.03	-0.13
S169	-1.03	-2.88	2.55	-0.17	-1.34	-0.19	-1.53
G170	-0.29	-0.85	0.45	-0.05	-0.10	-0.64	-0.74
E171	-0.18	0.32	-0.29	0.00	-0.09	-0.06	-0.15
L172	-1.09	-0.10	0.21	-0.21	-1.14	-0.05	-1.19

Energies are in kcal/mol.

Table S10. The ensemble docking results for C1 and C2.

Receptor	C1	C2
SIK2-Dasatinib-I-1	-8.07	-7.95
SIK2-Dasatinib-II-1	-8.04	-7.88
SIK2-HG-9-91-01-I-1	-8.15	-8.33
SIK2-HG-9-91-01-II-1	-9.19	-8.52
SIK2-KIN112-I-1	-7.31	-7.81
SIK2-KIN112-II-1	-8.09	-8.08
SIK2-MRT67307-I-1	-9.35	-9.38
SIK2-MRT67307-II-1	-7.79	-8.00
SIK2-MRT199665-I-1	-8.65	-8.86
SIK2-MRT199665-II-1	-8.93	-9.00

Energies are in kcal/mol.

Table S11. Binding free energy (ΔG_{bind}^{cal}) for C1 and C2 with SIK2 and decomposition to electrostatic interaction (E_{ele}), van der Walls interaction (E_{vdW}), solvation free energies (E_{GB}), and entropy (TS_{total}).

	C1/MRT199665-I-1	C1/HG-9-91-01-II-1	C2/MRT67307-I-1	C2/MRT199665-II-1
E_{vdW}	-66.12	-62.85	-53.60	-55.61
E_{ele}	-20.16	-27.53	-20.62	-15.18
E_{GB}	43.44	51.35	39.04	32.91
E_{surf}	-8.97	-7.36	-6.49	-6.59
G_{gas}	-86.28	-90.37	-74.23	-70.79
G_{solv}	34.47	43.99	32.55	26.32
$E_{gas} + G_{sol}$	-51.81	-46.38	-41.68	-44.47
TS_{total}	-27.46	-27.01	-22.25	-25.54
ΔG_{bind}^{cal}	-24.36	-19.36	-19.43	-18.92

Energies are in kcal/mol.